TURBULENT FLUID FLOW AND HEAT TRANSFER IN ANNULAR PASSAGES WITH ROUGH SURFACES AND MOVING CORES

by

Steven J. Keays, P.Eng

A thesis submitted to the School of Graduate Studies in partial fulfilment of the requirements of the degree of

MASTER OF APPLIED SCIENCE

in the

Department of Mechanical Engineering
University of Ottawa

ISBN 0-315-89674-4

Abstract

This study investigates the behaviour of fully developed fluid flows in concentric annuli with rough surfaces and moving cores, by analytically predicting the effects of surface roughness, core velocity and turbulent motion on the momentum and heat transfer characteristics of the flow, such as friction forces, velocity profiles, temperature profiles and heat transfer.

The analytical predictions are produced by a mathematical model based on an adaptation of Prandtl's mixing length theories and on the data of previous studies of turbulent flow in annuli and rectangular channels which were artificially roughened. The computer program developed for this study employs an iterative process to match velocity and temperature profiles with force and energy balances and calculates the desired momentum and thermal characteristics.

The results indicate excellent correlation with previous experimental data on rough annuli with static cores and smooth annuli with moving cores. From these results, the combined effects of surface roughness and moving cores are inferred. New equations are proposed for predicting the radius of maximum fluid velocity and the effects of core velocity on roughness, in terms of annulus radius ratio, roughness geometry, flow's Reynolds number and core velocity.

The study demonstrates the advantages, under certain conditions, of using roughness elements to increase heat transfer and enhance the overall efficiency in the energy transfer processes involved.

Acknowledgement

The author wishes to express his appreciation for the opportunity to have worked under the supervision and guidance of Dr. Yung Lee, whose help, patience and knowledge of the field of fluid heat transfer were paramount in bringing this study to fruition.

Thanks also go to the Department of National Defence Headquarters, who provided the computer resources to perform the computer simulations and draft this thesis.

Finally, special thanks go to the author's wife, whose continuous support and patience made it possible to persevere during the years of work.

Table of Contents

Chapter 4 - Computer Program

Chapter 5 - Results and analysis

List of Tables

List of Figures

Nomenclature

A_c: cross sectional area of the channel; constant

c_p: specific heat

C_1: constant

C_2: constant

D_H: hydraulic diameter. For annulus, $D_H = 2\ (R_{Ro} - R_{Ri})$

e: height of roughness elements

f_r: friction factor for annulus with rough surface(s)

f_s: friction factor for annulus with smooth surfaces

F: f_r/f_s

h: convective heat transfer coefficient

H: Nu_r/Nu_s

k: thermal conductivity

κ: Von Kármán's constant

l: Prandtl's mixing length

m: z/e, proportionality constant

Nu: Nusselt number

Nu_r: Nusselt number for annulus with rough surface(s)

Nu_s: Nusselt number for annulus with smooth surfaces

P: Pressure; pitch between roughness elements

Pr: Prandtl number

Pr_t: Turbulent Prandtl number; ϵ_M/ϵ_H

$\dot{q}_r$: heat flux

r: radial coordinate

R: Surface radius

Re: Reynolds number

R_M: radial location of maximum velocity

R_M^*: Non-dimensionalized $R_M = (R_M - R_{Ri}) / (R_{Ro} - R_{Ri})$

Rmc: Ratio of Rm calculated by computer iteration over Rm predicted by Eq [3.30]

S: annulus width; $(R_{Ro} - R_{Ri})$

t: time

T: temperature

T_b: bulk temperature (see Appendix A6, Eq [A6.10] and [A6.11])

u(r): axial velocity vector; also written in short form: *u*

v(r): radial velocity vector; also written in short form: v

U: Core velocity

U^*: Non-dimensional core velocity (see Eq [3.24])

v_r: Radial velocity

y_j: relative radial position, $|R_M - R_{Rj}|$

y_{mr}: relative location of maximum velocity in rectangular channel (see Eq [2.1], [3.29] and [3.30])

y_{os}: relative location of zero shear stress in rectangular channel (see Eq [5.3] and [5.4])

z: offset position for zero fluid velocity above root of rough surface (see Eq [3.28])

<u>Greek symbols</u>

α: radius ratio, R_{Ri}/R_{Ro} ; thermal diffusivity

β: constant

δ_i^+: $|R_M - R_{Rj}|$

Δ_i: δ_i^+/R_i^+

ζ_i: y_i^+/δ_i^+

$\mu_{\tau j}$: shear velocity

τ: shear stress

A_j: Van Driest's damping constant

ϵ_M: turbulent eddy diffusivity for momentum

ϵ_H: turbulent eddy diffusivity for heat

μ: dynamic viscosity

ρ: density

ν: kinematic viscosity

θ: angular coordinate

Ω: constant

Λ: constant

Υ: constant

Superscript

$\overline{}$: time averaged quantity

$+$: non-dimensionalized parameter using shear velocity

$^\circ$: time rate of change

': fluctuation

": per surface area

Subscripts

b: bulk

Bi: radial boundary of roughened core , $R_{Ri} + z_{or}$

Bj: Bi or Bo

Bo: radial boundary of roughened outer surface, $R_{Ro} - z_{or}$

Core: associated with the moving surface of the annulus

H: heat, hydraulic (for Diameter D_H)

i: inner surface; inner surface heated (see Appendix A, Eq [A.7])

ii: condition at core surface when core is heated

io: condition at core when outer surface is heated

j: *i* or *o*

jj: *ii* or *oo*

k: *o* or *i*

M: momentum; location of maximum velocity

m: condition of mean flow when core is heated

mo: condition mean flow when outer surface is heated

o: outer surface; outer surface heated (see Appendix A, Eq [A.7])

oo: condition at outer surface when core is heated oi: condition at outer surface when outer surface is heated

P: pressure

r: radius; rough surface

Ri: Core radius

Ro: outer surface radius

s: sublayer region; smooth surface

t: turbulent

τ: wall coordinate non-dimensionalized with wall shear stress

Chapter 1
Introduction

Fluid flows in internal passages have a long tradition of theoretical interest, in particular flows in circular passages and annuli. The theoretical aspect is indeed insightful; nevertheless, the problem has ramifications into the realm of practical applications that warrants serious investigation beyond mere intellectual curiosity. The class of problems concerning annulus flow with moving cores arises out of real engineering applications such as high speed trains in long tunnels, heavy traffic in tunnels, cooling of radioactive rods in nuclear reactors, etc. The generation of heat from inside a long passage makes its evacuation a dominant design problem. Analytical models for predicting the rate of heat transfer from the heat source to the surrounding fluid (such as air) are unfortunately scarce, as noted by Barrow and Pope [1]. Because turbulent boundary layers are well known for being more effective in convecting heat away from a surface, as explained by Dunn and Reay [2], there is heightened interest in modelling surface roughness. But rough surfaces increase friction losses, thereby placing an added burden on the pumping power required to evacuate heated fluids. Under certain combinations of artificial roughness and Re numbers, it is possible to improve overall energy efficiency of the energetic process. There lies the ultimate goal of the present study.

The problem investigated in this study can be ascribed this general description: a fluid flowing in a concentric annulus, with rough internal surfaces and a moving core. The boundary layer is fully developed (i.e., the velocity and temperature profiles are invariant along the axial and angular directions and time independent). The heat source generates a constant heat flux at the heated surface. Finally, the surfaces are artificially roughened by regular, square roughness elements, evenly spaced along the surface. The basic differential equation to be solved in this case is:

$$u(r)\,\frac{\partial u(r)}{\partial x} = -\frac{1}{\rho}\frac{\partial P}{\partial x} + \frac{\nu}{r}\frac{\partial}{\partial r}\left(r\,\frac{\partial u(r)}{\partial r}\right) \qquad [1.1a]$$

$$u(r)\,\frac{\partial T(r)}{\partial x} = \frac{\alpha}{r}\frac{\partial}{\partial r}\left(r\,\frac{\partial T(r)}{\partial r}\right) \qquad [1.1b]$$

The mathematical analysis of the problem has only been partially solved. In the case of laminar fluid flow, a complete solution to Eq [1.1] can be obtained analytically, as demonstrated in Appendix B. Turbulent fluid flows, on the other hand, exhibit added complications that make a closed analytical solution of Eq [1.1] impossible to achieve. Indeed, when the variables u(r) and T(r) are decomposed into a time averaged value and a fluctuating component, turbulent terms appear in the basic differential equations:

$$\overline{u(r)}\,\frac{\partial \overline{u(r)}}{\partial x} = -\frac{1}{\rho}\frac{\partial \overline{P}}{\partial x} + \frac{\nu}{r}\frac{\partial}{\partial r}\left[r\left(\frac{\partial \overline{u(r)}}{\partial r} - \overline{u'\,v'}\right)\right] \qquad [1.2a]$$

$$\overline{u(r)}\,\frac{\partial \overline{T(r)}}{\partial x} = \frac{\alpha}{r}\frac{\partial}{\partial r}\left[r\left(\frac{\partial \overline{T(r)}}{\partial r} - \overline{u'\,t'}\right)\right] \qquad [1.2b]$$

$$\textit{where}\quad u(r) = \overline{u(r)} + u'(r) \quad \textit{and}$$

$$t(r) = \overline{T(r)} + t'(r)$$

These new terms, called *apparent shear stresses* and *apparent heat fluxes* respectively, cannot be solved analytically (derivation of Eq [1.2] can be found in basic heat transfer text books such as [3], [4] and [5]).

The body of work on turbulent heat transfer in annulus passages is considerable for the case of an annulus with the core at rest and both annulus surfaces smooth (see Rothfus *et al* [6], Sleicher and Tribus [7], Shigechi *et al* [8] through [11], Nikuradse [12], Schlichting [13], Launder [14], Tanaka and Yabuki [15], Jones and Launder [16], Clauser [17] and Hama [18]). Surprisingly, the literature regarding annuli with rough surfaces is significantly more scant, owing perhaps to the inherent difficulty in modelling the roughness elements and their effects (see Lee [19], Lee and *et al* [20] through [23], Perry and Joubert [24], Wu [25] and Ahn [26]). The added complication of moving cores has not, to the author's knowledge, been the subject of scientific publication except for the case of laminar flow in a smooth annulus with moving cores (Lee [27]).

The modelling confronts numerous difficulties: the ineffective characterization of surface roughness by a single parameter; the establishment of the position of maximum fluid velocity; the impact of artificial roughness on the location of zero fluid velocity near a roughened wall; the determination of accurate profiles for the velocity and temperature in the fluid; and the combined effect(s) of a core velocity and surface roughness on the behaviour of the boundary layer. Thus, to solve the closure problem of Eq [1.2], it is necessary to model the turbulent terms and roughness variables.

In this context, the research objectives of this study are set as follows:

- To determine the velocity and temperature profiles across a concentric annulus, and their variations caused by varying α, core velocity, Re, Pr and roughness geometry;
- To predict the fluid characteristics such as mean velocity, mean temperature and friction factor, and the local Nusselt number;
- To compare the predictions with experimental data and verify the adequacy of the models;
- To derive empirical formulations for predicting the location of maximum velocity R_M and the position of zero velocity z_{0r}, in terms of α, core velocity and roughness elements; and
- To determine the overall efficiency of the heat transfer process by comparing the heat transfer with viscous forces. The efficiency is measured in terms of the following expression:

$$H/F = (Nu_r/Nu_s) \ / \ (f_r/f_s) \qquad [1.3]$$

Chapter 2

Literature Survey

2.0 General

The study of turbulent fluid flow in smooth surface conduits has been the subject of intense research over the years, due to the numerous engineering applications in which turbulent fluid flow occurs. The research has been successful in establishing with high degrees of correlation the characteristics of flows in circular pipes, annuli and long ducts with large aspect ratios. Such flows grow quickly into a fully developed state, usually within a few diameters of the tube entrance. The thermal boundary layer also reaches an invariant state within approximately the same distance (see Chapman [4], p. 280 and Schlichting [13], p. 560). However, the majority of the work done on channels has dealt with conduits whose internal surfaces were smooth. Early attempts to investigate the effects of artificial roughness on the flow encountered at least one severe constraint: one variable could not adequately describe the geometry of the roughness elements, which led to wide variations in results in the literature[1]. Better modelling has only recently been introduced with the advent of Computational Fluid Dynamics and higher order turbulence models, such as discussed by Kays and Leung [3] and presented by Launder [14], Tanaka and Yabuki [15] and Jones *et al* [16][2].

---

1 Bhuiyan [22] investigated a number of values for the parameter "m", which represents a proportionality constant for predicting the hypothetical position of the location of zero fluid velocity in the immediate neighbourhood of a rough surface. The variation in the "measured" value of m by numerous authors, led Bhuiyan to devise a new way to describe the effect of roughness elements.

2 It should be noted that these higher order turbulence models still contain shortfalls, one of which is the often-required need to tailor the turbulence models to the application. Hence, one needs *a priori* knowledge of the flow characteristics before applying the model. Also, these higher order models do not propose stand-alone expressions for calculating the quantities but rather they propose sets of differential equations, necessitating powerful computer resources.

2.1 Fully developed turbulent flow in smooth annuli

2.1.1 Turbulence terms

A complete analytical solution of Eq [1.2] cannot be obtained, even for the simplified problem involving a fully developed velocity and temperature profile, time independent, and with constant fluid parameters. Consequently, the development of a mathematical model for the problem in question necessarily requires artificial modelling of the turbulent parameters such as u'v', u'u' and u'p', etc. An early and highly successful attempt to model the turbulent terms was proposed by Prandtl (See Chapman [4] for a brief overview of the origins and basis for the theory). The mixing length theory[3] provided excellent insight into the mechanisms involved in the transport of momentum in locally fluctuating regions of a flow. However, the mixing length theory had serious shortfalls[4], as can be seen in Figure 2.1.

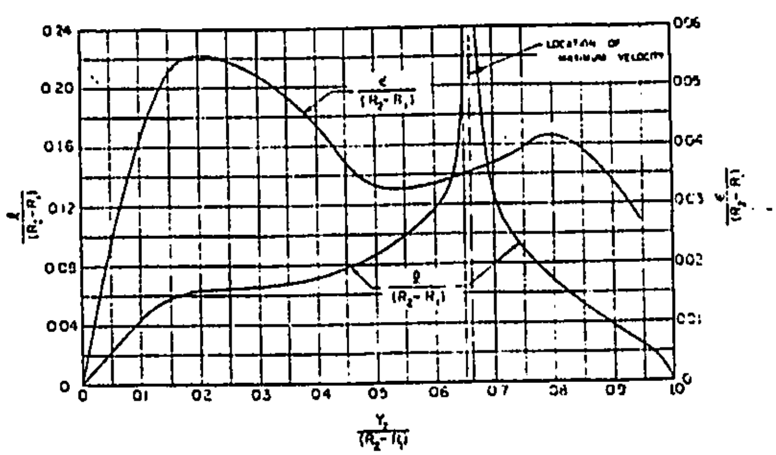

Figure 2.1: Calculated Prandtl's mixing length and eddy viscosity, α = 0.125 (from Brighton *et al* [32], page 840)

---

[3] Essentially, Prandtl assumed that a turbulent term was proportional to the mean velocity gradient of the fluid, in the direction normal to the velocity's direction, with the proportionality constant varying according to its distance from the wall.

[4] Brighton *et al* [32], for example, indicated that the measured turbulence parameter u'v' in an annulus flow exhibited a pseudo parabolic distribution across the channel, but that the mixing length theory predicted an asymptotic progression of the proportionality constant, with a value of infinity at the point of maximum velocity, a fact that is physically impossible.

Von Kárman [28] expanded on Prandtl's hypothesis by adding the second derivative of the mean velocity into the equation. Von Kármán's mixing length theory does not, however, improve significantly upon the predictions of Prandtl.

Despite these shortcomings, Prandtl's mixing length theory has been successfully used in numerous calculation schemes to predict momentum and heat transfer characteristics. It has also been the subject of numerous improvements, particularly by Van Driest [29] and Reichardt [30]. The works of Lee *et al* [11], [19], [20], [21] and [27], as well as those of Kays and Leung [31], Brighton & Jones [32], Barrow *et al* [33], Anderson *et al* [34] and Allan and Sharma [35] have demonstrated that the modified model is able to predict with high confidence flow parameters across most of an annulus' cross-section.

2.1.2 Higher-order turbulence models

In recent years, the advent of powerful computers encouraged scientists to develop more complicated turbulence models, such as the κ-ϵ model, first published by Harlow and Nakayama [36][5]. The κ-ϵ model offers significant improvements in the predictions of flow behaviour (see Jones *et al* [38] [39] and Lam and Bremhorst [40][6] but has the drawback of being more difficult to apply because of the requirement to simultaneously solve two third-order non-linear differential equations. In addition, the model does not escape the necessity of modelling turbulence terms. In fact, the modelling's difficulty has increased by one order of magnitude, dealing with tensors instead of vectors or scalars. But perhaps the biggest disadvantage of the model is the need to have *a priori* knowledge of the solution before applying the model.

2.1.3 Theoretical Statistical Turbulence

Another approach to the investigation of analytical means of quantifying turbulent terms

---

5 Hinze [37] discusses the driving motivation in developing the κ-ϵ model. See also [17].

6 Impressive results have been published on the investigation of the model by contemporary workers. The model has been undergoing constant improvements and is still under study.

is to study the problem statistically. *Theoretical Statistical Turbulence*[7], as it is called, was developed to mathematically describe the interaction of turbulent eddies that swirl around in isotropic turbulence. The model does provide a straightforward means of characterizing turbulent parameters, such as the eddy viscosity, based on the Dynamic Equation for isotropic Turbulence. This powerful equation equates the net rate of change of Total Kinetic Energy (TKE) to the sum of the net rate of energy transfer between eddies of larger sizes to eddies of smaller sizes, and the rate of TKE dissipation by viscous forces[8]. Unfortunately, there exists no accurate mathematical expression for the TKE dissipation term; the model is therefore restricted to an extremely limited class of problems and has not bridged the gap to extend to channel flows.

2.1.4 Turbulent velocity and temperature profiles

Concurrent to the search for modelling the turbulent parameters has been the effort to derive expressions for predicting the velocity and temperature profiles across the annulus. One simple yet effective expression can be obtained from the Prandtl's mixing length theory: the *logarithmic law of the wall.* Workers previously noted have had equal success in matching experimental data to computer predictions. Data have shown that the law of wall works very well for circular cylinders (see Kays and Crawford [3], p. 197), and for the flow region in an annulus bounded by the outer radius and the position of maximum velocity, R_M. For the inner region, the law of the wall is deficient and requires some modifications to better reflect the experimental evidence (Lee [19], Kays and Leung [31], Brighton and Jones [32], Barrow and Lee [33], Anderson *et al* [34], Allan and Sharma [35], Launder [43]). The temperature profile can also be derived from Prandtl's mixing length theory (Kays and Crawford [3], p. 241) but workers have traditionally reverted to performing numerical integration to obtain these profiles. The technique, used notably by Lee *et al*, [19] and [20], has correlated well experimental data.

[7] Hinze [37], pp. 200 to 260, presents a thorough development of the *Dynamic Equation for isotropic turbulence*. The subject is also discussed at length by Monin and Yaglom [41], pp.337-346 and Stănisik [42] pp. 40-60.

[8] TKE expresses the energy contained in the motion of lumps of fluids moving spatially as swirling eddies.

2.1.5 Position of maximum velocity

Research efforts have placed a high emphasis on finding empirical expressions for calculating the position of maximum velocity, R_M. That emphasis was justified by the importance of R_M; indeed, regardless of the models used, one must know where R_M lies in order to satisfy the forces and energy balances of the flow. For the laminar case, R_M can be analytically derived (see Appendix B). For the turbulent case, it cannot. Empirical expressions have been proposed, notably those of Kays and Leung [31] and Barrow *et al* [33]. An obvious limitation of any of these expressions is their inability to account for surface roughness; they were derived for smooth annuli only (the topic is discussed in greater detail in Chapter 5, Section 5.2.2). The expressions are not applicable when a moving core is involved. Other workers have elected to estimate R_M by computer iterations and have had good success in duplicating experimental data (see for example Lee [20] and Ahn [26]).

2.2 Fully developed turbulent flow in rough annuli

2.2.1 Annulus with rough surfaces and static core

Nikuradse [12] was the first to experiment with pipes artificially roughened with grains of sand uniformly spread over the inside wall. Using the average size of the sand grains, he provided the first means of asserting the roughness of a surface. He defined a roughness Reynolds number Re_k. For $Re_k < 5$, the surface was perfectly smooth. Above 70, the surface was fully rough. Middle values indicated a transition towards a fully rough surface.

The difficulty with Nikuradse's formulation lies in determining the roughness size k. Schlichting [13] later proposed the concept of *equivalent sand grain roughness* but did not completely remove the difficulty in assessing the roughness size and geometry.

To circumvent the problem, workers introduced the notion of a shift, from the surface, of the position of zero fluid velocity. Bhuiyan [22], working on rectangular channels with one surface roughened, looked into the many schemes of calculating this shift, usually found in the literature as the letter *m*. Workers such as Hanjalic [44] found that the velocity of a fluid near a surface roughened with geometric elements could be modelled to reach zero at an imaginary radial position above the root of the roughness gap and named that distance "z". "z" is directly proportional to the depth of the roughness, *e*, the proportionality constant being given by *m*. Bhuiyan [22] observed a wide spread in the predicted values of *m*, which indicated a deficiency in the methodology for defining *m*. Bhuiyan departed from the use of *m* and derived an analytical expression for predicting the imaginary position z_{mr}, based on an empirical equation for predicting the location of maximum velocity. The formula was applied successfully in subsequent work by Lee *et al* [19], [20], [21], [27], Hama [18] and others [24], [25]:

$$\frac{y_{mr}}{S} = 0.299 \times Re^{0.066} \times \left(\frac{S}{e}\right)^{0.140} \times \left(\frac{P}{S}\right)^{0.201} \qquad [2.1]$$

where y_{mr} is the relative location of maximum velocity, S is the channel's height, e is the roughness element's height and P, the roughness element's pitch.

The findings of subsequent investigations clearly demonstrated that surface roughness influences all flow parameters. In the smooth case, R_M is closer to the inner surface than in the laminar case, with a tendency to get closer as the radius ratio decreases, as the data from Brighton and Jones [32] and Barrow *et al* [33] demonstrated. In the case of an annulus with inner surface roughened, R_M is pushed radially outward, as the roughness increases in severity (see Lee and co-workers [19], [20], [21], [22], Ahn [26] and Randhave [45]). Whereas in the smooth case the position of zero shear stress is almost coincident with that of R_M[9], Bhuiyan found the two positions separated. Nusselt numbers were higher than for the smooth case, as was the friction factor and heat transfer near (although not necessarily by the same increase). The result is an increased overall efficiency in the heat transfer process (see Lee *et al* [20] [21])[10].

[9] As observed experimentally by several workers, including [7], [20], [31], [32] and [33].

[10] The efficiency of the energy exchange process is represented by the ratio H/F, Equ [1.3], and is also dependent also on the Prandtl number Pr.

2.2.2 Annulus with moving core

The latest development in annulus research has been the extension of the analysis to that of annuli with moving cores. Motivated by considerations of long tunnels used in train transportation and cooling of nuclear rods in a nuclear power reactor, numerous workers have laid down the mathematical models for calculating the heat and momentum transfer parameters of such cases, in particular Shigechi *et al* [8], [9], [10], [11] and Lee *et al* [23], [27]. Their work has been primarily in modelling the problem for computer calculations and not focused on experimental research. Nevertheless, the results obtained were, by extension from the static core case, favourable and realistic. A moving core will increase in general the values of Nu and H/F but decrease the friction factor, f. The computer models developed by these workers all used the principles of Prandtl's mixing length theory, along with the improvements made by Van Driest [29] and Reichardt [30].

The additional effect of surface roughness on a fluid moving relative to a moving core has not been the subject of investigation, at least not in the published literature. Therefore, a new modelling of the conjugated effects of moving core and core roughened was investigated in this study.

Chapter 3
Mathematical model

3.1 Problem definition and assumptions

The modelling of the equations for the problem at hand is based on a series of necessary assumptions to adequately control the computer simulation. The fluid flow to be analyzed is subjected to the following conditions:

1. The annulus is concentric;
2. The fluid's properties (density, viscosity, specific heat) are constant. The turbulent Prandtl number Pr_t is assumed to be unity;
3. The velocity and temperature profiles are fully developed and turbulent;
4. The roughness elements are square, equally spaced along a surface, and radially aligned on opposing surfaces;
5. The location of maximum velocity coincides with the position of zero shear stress;
6. For the smooth surface, the boundary layer can be divided into two regions: the viscous sublayer and the fully turbulent layer;
7. For the rough surface, the roughness Reynolds number is taken as being greater than 70; therefore, the boundary layer is assumed to be fully turbulent down to the surface;
8. The effects of roughness elements observed for flat plate channels are applicable to the annulus geometry;
10. There exists a non-zero axial pressure gradient in the fluid sufficient to maintain a radially variable velocity profile; and
11. The eddy viscosity expression derived by Van Driest is valid in the viscous sublayer region. The expression derived by Reichardt is applicable in a modified form in the fully turbulent region of the boundary layer, near a smooth surface.

12. The Prandtl's mixing length assumption is valid for the flow region near a roughened surface.

3.2 Modelling of eddy viscosity ratio ϵ_M/ν

3.2.1 The closure quandary that evolves from the fluctuation terms u'v' and u't' [11] in Eq [1.2] must be resolved first if a closed solution to the equation set is to be devised.

For the momentum equation, Prandtl hypothesized that the behaviour of the apparent shear stress was similar to the laminar stress, and proposed the identity:

$$\overline{u'v'} = -\epsilon_M \frac{\partial \bar{u}}{\partial r} \qquad [3.1]$$

$$\textit{where } \epsilon_M = \textit{proportionality constant} = l \frac{\partial \bar{u}}{\partial r} \qquad [3.2]$$

$$\textit{and } l = \textit{Prandtl's mixing length} = \kappa y$$

The proportionality constant is known as the *Eddy viscosity*. Eq [3.1] can be inserted back into Eq [1.1] to yield an expression for the *total shear stress* term:

$$\frac{\tau}{\rho} = (\nu + \epsilon_M) \frac{\partial \bar{u}}{\partial r} \qquad [3.3]$$

3.2.2 <u>Eddy viscosity near a smooth surface</u>

The boundary layer near a smooth surface will grow from a viscous sublayer to a fully turbulent layer. Using the basic definition given in Eq [3.1] and [3.2], two expressions for the eddy viscosity can be established to provide a continuous description of the boundary layer throughout the transition, based on a modified form of the original models proposed by Van Driest [29] and Reichardt [30] (also Shigechi [8]):

---

[11] For clarity, the time averaged symbol ___, and the variable dependency *(r)* will be omitted in the remainder of the text.

$$\frac{\epsilon_M}{\nu} = (\kappa_j y_j^*)^2 \left[1 - \exp\left(-\frac{y_j^*}{A_j^*} \right) \right]^2 \left| \frac{\partial u_j^*}{\partial y_j^*} \right| \qquad \textit{for the viscous sublayer and}$$

$$\frac{\epsilon_M}{\nu} = \frac{\kappa\, y_j}{6} \left[1 - \left(1 - \frac{y_j^*}{\delta_j^*} \right)^2 \right] \left[1 + 2 \left(1 - \frac{y_j^*}{\delta_j^*} \right)^2 \right] \qquad \textit{for the fully turbulent layer}$$

These two expressions can be made dimensionless, as shown in Appendix A5 at Eq [A5.6] and [A5.8]. The resulting expressions are:

$$\frac{\epsilon_M}{\nu} = \frac{1}{2} \left\{ -1 + \sqrt{ 1 + 4(\kappa_j \delta_j^* \zeta_j)^2 \left[1 - \exp\left(-\frac{\delta_j^* \zeta_j}{A_j^*} \right) \right]^2 \left| \delta_j^* \left(\frac{\tau}{\tau_R} \right)_j \right| } \right\} \qquad [3.4]$$

and

$$\frac{\epsilon_M}{\nu} = \frac{\kappa_j\, \delta_j^*\, \zeta_j}{6} \left[2 - \zeta_j \right] \left[3 - 4\zeta_j + 2\zeta_j^2 \right] \qquad [3.5]$$

The limiting domain for both equations is determined by the thickness of the viscous sublayer ζ_{js}, where $\zeta_{js} = y_{js}^+/\delta_j^+$ and $y_{js}^+ = A^+$, the Van Driest damping function[12]. Again in dimensionless form, the domains are given by the ranges:

For the viscous sublayer:	$0 < \zeta_j < \zeta_{js}$
For the fully turbulent layer:	$\zeta_{js} < \zeta_j < 1$

3.2.3 Eddy viscosity near a rough surface

Near a rough surface, Eq [3.4] and [3.5] cannot be applied because the boundary layer does not make a transition from a viscous regime to a turbulent regime. The viscous sublayer is annihilated by the effects of the roughness elements and the boundary layer is turbulent from the onset. Instead, Eq [3.2] and [3.3] are applied directly to the flow, starting from the surface and ending at R_M ($\zeta_{Bj} < \zeta_j < 1$, where ζ_{Bj} is equal to z_j^+/Δ_j^+).

[12] See [3] pp. 182-183 for a discussion of the concept of the damping function, utilized to make the eddy viscosity continuous over the viscous sublayer, down to the surface.

The mixing length l appearing in Eq [3.2] has been modeled by workers such as Lee *et al* [19], [20] and Ahn [26] by the equation[13]:

$$l = \kappa(y + z)$$

However, that equation implies that the variable y be set at zero at the position of z (thus, y = 0 will vary according to the geometry and dynamics of the fluid under study). The difficulty in using a "variable lower boundary" motivated the author to revert to the basic definition of l, from Eq [3.2] and adjust the domain according to z, in the following manner:

$$l = \kappa\, y$$

$$\text{where } z < y < y_{max}$$

3.3 Modelling of velocity profile

3.3.1 Velocity profile

The velocity profile of the flow, for any surface condition, is derived from Eq [3.3]. The equation is derived in Appendix [A.5] as Eq [A5.3], in the following non-dimensional form:

$$\frac{\partial u_j^*}{\partial \zeta_j} = \frac{\delta_j^* \left(\frac{\tau}{\tau_R}\right)_j}{\left(1 + \frac{\epsilon_M}{\nu}\right)} \qquad [3.6]$$

The term ϵ_M/ν is calculated using either Eq [3.4], [3.5] or [3.2], depending on the surface condition nearest to the flow area considered. Eq [3.6] is also a function of the shear stress ratio τ/τ_{Rj}, which is obtained from a force balance on the annulus' cross-section.

3.3.2 Force balance on the fluid

A force balance invariant of flow position can be established for a given geometry, owing to the fully developed nature of the flow. The relationship that arises between the shear stress at a radial position r and its adjacent surface shear stress is given by the expressions (see next page):

[13] See for example [27], [28] and [48].

$$\frac{\tau_r}{\tau_{R_i}} = \frac{R_{R_i}}{r}\left\|\frac{R_m^2 - r^2}{R_m^2 - R_{R_i}^2}\right\| \qquad [3.7]$$

and

$$\frac{\tau_{Ri}}{\tau_{Ro}} = \frac{R_{Ro}}{R_{Ri}}\left(\frac{R_M^2 - R_{Ri}^2}{R_{Ro}^2 - R_M^2}\right) \qquad [3.8]$$

Details of the derivation for both inner and outer regions of the flow are found in Appendix A1. Eq [3.7] can also be expressed in non-dimensional form for the particular flow region, as shown by Eq [A3.1] and [A3.2] in Appendix A3, for a smooth surface. The more general expressions, which include the effects of surface roughness, are given by Eq [A4.1], [A4.2] and [A4.3], in Appendix A4. They are:

InnerRegion:

$$\frac{\tau_r}{\tau_{R_{Ri}}} = \frac{1 + \frac{z_{Ri}}{R_{Ri}}}{1 + \Delta_i\zeta_i}\left[\frac{(1 + \Delta_i)^2 - (1 + \Delta_i\zeta_i)^2}{(1 + \Delta_i)^2 - \left(1 + \frac{z_{Ri}}{R_{Ri}}\right)^2}\right] \qquad [3.9]$$

OuterRegion:

$$\frac{\tau_r}{\tau_{R_{Ro}}} = \frac{1 - \frac{z_{Ro}}{R_{Ro}}}{1 - \Delta_o\zeta_o}\left[\frac{(1 - \Delta_o\zeta_o)^2 - (1 - \Delta_o)^2}{\left(1 - \frac{z_{Ro}}{R_{Ro}}\right)^2 - (1 - \Delta_o)^2}\right] \qquad [3.10]$$

$$\frac{\tau_{Bi}}{\tau_{Bo}} = \alpha \left(\frac{1 - \frac{z_{Ro}}{R_{Ro}}}{1 + \frac{z_{Ri}}{R_{Ri}}} \right) \left[\frac{(1 + \Delta_i)^2 - \left(1 + \frac{z_{Ri}}{R_{Ri}}\right)^2}{\left(1 - \frac{z_{Ro}}{R_{Ro}}\right)^2 - (1 - \Delta_o)^2} \right] \qquad [3.11]$$

Eq [3.9], [3.10] and [3.11] can be applied to any surface, rough or smooth. The domain limits for [3.9] and [3.10] are:

For the inner region : $\zeta_{Bi} < \zeta_i < 1$

For the outer region: $\zeta_{Bo} < \zeta_o < 1$

where ζ_{Bi} is equal to z_i^+/Δ_i^+ and ζ_{Bo} is equal to z_o^+/δ_o^+. In the case of a smooth surface, the term z goes to zero. The above shear stress equations are physically correct, in the sense that no assumption is made regarding the nature of the flow (whether it is laminar or turbulent).

3.4 Modelling of temperature profile

3.4.1 Eddy diffusivity ratio ϵ_H/ϵ_M

The apparent heat flux appearing in Eq [1.2] can be modelled following the classical analogy method[14]. The analogy equates the two eddy terms, such that their ratio $\epsilon_H/\epsilon_M = 1.0$.

Similar to the Eq [3.1], a total heat flux equation can be re-written to combine the effect of the apparent heat flux:

$$-\frac{\dot{q}_j''}{\rho\, c_p} = \alpha \left(1 + \frac{\epsilon_H}{\alpha}\right) \frac{\partial T_j}{\partial r} \qquad [3.12]$$

[14] See [3] pp. 205-207. Reynolds hypothesized that the eddy diffusivity ϵ_H was equal to the eddy viscosity ϵ_M, which finds strong support in the scientific community for Pr >0.5. Jenkins [27] and Sleichter *et al* [28] proposed a more complex expression for the ratio ϵ_H/ϵ_M based on a series solution of eigenvalues of the energy differential equation. The model predicts a ratio of unity when Pr = 1. See Appendix A5, Figure A5.1 for a graphical representation of the function.

3.4.2 Temperature profile

Eq [3.12] can be transformed into a non-dimensional equation and re-arranged to yield a corresponding expression for the temperature gradient. Details of the development are given in Appendix A5, Eq [A5.11]. The resulting equation is :

$$\frac{\partial T_j^+}{\partial \zeta_j} = \frac{\pm \delta_j^+ \left(\dfrac{\dot{q}_r''}{\dot{q}_{R_j}''} \right)}{\left(\dfrac{1}{Pr} \right) \left(1 + \dfrac{Pr}{Pr_t} \dfrac{\epsilon_M}{\nu} \right)} \qquad [3.13]$$

Again, in order to solve Eq [3.13], the expression for the heat flux ratio must be found via an energy balance of the fluid. The combination of heat sources at both annulus surfaces is calculated using *influence coefficients* (first proposed by Kays and Leung [31]), which are expressed by the equations (see Lee *et al* [22]):

$$\theta_i^* = \frac{\mu_{\tau_i}}{\mu_{\tau_o}} \frac{(T_{io}^+ - T_{mo}^+)}{T_{mi}^+} \qquad \theta_o^* = \frac{\mu_{\tau_o}}{\mu \tau_i} \frac{(T_{oi}^+ - T_{mi}^+)}{T_{mo}^+} \qquad [3.14]$$

3.4.3 Energy balance on the fluid

A complete solution to Eq [3.13] can be obtained if the heat ratio term is known. That term can be obtained by performing an energy balance on the fluid, as demonstrated in Appendix A2, Eq [A2.3] and [A2.4]. The general expression for the heat flux, at a radial position r in the annulus, (in the case of one surface heated) is:

$$\frac{\dot{q}_r''}{\dot{q}_{R_j}''} = \frac{R_{R_j}}{r} \left\| \frac{r^2 - R_{R_k}^2}{R_{Ro}^2 - R_{Ri}^2} \right\| \qquad [3.15]$$

where k = o when j = i; k = i when j = o

Non-dimensional forms of this equation can be derived in a manner similar to that of the shear stress ratios. There cannot be one single expression to account for the three different cases of heat generation (core heating, outer surface heating, combined core/outer surfaces heating). For the first two cases, the four heat flux ratios are given by the expressions:

Inner core heating - inner region

$$\frac{\dot{q}_r''}{\dot{q}_{Ri}''} = \frac{1 + \frac{z_{Ri}}{R_{Ri}}}{1 + \Delta_i\zeta_i}\left[\frac{(1 - \frac{z_{Ro}}{R_{Ro}})^2 - \alpha^2(1 + \Delta_i\zeta_i)^2}{(1 - \frac{z_{Ro}}{R_{Ro}})^2 - \alpha^2(1 + \frac{z_{Ri}}{R_{Ri}})^2}\right] \qquad [3.16]$$

Inner core heating - outer region

$$\frac{\dot{q}_r''}{\dot{q}_{Ri}''} = \alpha\frac{1 + \frac{z_{Ri}}{R_{Ri}}}{1 - \Delta_o\zeta_o}\left[\frac{(1 - \frac{z_{Ro}}{R_{Ro}})^2 - (1 - \Delta_o\zeta_o)^2}{(1 - \frac{z_{Ro}}{R_{Ro}})^2 - \alpha^2(1 + \frac{z_{Ri}}{R_{Ri}})^2}\right] \qquad [3.17]$$

Outer surface heating -inner region

$$\frac{\dot{q}_r''}{\dot{q}_{Ro}''} = \alpha\frac{1 - \frac{z_{Ro}}{R_{Ro}}}{1 + \Delta_i\zeta_i}\left[\frac{(1 + \Delta_i\zeta_i)^2 - (1 + \frac{z_{Ri}}{R_{Ri}})^2}{(1 - \frac{z_{Ro}}{R_{Ro}})^2 - \alpha^2(1 + \frac{z_{Ri}}{R_{Ri}})^2}\right] \qquad [3.18]$$

Outer surface heating - outer region

$$\frac{\dot{q}_r''}{\dot{q}_{Ro}''} = \frac{1 - \frac{z_{Ro}}{R_{Ro}}}{1 - \Delta_o\zeta_o}\left[\frac{(1 - \Delta_o\zeta_o)^2 - \alpha^2(1 - \frac{z_{Ro}}{R_{Ro}})^2}{(1 - \frac{z_{Ro}}{R_{Ro}})^2 - \alpha^2(1 + \frac{z_{Ri}}{R_{Ri}})^2}\right] \qquad [3.19]$$

3.5 Boundary conditions and matching conditions

The division of the flow into two regions, inner and outer, and the subdivision of each region, for the smooth case, into a viscous sublayer and a fully turbulent layer, automatically gives rise to the issue of continuity at the intersection of those divisions. The velocity, temperature and eddy viscosity must be equal on each side of a boundary. Furthermore, at the surfaces, those parameters <u>must</u> take on specific values, in order to be physically meaningful.

3.5.1 <u>Velocity Profile</u>

At the surface, the fluid is at rest, by virtue of viscosity. Also, because of that constraint, ϵ_M must also be zero at the surface. Therefore, the boundary conditions for u(r) and ϵ_M at the wall are:

$$\epsilon_M = 0 \text{ and } u(r) = 0 \qquad \text{at } y_j = z_{Rj} \quad (\zeta_j = z_{Rj}/\delta_j')$$

In the case of a smooth surface, the term $z_{Rj} = 0$.

At the location of maximum velocity, the velocity gradient is zero. Therefore, because of the continuity consideration, the velocity u(r) at R_M, calculated by integrating Eq [3.6] between the surface and $\zeta_j = 1.0$, must be equal on either side of R_M, i.e:

$$u(R_M)_i = u(R_M)_o$$

By substituting the non-dimensional equivalences from Appendix A3, one obtains:

$$\frac{\mu_{\tau_{Ri}}}{\mu_{\tau_{Ro}}} = \frac{(u_o^+)_{max}}{(u_i^+)_{max}} \qquad [3.20]$$

3.5.2 <u>Temperature profile</u>

At the wall, the non-dimensional temperature $T_j^+ = 0.0$, at $r = R_{Rj}$, from the definition given in Appendix A3.

At the location of maximum velocity, where $\zeta_i = \zeta_o = 1.0$, the non-dimensional temperatures T_o and T_i are equal, which, by straight substitution, gives:

$$\frac{(T_o^*)}{(T_i^*)} = \frac{\mu_{\tau_{Ro}}}{\mu_{\tau_{Ri}}} \qquad [3.21]$$

$$\text{and} \qquad \frac{\partial T_i^*}{\partial \zeta_i} = -\frac{\partial T_o^*}{\partial \zeta_o}\left(\frac{\delta_i^*}{\delta_o^*}\right) \qquad [3.22]$$

$$\text{both at} \quad r = R_M$$

Eq [3.22] is obtained by setting $\zeta_i = 0$ in Eq [3.13] and equating the two expressions for the inner and outer region.

3.5.3 Proportionality constants κ_i and κ_o - Smooth surface

At the junction of the inner and outer regions, Eq [3.5] must yield the same value of ϵ_M/ν as ζ_i approaches $\zeta_o \to 1.0$. Equating both expressions yields the condition:

$$\kappa_i \, \delta_i^* = \kappa_o \, \delta_o^* \qquad [3.23]$$

3.5.4 Proportionality constants κ_i and κ_o - Rough Core

In the case of a core that is artificially roughened, Eq [3.2] is applied throughout the inner region. Hama [18], Lee and co-workers [19], [20], [21], Bhuiyan [22], Ahn [26], Kays and Leung [31], Brighton and Jones [32], Barrow *et al* [33] have noted that the logarithmic law of the wall works well for the outer region of the flow but not the inner region, making it necessary to express κ_i in terms of κ_o for continuity considerations at the location R_M. Convex curvature effects are known to disrupt the validity of the logarithmic law of the wall, as Kays and Leung [31] and Barrow *et al* [33] remarked. On the other hand, Lee and others [19], [20] and [21] noted that these curvature effects are somewhat eliminated by the presence of roughness elements on the inner surface. These workers have therefore assumed that, in the case of an annulus with a rough core, both κ_i and κ_o are equal.

3.5.5 Core velocity

The relative velocity U* and the dimensionless velocity U' (refer to Appendix A3 for definitions) are related to one another by the relationship:

$$U^* = \frac{2\,(1-\alpha)\,U'\,R_{Ri}'}{\alpha\,Re} \qquad [3.24]$$

Eq [3.24] is derived from the definition of the Re number, discussed in the next section 3.6. Starting with Re = $2u_b(R_{Ro} - R_{Ri})/\nu$, and the definition of U*, R_{Ri}' and U' (refer to Appendix A3), the formula is derived as follows:

$$Re = \frac{2\,u_b\,(R_{Ro} - R_{Ri})}{\nu}$$

$$= \frac{2\,U\,R_{Ri}\left(\frac{1}{\alpha} - 1\right)}{U^*\,\nu} \qquad \textit{by substituting for } u_b,$$

$$= \frac{2\,U'\,U_{\tau_{Ri}}\,R_{Ri}\,(1-\alpha)}{U^*\,\nu\,\alpha} \qquad \textit{by substituting for } U$$

$$= \frac{2\,U'\,R_{Ri}'\,(1-\alpha)}{U^*\,\alpha} \qquad \textit{by substituting } \frac{U_{\tau_{Ri}}\,R_{Ri}}{\nu} = R_{Ri}'$$

Re-arranging the last expression directly yields Eq [3.24].

3.6 Reynolds number, friction factor, z and Nusselt number

3.6.1 Reynolds number

The Reynolds number has already been *defined* as:

$$Re = \frac{2\,u_b\,D_H}{\nu} = \frac{2\,u_b\,(R_{Ro} - R_{Ri})}{\nu}$$

$$Re = \frac{2\,u_b\,R_{Ro}\,(1-\alpha)}{\nu}$$

The bulk velocity u_b is derived in Appendix A6, Eq [A6.1]. Its form is:

$$u_b = \frac{2\ \nu\ \alpha}{R_{Ro}(1 - \alpha^2)}\left[\delta_i^* \int_0^1 u_i^*(1 + \Delta_i\zeta_i)d\zeta_i + \delta_o^* \frac{1}{\alpha}\int_0^1 u_o^*(1 - \delta_o\zeta_o)\ d\zeta_o\right]$$

[3.25]

Inserting this expression into the Reynolds expression above yields the equation:

$$Re = \frac{4\ \alpha}{(\ 1 + \alpha)}\left[\alpha\ \delta_i^* \int_0^1 u_i^*\ (1 + \Delta_i\zeta_i)d\zeta_i\ +\ \delta_o^* \int_0^1 u_o^*\ (1 - \delta_o\zeta_o)d\zeta_o\right]$$

[3.26]

See Appendix A6, Eq [A6.2] for details.

3.6.2 Friction factor

The friction factor is *defined* in the usual way:

$$f = \frac{R_{Ro} - R_{Ri}}{\rho\ u_b^2}\left(-\frac{\partial P}{\partial x}\right)$$

Appendix A6 demonstrates how this equation can be reduced to a non-dimensional form, by expressing the pressure gradient in terms of the surface shear stresses. The result is:

$$f = 8\left(\frac{R_{Ri}}{Re}\right)^2 \frac{(\ 1 - \frac{1}{\alpha})^2}{(\ 1 + \frac{1}{\alpha})}\left(1 + \frac{\tau_{R_{Ro}}}{\tau_{R_{Ri}}}\frac{1}{\alpha}\right) \qquad [3.27]$$

3.6.3 Position of z

Bhuiyan [22] derived a mathematically correct expression for calculating the position z as a function of Re, S/e and P/e. The equation is based on *a priori* knowledge of the position of maximum velocity:

$$\frac{z}{y_{mr}} = \exp\left\{ -\frac{\mu_{\tau_s}}{\mu_{\tau_r}} \left[Ln\left(\frac{\mu_{\tau_s}}{\nu} (S - y_{mr}) \right) + 5.52\ \kappa_o \right] \right\} \qquad [3.28]$$

$$where \quad \frac{y_{mr}}{s} = 0.299\ Re^{0.066} \left(\frac{S}{e}\right)^{0.140} \left(\frac{P}{S}\right)^{0.201} \qquad [3.29]$$

Here, the subscripts s and r stand for smooth and rough surface, respectively. Eq [3.29] for y_{mr} is empirical and predicts the location of maximum velocity, relative to the rough surface. The ratio $\mu_{\tau s}/\ \mu_{\tau r}$ is always calculated from the geometry of a rough core surface and a smooth outer surface.

A better formula for predicting y_{mr} was derived in the course of this study. That formula, shown here, was utilized in lieu of Bhuiyan's formula[15]:

$$\frac{y_{mr}}{S} = \frac{R_M - R_{Ri}}{R_{Ro} - R_{Ri}} = A + B\ Log_{10}\ (Re) \qquad [3.30]$$

$$where \quad A = 0.4715 + 0.01521 \left(\frac{S}{e}\right) - 0.09876 \left(\frac{S}{P}\right)$$

$$and \quad B = 0.016155 - 0.001665 \left(\frac{S}{e}\right) + 0.01337 \left(\frac{S}{P}\right)$$

$$and \quad 2 \leq P/e \leq 16 \quad , \quad 15 \leq S/e \leq 30$$

A new empirical formula was also developed in the course of this study to express z directly from Re, S/e and P/e (refer to Chapter 5). The equation is:

$$\frac{z}{S} = 10^{C_1} + Re^{C_2} \qquad [3.31]$$

$$where \quad C_1 = 0.9534 - 17.68 \left(\frac{e}{S}\right) - 0.3859 \left(\frac{S}{P}\right)$$

$$and \quad C_2 = -\ 0.2789 + 1.847 \left(\frac{e}{S}\right) + 0.03921 \left(\frac{S}{P}\right)$$

15 That formula was utilized ONLY for the purpose of calculating z, using Equ [3.28]. The formula was not used for predicting the location of R_M in the computer simulation. The value of R_M was calculated through an iterative process (see Chapter 4). However, as will be seen in Chapter 5, Eq [3.30] proved highly reliable and could therefore have been used.

3.6.4 Effects of U^* on z

Eq [3.31] was developed from data applicable to an annulus with static core. When applied directly to the case of a moving core, the typical results, shown in Figure 3.1, were erratic and unrealistic. Therefore, a relationship between U^* and z was sought to improve on the predictions of R_M^*. To do so, the data obtained by Bhuiyan [22] was studied in more details.

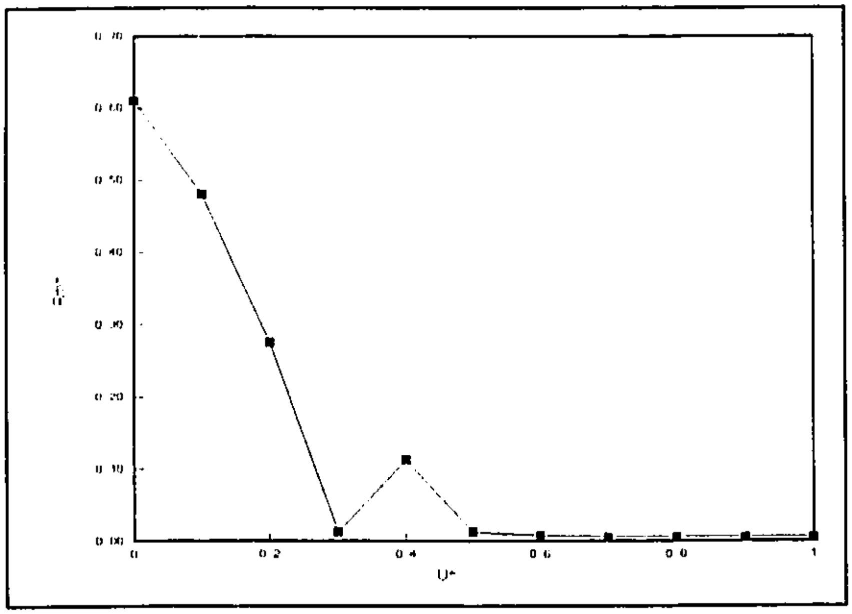

Figure 3.1: Variations of R_M^* with U^* (Re = 50000, α = 0.2, S/c = 15.0, P/c = 2.0)

The experimental evidence from Bhuiyan [22] indicates that z does not seem to follow a predictable pattern, as shown in Figure 3.2 on the next page. In some cases, z will decrease and move towards R_{Ri} as Re increases. In other cases, the opposite occurs. However, z appears to be directly influenced by the momentum carried by the flow. The data from Bhuiyan may be explained in part by the difficulty in measuring z. Dynamically, a higher flow momentum (i.e. Re number) should have the effect of "lifting" z away from the roughness elements. As the fluid passes over the leading edge of a square element, it is accelerated and locally depressurized. Lumps of fluid inside a roughness cavity would then be "sucked" up.

The key element in understanding the mechanisms involved lays in the magnitude of the momentum carried by the flow *relative* to the core surface. One would expect that an increase in U* would have similar effects as a decrease in Re, since both cases lower the fluid momentum as seen relative to the moving core. This relative magnitude can be expressed in mathematical form by relating the *variation* of z with the corresponding *but opposite variation in Re*. An empirical expression was therefore sought to express the *relative* influence of the momentum on z in mathematical terms. The expression found is Eq [3.32]:

$$\frac{Z - Z_{Ref}}{Z_{Ref}} = C_1 + C_2\left(\frac{Re}{Re_{Ref}}\right) \qquad [3.32]$$

$$where\ C_1 = 0.1194 + 1.256\left(\frac{\epsilon}{S}\right) + 0.03933\left(\frac{S}{P}\right)$$

$$and\ C_2 = -0.1782 - 0.002299\left(\frac{S}{\epsilon}\right) - 0.02594\left(\frac{S}{P}\right)$$

The variable Re_{Ref} is the largest value of Re, recorded by Bhuiyan [22], for a given set of S/e and P/e values. This expression predicts the relative decrease in z with the corresponding increase in Re. The limits of the equation are $0.1 < Re/Re_{Ref} < 1.0$.

Eq [3.32] helps to understand how the momentum of the flow, relative to the position z, affects the latter and, by extension, can explain the relationship with U*. A new hypothesis is proposed, whereby the effect of U* can be modelled by subsituting the Re ratio bu U* in Eq [3.32]:

$$\frac{Z - Z_{Ref}}{Z_{Ref}} = C_1 + C_2\,(U^*) \qquad [3.32a]$$

$$where\ C_1 = 0.1194 + 1.256\left(\frac{\epsilon}{S}\right) + 0.03933\left(\frac{S}{P}\right)$$

$$and\ C_2 = -0.1782 - 0.002299\left(\frac{S}{\epsilon}\right) - 0.02594\left(\frac{S}{P}\right)$$

With $(z)_{Ref}$ calculated at $U^* = 0$.

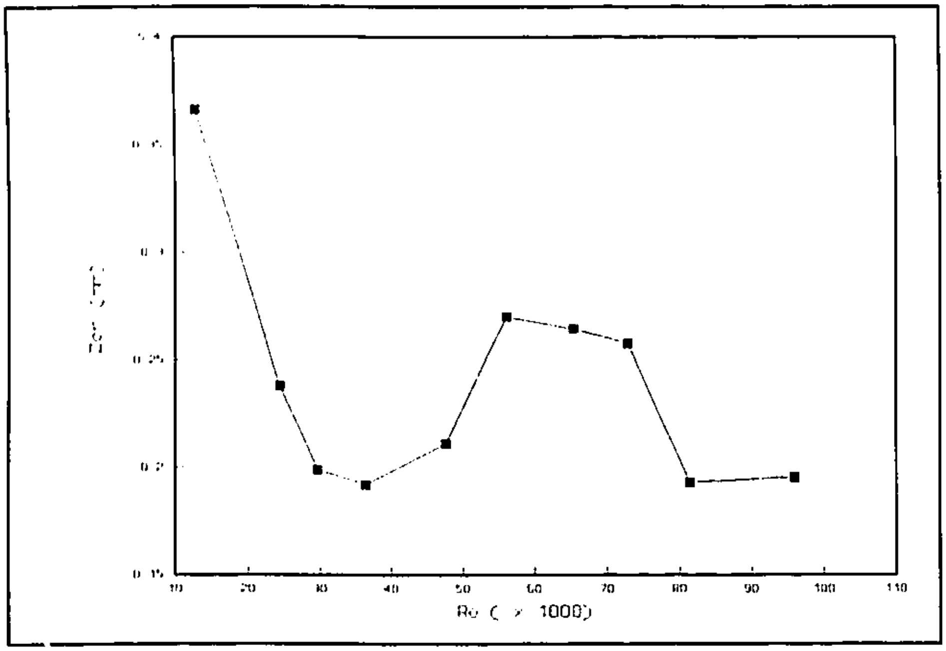

A. S/c = 8.0 P/c = 2.0

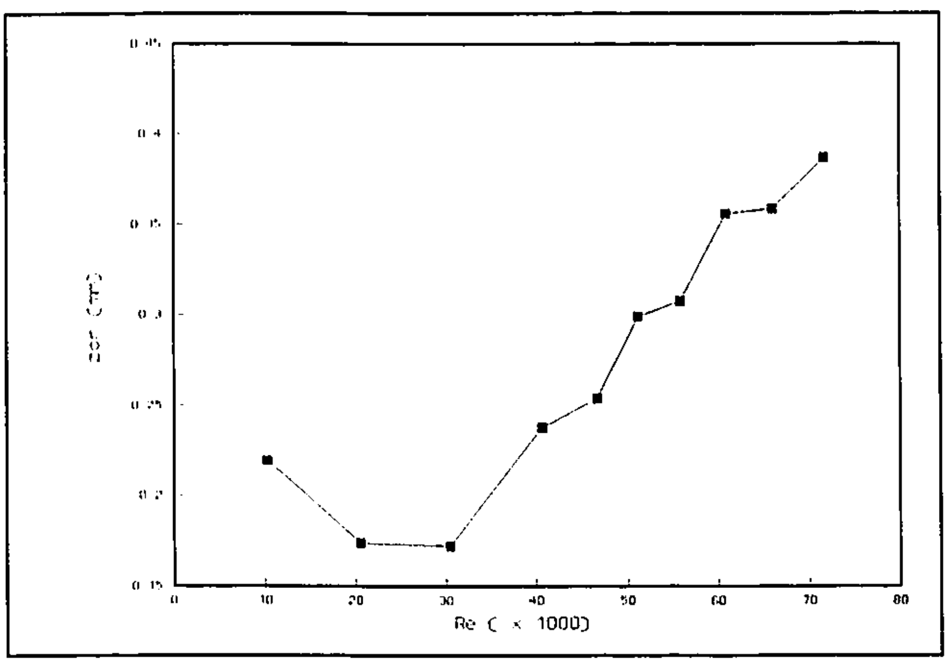

B. S/c = 8.0 P/c = 8.0

Figure 3.2: Experimental measurements of z vs Re (according to Bhuiyan [22])

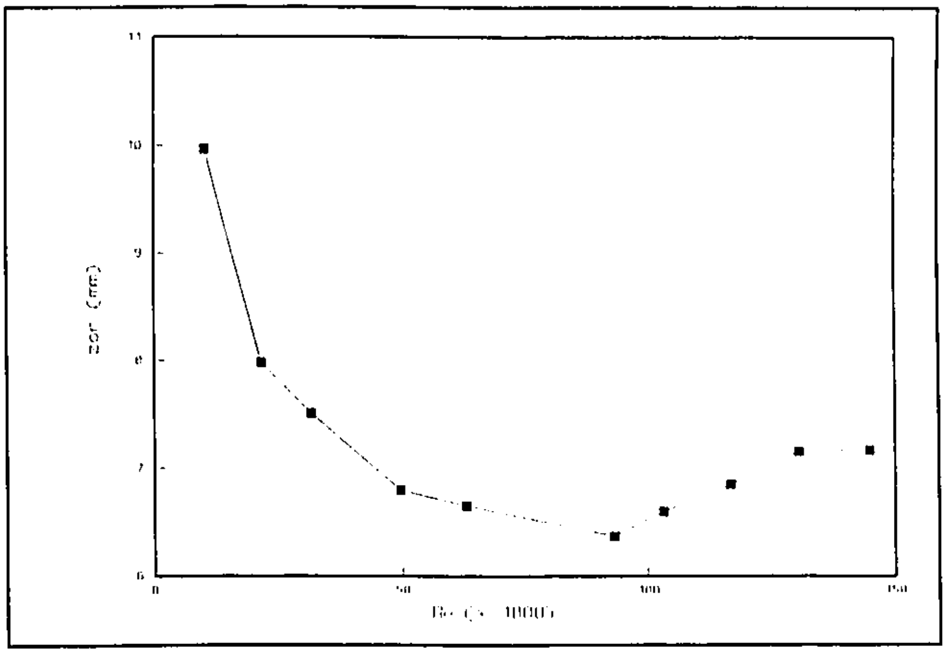

D. S/c = 29.5 P/c = 16.0

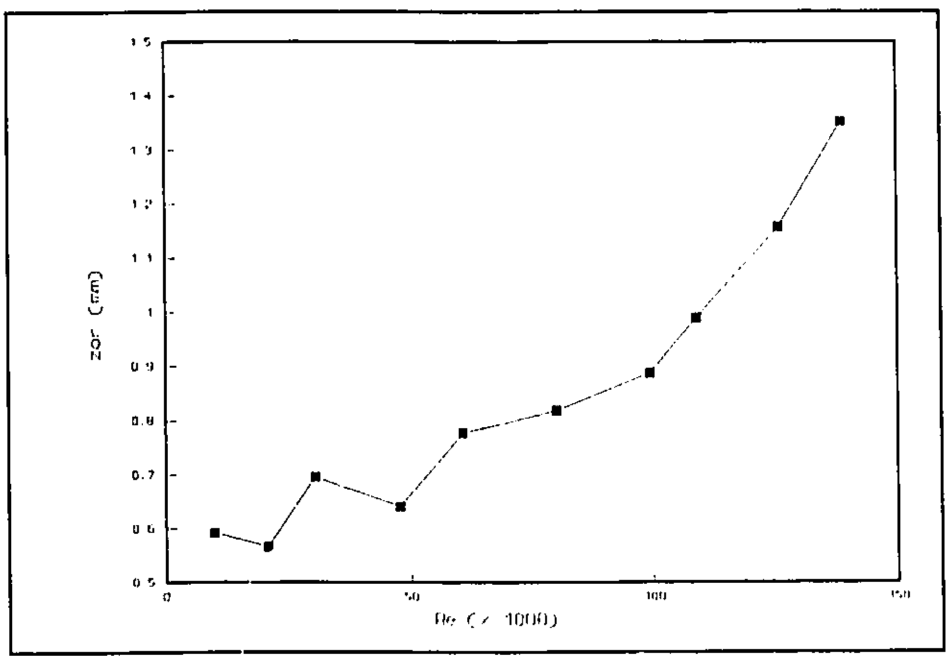

C. S/c = 29.5 P/c = 4.0

3.6.5 Nusselt number

The Nusselt number is given by the basic formulation:

$$N_{jj} = \frac{h_{jj}\, D_H}{k}$$

$$= \frac{2\ \rho\ c_p\ (R_{Ro} - R_{Ri})}{T_b^+\ k}\ \mu_{\tau_j}$$

where the last expression is obtained by substituting the definition of T_b^+ (see Appendix A6). For core heating, the inner Nu number, Nu_{ii} is given by:

$$Nu_{ii} = 2\ Pr\ R_{Ri}^+ \frac{\left(\frac{1 - \alpha}{\alpha}\right)}{T_{b_i}^+} \qquad [3.33]$$

$$where\ \alpha = radius\ ratio\ \frac{R_{Ri}}{R_{Ro}}$$

For outer surface heating, the outer Nu number, Nu_{oo} is given by:

$$Nu_{oo} = 2\ Pr\ R_{Ro}^+ \frac{(1 - \alpha)}{T_{b_o}^+} \qquad [3.34]$$

In both cases, the non-dimensional bulk temperature is given by:

$$T_{b_j} = \Omega \times \left[\alpha\ \delta_i^+ \left(\frac{\mu_{\tau_k}}{\mu_{\tau_i}}\right) \int_0^1 u_i^+\ R_{Ri}\ (1 + \Delta_i \zeta_i)\ T_i^+\ d\zeta_i\right]$$

$$+ \Omega \times \left[\delta_o^+ \left(\frac{\mu_{\tau_k}}{\mu_{\tau_o}}\right) \int_0^1 u_o^+\ R_{Ro}\ (1 - \delta_o \zeta_o)\ T_o^+\ d\zeta_o\right]$$

$$where \quad \Omega = \frac{4}{Re\ (1 + \alpha)}$$

[3.35]

where, for core heating, j = i and k = i, for outer surface heating, j = o and k = o.

Chapter 4
Computer Program

4.1 General approach

The computer program developed for this study was partitioned into three sections:

Section 1: Calculate the position of maximum velocity R_M and the non-dimensional parameter $R_{R_0}{}^+$, for a given set of input parameters (α, U^*, Re, Pr, S/e and P/e). The process utilized an iterative approach for finding both parameters[16] based on an iterative approach for calculating the flow's principal parameters R_M and $R_{R_0}{}^+$.

Section 2: Calculate the velocity and temperature distributions and the bulk parameters .

Section 3: Calculate the friction factor, Nusselt numbers, influence coefficients and output the results.

Section 1 is critical in determining the validity of the results. Indeed, of all parameters involved, $R_M{}^*$ will have the greatest influence (an error of 0.1 in its calculated value was found to produce variations of up to 15-20 % in the expected values of f and Nu).

4.2 Methodology for Section 1

<u>Input parameters</u>

The flow characteristics were calculated for the following conditions:

α = 0.2 through 0.8 in increments of 0.1

U^* = 0.0 to 1.0 in increments of 0.1

[16] Other workers, notably Ahn [26], utilized a more complex process called a *two-dimensional iteration method* coupled with a *Five point Gaussian quadrature integration method*. Although that approach was not utilized for this work, the comparison of the results obtained equally support either method.

Re = 10 000 to 150 000 in increments of 15 000

Pr = 0.01, 0.72, 1.0, 30.0

S/e = 15.0, 30.0

P/e = 2.0, 16.0

Fixed parameters

Pr_t = 1.0

Viscous sublayer thickness y_{js}^+ = 26.0

Van Driest's damping constant A_o^+ = 26.0

Searching for R_M^* and R_{Ro}^+

For a given set of input parameters, the procedure for finding R_M^* is as follows:

- a. Assume an initial value for R_{Ro}^+, equal to $Re/5.0$
- b. Divide flow cross section area into 450 steps
- c. Set initial value of R_M^* at $1/\alpha$ - one step
- d. Calculate the velocity gradient using Eq [3.6] for one flow region
- e. Integrate Eq [3.6] to yield the velocity $u(\zeta_j)$
- f. Repeat steps a) through e) for the other flow region.
- g. Compare u_{om} and u_{im} using Eq [3.20].
- h. Reduce R_M^* by one step and repeat steps a) through g)
- i. R_M^* is found with the value closest to the ratio predicted by Eq [3.20]

Once R_M^* is established, the next step is to find R_{Ro}^+:

- j. Calculate Re (called Re_{12}) using Eq [3.26] and compare with initial Re set
- k. if $Re_{12} > Re$, reduce R_{Ro}^+ and repeat steps a) through j)
- l. R_{Ro}^+ is found when the subsequent trial yields a $Re_{12} < Re$

The correct value of R_{Ro}^+ converged quickly once it is within 100 of the true value. The value of R_M^* converges toward a stable and constant value when R_{Ro}^+ is within 1000 of its true value.

The number of steps for R_M^* was chosen after a series of computer trials were made for the case of a static annulus with smooth surfaces (allowing a comparison with the accepted data of Kays and Leung [24]). The fidelity of the computed values for R_M^* improved as the number of steps was increased from 50 to 400. After 500, the accuracy levelled off to a plateau. The number 450 was therefore chosen at the mid-point between 400 and 500 hundred.

The threshold for R_{Ro}^+ was set at ± 0.5 after another set of computer trials, from a high of ± 5. A threshold of ± 1 was found to produce variations of the order of 5 to 10 in the calculated values of Re_{12}. At ± 0.5, that variation was reduced to a fraction of one.

4.3 Methodology for Sections 2 and 3

The velocity profile

The velocity profile for each region is calculated by performing a numerical integration of the velocity gradient, Eq [3.6], using Simpson's rule. The region of interest (inner or outer) is divided into 6000 steps (for the smooth surface, the viscous sublayer and the fully turbulent layer are each divided into 3000 steps), or 12 000 for the entire cross-section.

The number of steps were varied to investigate the ultimate size of the subdivisions. Again, the fidelity of the results was improved as the number of steps was increased from 600 to 6000, at which point any increase in the number of steps produce insignificant improvements.

The temperature profile

This profile was calculated using Eq [3.13] and by performing a numerical integration using Simpson's rule for each region. Calculations are started for the region adjacent to the heated surface. Calculations for the other region are started from the location of maximum velocity, using Eq [3.21] and [3.22], and carried in reverse order up to the opposing surface. Each region is divided into 6000 steps, the same as the velocity.

For a given set of initial parameters, the program requires approximately 4 minutes to run. The program was written in FORTRAN 77 and was carried out on the Department of

National Defence (DND) navigation simulation computer *Sun SPARCstation 1* (32 bit SPARC CPU, 12.5 MIPS)[17], equipped with SunOS 4.1.2 operating system.

The figures in Appendix D and E, and those found throughout the text, were produced by Lotus 1-2-3, Release 3.1 and edited using Harvard Graphics, Release 3.0.

[17] T.M. of Sun microcomputer systems, CA.

Chapter 5
Results and analysis

5.1 Validation of program algorithms

The computer program described in Chapter 4 was originally tested against experimental data from previous workers Lee *et al* [20], [21], Kays and Leung [31], Shigechi and co-workers [8] [11], and Park [46] in order to establish the validity of the algorithms. Trial runs were first carried out for the case of a static and smooth annulus, with varying values of α, Re and Pr. Graphical results for the smooth annulus and the rough core annulus are found in Annex D. Results for the rough core and outer surface annulus are found in Annex E.

Annex D, Figures 1 and 2 depict the normalized velocity profile for a smooth annulus with moving core. The profiles are virtually identical to those obtained experimentally by Kays and Leung [31] (for static core) and to those predicted by Shigechi *et al* [8] for the moving core case (see Figure 2). Figure 3 illustrates the variation of Nu_{ii} for the same geometry and is seen to be is excellent agreement with the data from Kays and Leung [31] (for zero core velocity) and the predictions of Shigechi *et al* [8] [11]. Table 5.1 also illustrates how the results compare to those of the latter workers. The friction factor f, shown in Figure 4, was found to be in equally good agreement with the smooth case data of Park [46] for static core, and with the predictions of Shigechi *et al* [8] [11] for the moving core case. The location of maximum velocity R_M was found to be independent of Re, as predicted by Kays and Leung [31], Brighton and Jones [32] and Barrow *et al* [33], and can be seen in Figure 5. The influence of U^* on R_M, for the smooth annulus, is presented in Figure 6 and was observed to mirror precisely the predictions of Shigechi *et al* [8].

The addition of surface roughness to the static core annulus was also used to test the algorithms. Figures 7, 8 and 9 compare the computer predictions of the velocity profiles with the experimental data from Ahn [26]. Again, the results are in excellent agreement with the data. Figure 10 shows the results obtained by Ahn [26] for the friction factor f. One can observe that the predictions tend to be less accurate as the roughness factor P/e is increased. This deficiency is attributed to the inability of Eq [3.29] to accurately predict the position of R_M, discussed further in Section 5.2.1. In Figure 11, the friction ratio F predicted by Ahn and by the present algorithm is charted against Re. It can be seen that the predictions based on the new Eq [3.30] are greater than those made with Eq [3.29]. The effect of Eq [3.30] on the heat transfer ratio H is also seen, in Figure 12, to be different than the effect of Eq [3.29]. Figure 13 depicts the effect of Eq [3.30] on the efficiency ratio H/F, compared to those of Eq [3.29]. There are some significant differences in the predictions, which is again attributed to the use of the new equation. These differences will be seen later to permeate the entire set of results.

5.2 New empirical formulations

5.2.1 Location of maximum velocity R_m - Rough surfaces

Eq [3.28] for calculating z was analytically derived by Bhuiyan [22] and required *a priori* knowledge of the position of the maximum velocity in the channel. Bhuiyan solved the quandary by devising an empirical equation for calculating R_M^*. Bhuiyan himself noted that Eq [3.29] was only accurate to within $\pm 15\%$.

A closer look at the experimental data from Bhuiyan [22] revealed further limitations of Eq [3.29]. It will not predict a y_{mr}/S value lower than 0.5, although the experimental data did show this case to happen when $S/e = 24.2$, $P/e = 2.0$, $Re \leq 87\ 000$; or $S/e = 29.5$, $P/e = 2.0$ when $Re \leq 50\ 000$. In fact, Eq [3.29] will only yield good predictions when the true value of y_{mr}/S lies in the range 0.50 - 0.80. In the limiting smooth case for the rectangular channel ($S/e = \infty$ or $P/S = 0.0$), the y_{mr}/S equation does not predict the ratio of ½. Thus, the author undertook to investigate new expressions to better correlate the data by Bhuiyan. By using a modified least square fitting algorithm [see Appendix C], a better expression was found, for $S/e \geq 13.8$ (all P/e except $P/e = 2.0$ when $S/e = 13.8$), with $Re \leq 120\ 000$:

$\alpha = 0.2$, $U^* = 0.0$, $Re = 100\ 000$

Pr	Nu calculated		Nu from [31]		Nu from [11]	
	Nuii	Nuoo	Nuii	Nuoo	Nuii	Nuoo
0.72	224	163	196	165	224	163
1.00	276	200	247	206	Not Available	
30.0	1405	1021	1210	1030		

$\alpha = 0.2$, $U^* = 0.0$, $Re = 100\ 000$

Pr	Nu calculated		Nu from [31]		Nu from [11]	
	Nuii	Nuoo	Nuii	Nuoo	Nuii	Nuoo
0.72	159	154	157	156	159	153
1.00	197	191	202	197	Not Available	
30.0	1075	1032	1050	1040		

$Pr = 0.72$, $U^* = 1.0$, $Re = 100\ 000$

α	Nu calculated		Nu from [11]	
	Nuii	Nuoo	Nuii	Nuoo
0.2	317	170	323	171
0.8	250	161	254	161

Table 5.1: Comparison of Nu predicted with published data

S/e = 24.2 P/e = 2.0			S/e = 29.5 P/e = 2.0	
Re	y_{mr}/S		**Re**	y_{mr}/S
11211	0.294		10493	0.418
21468	0.367		20922	0.428
32148	0.403		31393	0.443
51241	0.457		50003	0.472
64079	0.466			
86843	0.480			

Table 5.2: Low experimental values of y_{mr}/S according to Bhuiyan [22]

$$\frac{y_{mr}}{S} = A + B \times Re \qquad where$$

$$A = 0.7150 + 0.00875\left(\frac{S}{e}\right) - 0.0427\left(\frac{S}{P}\right)$$

$$B = -2.685\times10^{-7} + 8.082\times10^{-6}\left(\frac{e}{S}\right) + 9.904\times10^{-8}\left(\frac{S}{P}\right)$$

The two expressions were compared in term of the standard statistical correlation factor. The higher correlation of Eq [3.30] over [3.29] is obvious:

y_{mr}/S (Eq [3.29]):	0.7640
y_{mr}/S (New Equation):	0.9045

However, neither expression predicted physically meaningful values for y_{mr}/S when Re exceeded 500 000, under certain combinations of S/e and P/e. To address this deficiency, a new expression for y_{mr} was sought, using the data from Bhuiyan, but this time assuming a logarithmic form. The result was Eq [3.30]:

$$\frac{y_{mr}}{S} = A + B \times Log_{10}(Re) \qquad where$$

$$A = 0.4715 + 0.01521\left(\frac{S}{e}\right) - 0.09876\left(\frac{S}{P}\right)$$

$$B = 0.06155 - 0.001665\left(\frac{S}{e}\right) + 0.01337\left(\frac{S}{P}\right)$$

with a correlation factor of 0.9092, applicable to the entire range of Re (up to 10^6). A comparison of the expressions of Bhuiyan and the logarithmic expression, for extreme cases of Re, S/e and P/e is shown in Table 5.3. The highlighted numbers indicate physically meaningless predictions of y_{mr}/S (a ratio of 1.0 being the limiting case).

A comparison of the predictions of Bhuiyan and the two other formulae, based on the experimental data of Bhuiyan, is shown in Table 5.4. The comparison is expressed in terms of the ratio of the predicted value over the experimental data. Table 5.4 clearly shows the better fit obtained by Eq [3.30] vis-a-vis Eq [3.29].

Eq [3.30] proved highly reliable when compared to the calculated values of R_M^* by the computer simulations. In Table 5.5, the effectiveness of Eq [3.30] was measured by a variable *Rmc*. The ratio is very close to unity throughout the range of α, U^* and Re tested, which indicates the validity of Eq [3.30] when the annulus has one surface roughened. The equation is not as reliable when applied to an annulus with both surfaces roughened, as can be seen in Table 5.6. These results also revealed the surprising absence of dependence of R_M on α.

5.2.2 <u>Location of maximum velocity R_m - smooth surfaces</u>

Numerous expressions have been proposed in the literature for determining R_M. Kays and Leung [31] proposed the equation:

$$\frac{R_M - R_{Ri}}{R_{Ro} - R_{Ri}} = \alpha^{0.343}$$

while Barrow, Lee and Roberts [33] proposed the formula:

$$R_M = R_{lam}\left(\frac{1}{\alpha}\right)^{0.027}$$

where R_{lam} is the value of R_M for a laminar flow[18].

Figure 14 gives a overview of the computer predictions for R_M, for various combinations of α and U^* in a smooth annulus. Based on these data, the curve fitting algorithm defined at Annex C was used to derive a better expression for R_M:

---

[18] See Equ [B1.5], Appendix B for the expression for R_{lam}.

Table 5.3: Comparison of y_{mr}/S by Bhuiyan's Equation [3.29] with Eq [3.30]

Roughness condition	Re = 50 000		Re = 100 000		Re = 500 000		Re = 1 000 000	
	Eq [3.29]	Eq [3.30]	Eq [3.29]	Eq [3.30]	Eq [3.29]	Eq [3.30]	Eq [3.29]	Eq [3.30]
A	0.5951	0.6020	0.6229	0.6432	0.6927	0.7388	0.7252	0.7800
B	0.9038	0.8378	0.9461	0.8526	1.0520	0.8869	1.1014	0.9017
C	0.5704	0.4433	0.5971	0.5071	0.6641	0.6554	0.6951	0.7193
D	0.8664	0.9149	0.9070	0.9250	1.0090	0.9516	1.0558	0.9626

A: S/e = 15.0, P/e = 2.0 B: S/e = 15.0, P/e = 16.0

C: S/e = 30.0, P/e = 2.0 D: S/e = 30.0, P/e = 16.0

Table 5.4: Comparison of predictions by Bhuiyan with new equations

(for various values of S/e and P/e)

Legend

(1) = Ratio (y_{mr}/S over *y_{mr}/S predicted by Bhuiyan's Equation [3.29]*)
(2) = Ratio (y_{mr}/S over *y_{mr}/S predicted by Eq [3.30]*)
(3) = Ratio (Yos/S over *Yos/S predicted by Bhuiyan's Equation [5.3]*)
(4) = Ratio (Yos/S over *Yos/S predicted by Eq [5.4]*)
(5) = Ratio (Zor/s over *Zor/S predicted by Eq [3.31]*)

S/e = 8.6 P/e = 2.0

Re	y_{mr}/S	(1)	(2)	Yos/S	(3)	(4)	Zor/S	(5)
12865.	0.6220	1.6265	0.9775	0.6400	0.9937	1.0381	0.0024	0.2613
24410.	0.6280	1.6805	1.0145	0.6470	1.0039	1.0643	0.0019	0.3523
29618.	0.6400	1.6702	1.0092	0.6490	1.0072	1.0723	0.0019	0.3649
36389.	0.6470	1.6747	1.0128	0.6530	1.0079	1.0776	0.0018	0.3963
47620.	0.6530	1.6891	1.0222	0.6590	1.0076	1.0833	0.0016	0.4684
56079.	0.6590	1.6919	1.0242	0.6610	1.0100	1.0893	0.0014	0.5600
65348.	0.6650	1.6936	1.0254	0.6660	1.0075	1.0899	0.0014	0.5730
72778.	0.6710	1.6904	1.0235	0.6750	0.9976	1.0814	0.0015	0.5353
81368.	0.6710	1.7029	1.0311	0.6820	0.9910	1.0765	0.0017	0.4787
95932.	0.6710	1.7215	1.0423	0.6840	0.9935	1.0824	0.0016	0.5363

S/e =13.8 P/e = 2.0

10901.	0.5710	2.0592	0.9250	0.6290	1.0050	1.0544	0.0023	0.2663
22865.	0.5760	2.1436	0.9900	0.6380	1.0154	1.0796	0.0016	0.4205
33891.	0.5800	2.1848	1.0217	0.6470	1.0143	1.0856	0.0014	0.5107
54576.	0.5980	2.1868	1.0362	0.6560	1.0163	1.0958	0.0012	0.6221
67549.	0.6070	2.1849	1.0408	0.6640	1.0111	1.0937	0.0012	0.6543
91114.	0.6110	2.2139	1.0619	0.6730	1.0075	1.0945	0.0012	0.7200
113702.	0.6250	2.1962	1.0582	0.6870	0.9942	1.0833	0.0013	0.6545
125870.	0.6470	2.1358	1.0312	0.6910	0.9918	1.0821	0.0014	0.6150
138799.	0.6600	2.1073	1.0193	0.6990	0.9836	1.0746	0.0015	0.5837
156099.	0.6640	2.1109	1.0232	0.7010	0.9846	1.0773	0.0017	0.5169

Table 5.4: Comparison of predictions by Bhuiyan with new equations
(Continued)

S/e =13.8 P/e =16.0

Re	y_{mr}/S	(1)	(2)	Yos/S	(3)	(4)	Zor/S	(5)
10721.	0.7780	0.9939	1.0259	0.8730	1.0052	0.9862	0.0688	1.1414
22489.	0.7810	1.0397	1.0426	0.8780	1.0243	0.9920	0.0550	1.3490
33904.	0.7820	1.0669	1.0527	0.8800	1.0359	0.9961	0.0499	1.4436
42885.	0.7840	1.0808	1.0565	0.8830	1.0404	0.9964	0.0474	1.4901
52523.	0.7870	1.0912	1.0581	0.8850	1.0450	0.9972	0.0462	1.5074
63125.	0.7910	1.0990	1.0578	0.8870	1.0490	0.9978	0.0453	1.5162
78297.	0.7940	1.1105	1.0597	0.8900	1.0529	0.9977	0.0446	1.5144
92643.	0.7960	1.1201	1.0617	0.8920	1.0564	0.9981	0.0435	1.5333
102087.	0.7980	1.1244	1.0616	0.8940	1.0574	0.9973	0.0437	1.5147
116792.	0.8000	1.1316	1.0626	0.8980	1.0574	0.9949	0.0455	1.4397

S/e =24.2 P/e = 4.0

10194.	0.5520	2.2343	1.1803	0.7000	1.0048	1.0768	0.0041	2.3574
21323.	0.6170	2.0987	1.1090	0.7090	1.0165	1.0869	0.0038	2.5793
31213.	0.6630	2.0029	1.0576	0.7140	1.0222	1.0915	0.0039	2.5597
49022.	0.6950	1.9684	1.0377	0.7190	1.0303	1.0983	0.0036	2.8243
62426.	0.7000	1.9858	1.0456	0.7240	1.0314	1.0984	0.0034	2.9676
82183.	0.7160	1.9770	1.0393	0.7280	1.0351	1.1010	0.0031	3.3247
101941.	0.7200	1.9941	1.0468	0.7330	1.0354	1.1002	0.0031	3.3163
111671.	0.7290	1.9814	1.0394	0.7380	1.0314	1.0956	0.0033	3.0977
128947.	0.7330	1.9894	1.0424	0.7430	1.0294	1.0926	0.0032	3.1731
142353.	0.7410	1.9808	1.0371	0.7470	1.0272	1.0898	0.0033	3.0933

S/e =29.5 P/e =16.0

10311.	0.8770	1.1395	1.0113	0.9000	0.9731	1.0091	0.1384	0.5689
21567.	0.8800	1.1923	1.0214	0.9030	0.9938	1.0108	0.1108	0.6721
31570.	0.8820	1.2199	1.0260	0.9060	1.0030	1.0100	0.1043	0.6939
49583.	0.8850	1.2526	1.0308	0.9080	1.0158	1.0109	0.0944	0.7408
63140.	0.8880	1.2684	1.0317	0.9110	1.0206	1.0092	0.0924	0.7432
93128.	0.8920	1.2955	1.0341	0.9130	1.0315	1.0096	0.0885	0.7536
103108.	0.8940	1.3013	1.0336	0.9180	1.0293	1.0048	0.0916	0.7219
116653.	0.8960	1.3091	1.0335	0.9220	1.0290	1.0013	0.0952	0.6887
130422.	0.9000	1.3129	1.0309	0.9250	1.0295	0.9988	0.0994	0.6538
144902.	0.9030	1.3176	1.0293	0.9260	1.0320	0.9984	0.0995	0.6477

Table 5.5: Comparison of Rmc for annulus with rough core

Re (x 1000)	α = 0.1							
	U* = 0.0				U* = 1.0			
	A	B	C	D	A	B	C	D
50	0.9829	1.0155	0.9432	1.0110	0.9829	1.0155	0.9432	1.0110
100	0.9820	1.0031	0.9524	1.0065	0.9820	1.0031	0.9524	1.0065
150	0.9777	1.0015	0.9553	1.0026	0.9777	1.0015	0.9553	1.0026
200	0.9812	0.9999	0.9597	1.0021	0.9812	0.9999	0.9597	1.0021
250	0.9826	0.9967	0.9619	1.0006	0.9826	0.9967	0.9619	1.0006
300	0.9806	0.9983	0.9657	0.9984	0.9806	0.9983	0.9657	0.9984
350	0.9831	0.9964	0.9690	0.9983	0.9831	0.9964	0.9690	0.9983
400	0.9839	0.9968	0.9693	0.9979	0.9839	0.9968	0.9693	0.9979
450	0.9833	0.9968	0.971	0.9973	0.9833	0.9968	0.971	0.9973
500	0.9851	0.9966	0.9746	0.9964	0.9851	0.9966	0.9746	0.9964

Re (x 1000)	α = 0.8							
	U* = 0.0				U* = 1.0			
	A	B	C	D	A	B	C	D
50	1.0247	1.0249	1.0133	1.0194	1.0247	1.0249	1.0133	1.0194
100	1.0090	1.0090	0.9993	1.0065	1.0090	1.0090	0.9993	1.0065
150	1.0035	1.0044	0.9946	1.0026	1.0035	1.0044	0.9946	1.0026
200	0.9991	0.9941	0.9931	1.0021	0.9991	0.9941	0.9931	1.0021
250	0.9967	0.9996	0.9943	1.0006	0.9967	0.9996	0.9943	1.0006
300	0.9979	0.9983	0.9933	0.9984	0.9979	0.9983	0.9933	0.9984
350	0.9968	0.9992	0.9922	0.9983	0.9968	0.9992	0.9922	0.9983
400	0.9940	0.9968	0.9920	0.9953	0.9940	0.9968	0.9920	0.9953
450	0.9967	0.9968	0.9934	0.9947	0.9967	0.9968	0.9934	0.9947
500	0.9951	0.9966	0.9931	0.9964	0.9951	0.9966	0.9931	0.9964

A: S/e = 15.0 P/e = 2.0
B: S/e = 15.0 P/e = 16.0
C: S/e = 30.0, P/e = 2.0
D: S/e = 30.0 P/e = 15.0

Table 5.6: Comparison of Rmc for annulus with both surfaces rough

Re (x 1000)	α = 0.1, U* = 0.0, A	B	C	D	U* = 1.0, A	B	C	D
50	1.5842	1.7701	1.2546	1.6602	1.5842	1.7701	1.2546	1.6602
100	1.6540	1.7763	1.4001	1.6535	1.6540	1.7763	1.4001	1.6535
150	1.6965	1.7778	1.4850	1.6455	1.6965	1.7778	1.4850	1.6455
200	1.7302	1.7823	1.5387	1.6407	1.7302	1.7823	1.5387	1.6407
250	1.7442	1.7759	1.5846	1.6342	1.7442	1.7759	1.5846	1.6342
300	1.7615	1.7838	1.6199	1.6082	1.7615	1.7838	1.6199	1.6082
350	1.7744	1.7824	1.6480	1.6124	1.7744	1.7824	1.648	1.6124
400	1.7843	1.7802	1.6707	1.6038	1.7843	1.7802	1.6707	1.6038
450	1.7917	1.7853	1.6894	1.6010	1.7917	1.7853	1.6894	1.6010
500	1.8070	1.7818	1.7049	1.5978	1.8070	1.7818	1.7049	1.5978

Re (x 1000)	α = 0.8, U* = 0.0, A	B	C	D	U* = 1.0, A	B	C	D
50000	1.2202	1.5343	0.9150	1.5714	1.2202	1.5643	0.9150	1.5714
100000	1.2920	1.5788	1.0420	1.5664	1.2920	1.5788	1.0420	1.5664
150000	1.3345	1.5883	1.1137	1.5597	1.3345	1.5883	1.1137	1.5597
200000	1.3626	1.5866	1.1626	1.5616	1.3626	1.5866	1.1626	1.5616
250000	1.3890	1.5953	1.1990	1.5560	1.3890	1.5953	1.1990	1.5560
300000	1.4044	1.5959	1.2331	1.5494	1.4044	1.5959	1.2331	1.5494
350000	1.4226	1.6019	1.2562	1.5478	1.4226	1.6019	1.2562	1.5478
400000	1.4320	1.6071	1.2810	1.5401	1.4320	1.6071	1.2810	1.5401
450000	1.4458	1.6052	1.3029	1.5376	1.4458	1.6052	1.3029	1.5376
500000	1.4582	1.6093	1.3166	1.5348	1.4582	1.6093	1.3166	1.5348

A: S/e = 15.0 P/e = 2.0
B: S/e = 15.0 P/e = 16.0
C: S/e = 30.0, P/e = 2.0
D: S/e = 30.0 P/e = 15.0

$$For\ U^* = 0.0\ ,\quad Rm^* = 0.5017 + 0.062\ Ln(\alpha) \qquad [5.1]$$

For $U^* \geq 0.0,$

$$\frac{(Rm^*)_{U^*}}{(Rm^*)_0} = 1.0 + 0.0015\ U^* - 0.5795\ (U^*)^2 \qquad [5.2]$$

Table 5.7 shows how the two expressions from Kays and Leung [31] and Barrow *et al* [33] compare to Eq [5.1] and [5.2],and the computer iterated values of R_M^*:

α	R_M^*			
	From computer iteration	**From Eq [5.1]** (at $U^* = 0.0$)	**From Kays and Leung [31]**	**From Barrow *et al* [33]**
0.2	0.4022	0.4019	0.5758	0.5704
0.8	0.4867	0.4879	0.9263	0.9036

Table 5.7: Comparison of predictions of R_M^*

Table 5.7 demonstrates that neither formula from Kays or Barrow proved reliable when compared to the computer predictions for R_M in the smooth annulus. The computer predictions for R_M^* closely matched the experimental data from Kays and Leung [31].

5.2.3 Position of z

The discussion on the difficulty in applying Eq [3.28] directly has already been established in Chapter 3. In addition to the problems identified, Eq [3.28] was derived by Bhuiyan [22] based on an annulus with only the core surface roughened. Bhuiyan's work, or subsequent studies by Lee and co-workers [19] [20] [21] did not investigate modified forms of Eq [3.28] to account for the case of an outer surface roughened (alone or in pair with a rough core). Based on the data of Bhuiyan [22], the author investigated possible empirical forms of an equation for z, to remove the interdependency with the stress ratio. The equation obtained was Eq [3.31] (refer to Section 3.6.3). However, Bhuiyan's data for z was observed to be non-predictable (see Figure 3.2); for that reason, Eq [3.31] was not deemed reliable (see the predictions of Eq [3.31] with the actual data from Bhuiyan in Table 5.4).

Computer predictions for z showed that z will increase consistently with increasing Re, as Figures 15 and 16 demonstrate. Figure 17 also demonstrates that the effect of U^* is indeed similar and opposite to Re, as predicted by Eq [3.32]. New empirical equations were investigated for expressing z in terms of Re, S/e, P/e, U^* and α but none proved successful. There seems be no other alternative but to rely on the iterative process explained in Chapter 4 to determine z, using Eq [3.28] and Eq. [3.30]. This gave rise to the question: are the computed values of z physically representative? The excellent correlation between the velocity profiles obtained from experiment and from theory, shown in Figures 7, 8 and 9, indicates that the values of z found by computer iterations must be close to their "true" values, otherwise the predicted profiles would have been incorrect. Therefore, it is safe to consider the iterative process reliable when calculating z. Given that a small variation in z will cause a noticeable change in the velocity profiles, the use of an empirical equation to predict z is not recommended.

5.2.4 Location of zero shear stress y_{os}

Bhuiyan's data [22] and Ahn's data [26] indicated that the location of zero shear stress, y_{os}, was in fact not coincident with y_{mr}, although the differences were relatively small. Bhuiyan derived an empirical expression for the ratio y_{os}/S, based on his experimental data:

$$\frac{y_{os}}{S} = 0.418 \times Re^{0.033} \times \left(\frac{S}{e}\right)^{0.157} \times \left(\frac{P}{S}\right)^{0.158} \qquad [5.3]$$

Eq [5.3] closely matched another empirical formula proposed by Hanjalic [44]. As part of the present study, a better formula was derived using the same technique behind Eq [3.30] and data from Bhuiyan [22]. The equation, applicable to a range of Re number up to 10^6 is:

$$\frac{y_{os}}{S} = A + B \times Log_{10}\,(Re) \qquad [5.4]$$

$$where\ A = 1.129 - 4.669\left(\frac{e}{S}\right) - 0.06505\left(\frac{S}{P}\right)$$

$$and\ B = -0.02233 + 0.6457\left(\frac{e}{S}\right) + 0.007991\left(\frac{S}{P}\right)$$

Eq [5.4] performs slightly better than Eq [5.3], with their respective correlation factors at 0.8993 and 0.8566. Refer to Table 5.4 for a comparison of the data from Bhuiyan [22].

5.3 Analytical results for the rough core annulus

Tables 5.1 through 5.7 present only a fraction of the results obtained by computer simulations. The bulk of the results are presented in graphical form in Appendices D and E. A discussion of the data obtained will now be presented.

The introduction of roughness elements on the core surface disturbs the symmetrical characteristics of the flow and render the latter essentially asymmetrical. The asymmetry effect will be reflected in a shift in R_M and a change in the surface shear stress ratio, T_{Ri}/T_{Ro}, which will inevitably be reflected in the momentum and heat transfer behaviour of the fluid. These changes were noted in the results obtained during this study.

5.3.1 Velocity profiles

The velocity profiles obtained for the rough core annulus are shown in Figures 18 through 23. All profiles exhibit notable differences with the smooth case (Figures 1 and 2). The rough profiles are indeed asymmetrical and demonstrate the shift in the position of the maximum velocity. Whereas in the smooth annulus, α had little effect on the velocity profile, it has a significant impact for the rough annulus. Figures 18 through 23 show the approximate position of the shift in the location of zero velocity z, observed from the origins of the profiles. The shift increases as the roughness condition increases (S/e and P/e grow), as Figure 18 shows.

5.3.1.1 Effects of U^*

The effects of U^*, seen in Figures 19, 20, 21 and 23, are similar to those observed for the smooth annulus. The difference lies in the velocity gradients near the rough surface. The gradients are less pronounced in the rough annulus than the smooth annulus. Also, the location of R_M will be affected more for the rough annulus. In the outer region, the velocity gradients mirror the smooth annulus, as Figure 2 indicates. Finally, the effect of U^* on the rough annulus flow will diminish as α grows toward unity. This is observed by comparing the profiles of Figures 19, 20 and 21 with Figure 23. In Figure 23, z is smaller and the shift in R_M reduced.

5.3.1.2 Effects of Roughness

The geometry of the roughness elements is determinant of the shape of the velocity profiles. Figures 18 and 22 illustrate this observation. The *magnitude* of the effect, to speak figuratively, can be qualitatively measured by assessing how much departure from the smooth annulus profile is undergone. In both figures, a small P/e ratio gives rise to a profile akin to the smooth annulus case, a similarity that is accentuated as S/e grows. This would be an expected result since the smooth annulus can be viewed as the limiting condition of a rough surface: $S/e \rightarrow \infty$ as $P/e \rightarrow 0$. At the opposite end of the spectrum, a decrease in S/e combined with an increase in P/e ($S/e \rightarrow 1.0 \quad P/e >> 0$) will increase the magnitude of the roughness effect, thereby producing a strong departure in the velocity profiles, from the smooth annulus profiles. Figures 18 and 22 illustrate this condition clearly. It is interesting to note that as the roughness geometry increases (henceforth referred to as *roughness geometry*), the velocity gradient near the rough surface decreases, while R_M is pushed radially outward from the core surface[19]. The influence of the roughness geometry on the velocity gradient near the rough surface is lessened as U^* increase towards unity, as seen in Figure 23. The reduction would be anticipated, given the discussion presented in Section 3.6.4.

---

[19] The motion of R_M away from the rough surface had already been observed by Bhuiyan [22] and Lee & co-workers [19], [20], [21].

5.3.2 Location of maximum velocity R_M^*

The motion of R_M^* away from the rough surface has already been observed in Figures 18 and 22. That motion is the resulting effect of adding roughness to the core surface. How α, U^* and roughness geometry influence the motion is illustrated in Fig 5, 6 and 24 through 30.

5.3.2.1 Effects of U^*

In the smooth annulus, U^* causes R_M^* to decrease towards a convergent, limiting value (see Figures 6 and 24). Figure 25 and 26 indicate a similar trend but not towards a single value of R_M^*. The elimination of the convergence observed for the smooth annulus case is caused by the presence of roughness. α also has an effect on the influence of U^*, as Figures 27 & 28 and 29 & 30 demonstrate. Hence, U^* is working opposite the surface roughness, in that it tends to pull R_M nearer the rough surface. The discussion in Section 3.6.4 finds more support in that observation. Indeed, for the case of static core, Figures 27 and 29, a reduction in the fluid's momentum, indicated by lower Re numbers, also pulls R_M nearer the rough surface.

5.3.2.2 Effects of Re

In the smooth annulus, R_M^* has been known to be independent of Re (see Kays and Leung [31]). In a rough annulus, R_M^* becomes dependent on Re. At low U^*, Re will push R_M^* away from the rough surface (see Figures 27 and 29). At high U^*, the opposite effect will be felt, i.e., R_M^* will move towards the rough core (see Figures 28 and 30). One can infer from these observations that the influence of U^* is more severe than Re, for a given roughness condition.

5.3.2.3 Effects of Roughness

The roughness geometry is the predominant factor among U^*, α and Re. Low roughness geometry[20] will produce the least motion of R_M^* from its smooth annulus position, while the most severe roughness geometry[21] will generate the largest motion in R_M^*. At low α, the motion of R_M^* is always radially outward from its smooth annulus location, regardless of U^* (see

---

[20] Previously defined by $S/e \rightarrow \infty$ and $P/e \rightarrow 0$.

[21] Previously defined as $S/e \rightarrow 1$ as $P/e >> 0$.

Figures 27 and 28). As α and U^* increase towards unity, the motion is maintained for high roughness geometry but is reversed for low roughness geometry (see Figure 29 and 30). The combination of high α and U^* , for low roughness geometry conditions, results in a flow that is dominated by dynamic pressures which squash the fluid layer immediately adjacent to the rough surface. The flow is thus forced to grow from zero to large velocity in a radially short distance, thereby reaching its maximum velocity very rapidly. As roughness geometry increases, the turbulent exchange of momentum near the rough surface also increases and counteracts the dynamic pressures of the flow. This results in a fluid that is allowed more "space" to grow to full velocity, hence the larger R_M^*.

Bhuiyan [22] and Lee [19] hypothesized that the effects of roughness were felt only locally on the fluid; that is, away from the rough surface the fluid would not have "knowledge', so to speak, of the presence of roughness elements. Such an effect could be observed by comparing the velocity profiles in the outer region of the flow and the effects of S/e and P/e on R_M^*. The velocity profiles for the rough core have already been seen to reflect a smooth annulus in the outer region (see section 5.3.1.1). The influence of S/e and P/e is separately identified in Figures 25 through 30. The changes caused by a variation in P/e, for a given S/e, are always larger than a variation in S/e for a given P/e. That observation had already been made by Lee *et al* [20], [21]. P/e is a local parameter while S/e is a global parameter[22]. Because P/e has by far the largest impact, and because it is a local parameter, it lends credence to the hypothesis submitted by Bhuiyan and Lee.

5.3.3 Friction factor

The effects of Re, α and U^* on the smooth annulus flow are shown in Figures 4 and 31. While the effects of α are generally the same for the rough core annulus, Re and U^* have opposite effects. In the smooth annulus, f will decrease with increasing U^* and Re. Roughness geometry also plays a significant role by increasing the friction factor, sometimes by one order

---

[22] A local parameter contains variables related to a local spatial region. A global parameter contains variables that encompass the entire spatial region under consideration. S/e, S, Re are all global parameters for that reason. P/e, ν, y, Δ_i are local parameters.

of magnitude. Furthermore, the predictions of the present study, for the rough static core annulus, have already been seen to be higher than previous workers, as Figure 11 will show.

5.3.3.1 Effects of U^*

The effects of U^* can be observed clearly in Figures 32 and 33. There is a universal tendency for the friction ratio F to diminish with increasing U^*, no matter what α, S/e or P/e are set at. The strength of the influence of U^* is however a function of the roughness geometry and will decrease as the roughness geometry increases. That F should diminish as U^* increases is expected, since greater U^* values translate into lower relative momentum as seen by the rough surface and consequently less severe fluid mixing.

5.3.3.2 Effects of Re

Although F can be seen in Figures 32 and 33 to be constantly greater than unity, the influence of Re will work against the influence of U^*. Figures 34 through 37 show how F increases with Re. However, when U^* is increased, the result is a reduction in the magnitude of F (as a comparison of Figure 34 with 35, and 36 with 37, will show). Again, the concept of relative fluid momentum comes to play, the determining element being how turbulent (i.e. the Re number) is the flow *relative* to the rough core.

5.3.3.3 Effects of Roughness

Roughness geometry is the predominant element on the friction factor. Figures 32 and 33 indicate how a severe roughness condition (large values of S/e and P/e) will increase the friction factor beyond unity. As the roughness geometry approaches a pseudo-smooth condition, the ratio F for a static core annulus will move closer to unity, as Figure 34 and 36 show. The axial motion of the core creates a somewhat surprising result: the friction ratio F decreases 5 to 6 times from its static core value, *even below* unity (see Figures 35 and 37). The drop below the unity line is accentuated when α increases toward 1.0, as figure 37 shows.

A possible explanation for that result can be found in Figure 16, where it is seen that the shift in the zero velocity position near a rough surface is virtually null. When U^* equals unity, the momentum flow relative to the rough surface is very small. The intensity of the eddies at the leading edge of a roughness element is therefore relatively small. Thus, the dynamic pressures produced by the fluid immediately adjacent to the roughness elements are small and allow more lumps of fluid to reach the root of the roughness cavity. Because the roughness elements are small in low roughness geometry, the velocity profile starts to grow almost immediately at the root of the roughness cavity , which in turn reduces the pressure losses due to friction. Although the process is more complicated than in the smooth case, the end result is very similar to the effects of Re on the friction factor in a smooth annulus, seen in Figures 4 and 10.

5.3.4 Nusselt number Nu and Heat transfer ratio H

In the smooth annulus geometry, the behaviour of Nu shown in Figures 38, 39 and 40 is opposite that of the friction factor f. U^* and Re will increase the heat transfer at the heated surface as they increase individually. A decrease in α will also generate an increase in Nu. Perhaps most significant is the effect of the Prandtl number Pr on Nu. Figure 39 indicates how increasing Pr will dramatically increase Nu. When surface roughness is added to the geometry, there is also a general gain in heat transfer (expressed by the ratio Hii).

The effects of U^*, Re, α and roughness geometry, as well as the new variable Pr, are shown in Figures 41 through 48. The figures reveal that these independent parameters have the same effects on Hii as they have on F (see Section 5.3.3 above) except for α. In the case of Hii, increasing α will reduce Hii, as demonstrated by Figures 41 and 42. For any roughness condition, higher values of Pr will lead to higher heat transfer ratios (see Figure 43). The impact of the roughness geometry on Hii also follows the pattern observed for the friction ratio F (see Figures 44 through 48).

The thermal advantage of rough surfaces is revealed in Figures 44 through 48. As was the case for F, low roughness geometry geometries are actually detrimental to the heat exchange process. High roughness geometries, on the other hand, enhance the heat transfer process. In

Figure 45 for example, Hii for P/e values of 2 is consistently inferior to unity. High values of P/e push Hii beyond unity, reflecting a higher heat transfer ratio. The explanation for this observation borrows from the explanation given for a similar observation on F, at paragraph 5.3.3.3. In cases of low roughness geometry, more lumps of fluid are allowed to sink in the cavities of the roughness geometry. This confinement restricts the turbulent motion of the fluid lumps, which in turn reduces significantly the transport of heat energy by fluid motion. Slower rates of heat energy transport by convection necessarily produce lower heat transfer rates at the rough surface.

5.3.5 Efficiency factor H/F

The combination of the previous results for F and Hii is presented in Figures 49 through 56. Whereas both F and Hii are influenced in the same fashion by U^* , Re, S/e and P/e, the opposite effect of α does not allow one to extend the preceding observations to the efficiency ratio H/F.

5.3.5.1 Effects of U^*

Figures 49, 50 and 51 illustrate how U^* and α influence the efficiency ratio H/F. It is apparent that U^* cannot be dissociated from the effects of roughness geometry. For example, in Figure 49, high roughness geometry combined with high U^* values produce a net gain in overall efficiency of the process. Lower roughness geometry geometries result in a loss in efficiency, with the loss actually *increasing* with increasing values of U^*.

The radius ratio α also plays an important role. Comparison of Figures 49 and 50 shows that high α values will always produce a loss in efficiency in the energy transfer process. Low α values have the opposite effect.

The impact of Pr is seen in Figure 51. High Pr values ($Pr >> 1$) will always produce net gains in efficiency. This observation was found to apply across the spectrum of S/e and P/e values investigated.

5.3.5.2 Effects of Re

The momentum of the flow has a strong influence on Hii/F and is shown in Figures 52 to 56. In general, increasing Re will lead to an increase in Hii/F. There is one notable exception, in the case of very low roughness geometry (S/e = 30 and P/e = 2). In that case, increasing Re will have the opposite effect and reduce the magnitude of Hii/F (see Figures 52 and 54). Increasing U^*, for any roughness geometry, will reduce Hii/F.

5.3.5.3 Effects of roughness geometry

The influence of the roughness geometry is coupled with α. Figures 52 and 53 show how high roughness geometry will generate higher Hii/F values. Figure 55 and 56 indicate the same behaviour. However, when α is changed from a low value to a high value, the effects of low roughness geometry are greatly enhanced, as seen in Figures 55 & 56. When U^* is zero, having low roughness geometry is even beneficial to the overall efficiency of the process (see Figure 54). However, the best values of Hii/F are obtained at low α.

5.3.6 Comparison with other workers

The most recent results on hand are those of Ahn [26], for the case of a static core annulus. For that case only, the preceding observations are in line with the findings of Ahn, and other workers such as Lee *et al* [19], [20], [21]. Ahn recommended that, in order to achieve the most efficient system design for heat transfer, one should

a) decrease S/e

b) decrease α

c) increase P/e, Re and Pr

These recommendations are all verified by this study, except the first one. The results indicate that increasing S/e would produce better efficiency figures, with or without the added axial motion of the core.

5.4 Analytical results for the rough annulus

The presence of roughness elements on both surfaces of the annulus, core and casing, re-establishes some symmetry in the flow (provided that the roughness elements are of the same S/e and P/e). Therefore, one would expect that the location of R_M and the velocity profiles would approach those found for the smooth annulus. All results for the rough annulus are found in Annex E.

5.4.1 Velocity profiles

Figures 1 through 8 depict how the velocity profiles appear in a rough annulus. For a static core, the profiles exhibit a location of maximum velocity that is in line with the location found for the smooth annulus case (see Annex D, Figure 1). There is also good agreement with the predictions of Lee *et al* [21]. Again, the influence of z on the starting point of the profiles can be appreciated in all Figures, and especially Figures 1 and 5.

5.4.1.1 Effects of U^*

Figures 2, 3, 4, 6, and 8 illustrate how U^* shapes the profiles. The location of maximum velocity is shifted towards the core, as was the case for the rough core annulus. High values of α accelerate the growth of the profiles, making them flatter than at low α, seen here in comparing Figures 2 with 6.

5.4.1.2 Effects of roughness geometry

The effects identified for the rough core annulus appear once again in the rough annulus. Figure 1 demonstrates how low roughness geometry confers upon the velocity profiles characteristics associated with smooth annulus (compare the S/e = 30, P/e = 2 curve of Figure 1 with Figure 1 of Annex D). At high roughness geometry, the profile is completely different form a smooth flow, with lower velocity gradients near the surfaces and a motion by R_M away from the smooth flow position. High α values tend to slow down that outward motion but not the velocity's radial development.

5.4.2 Location of maximum velocity R_M^*

The similarity of the smooth annulus flow with the rough annulus flow is best revealed in Figures 9 through 14, which show how R_M^* is influenced by α, U^*, Re and roughness geometry. In practically all combinations of these parameters, R_M^* is almost invariant, even when the core is moving.

5.4.2.1 Effects of U^*

For the static core annulus, the behaviour of R_M^* is almost identical to that for the smooth annulus (refer to Figures 11 and 13), with the exception that a rough annulus will have an R_M^* value larger than the smooth annulus. The addition of core velocity hardly affects R_M^*, which is a rather surprising result. That constitutes a strong departure form the smooth annulus (Annex D, Figure 14). The location of R_M^* seems to hover around the annulus' geometric centre (R_M^* = 0.5), which is indicative of equal surface shear stresses and symmetry in the flow. High α values tend to push R_M^* radially outward, when compared to low α values, which is explained by relatively stronger curvature effects at low α[23].

5.4.2.2 Effects of Re

The pseudo-symmetry of the flow, established by the presence of roughness on both inside surfaces, is also found in the relative absence of effects by Re (Figure 11 through 14). R_M^* is almost invariant with Re, as was the case for the smooth annulus. Variations in R_M^* appear to be caused mainly by roughness geometry and U^*.

5.4.2.3 Effects of roughness geometry

For the static core annulus, the presence of roughness translates into a motion of R_M^*

---

[23] Bhuiyan's work [22] and Lee's predictions [19] had shown that, for the rectangular channel (limiting case of an annulus where α = 1.0), R_M^* always tends to move away from the rough surface of an asymmetric channel. By extension, when the two inside surfaces of an annulus are roughened, the strength of the turbulence, induced locally on the flow by the roughness elements, is enhanced by the effects of the convex curvature of the core. Small α, an therefore small core radii, will have stronger curvature effects, which will force the flow to accelerate faster than in the outer region, attracting R_M^* closer to the core surface. At high α, the curvature effects diminish and consequently, the tendency of R_M^* to move towards the core also diminishes.

away from the core, as the roughness geometry increases (Figures 11 and 13). High roughness geometry will always push R_M^* above the passage's centreline, while low intensity roughness causes the opposite effect. When the core is moving, Figures 12 and 14 indicate that there is a reversal in the effects of low roughness geometry. Whereas in the static core, any roughness geometry combined with increasing Re to yield increasing R_M^* values, a moving core will see the combined effect of low roughness geometry and increasing Re as lowering R_M^*. High roughness geometry will not be affected by the presence of a moving core. The explanation for that observation was already discussed in Section 5.3.3. Low roughness geometry tends to accentuate the smooth flow characteristics of the flow at hand, which implies that R_M^* will lower as U^* increase (Annex D, Figure 14).

5.4.3 Friction Factor F

Intuitively, one would expect that the friction factor for a fully rough annulus be greater than the smooth case or the rough core case. A comparison of Figure 15 through 20 with the results of Annex D (Figures 32 to 37) supports this intuitive result.

5.4.3.1 Effects of U^*

Figures 15 and 16 reveal a new effect that is opposite the one observed for the rough core annulus (Annex D, Figures 32 and 33). In the rough annulus, an increase in U^* actually increases the friction factor F, whereas in the rough core annulus, it had the effect of reducing it. The increase is more pronounced as the roughness geometry increases. How to account for this result? Prior discussions indicated that increasing U^* could be seen as a reduction in the momentum carried by the flow *relative* to the core surface. Thus, the friction losses at the core surface are reduced with increasing U^*. At the outer surface however, there is no such relative reduction in the flow's relative momentum. The results obtained during the study indicated that the surface shear stress ratio τ_{Ri}/τ_{Ro} decreased as U^* increased. Such a reduction indicated that the friction losses at the outer surface increased with increasing U^*. The magnitude of the increase for the outer surface exceeded the magnitude of the decrease of f at the core surface. The net result is a gain in the total friction factor F.

5.4.3.2 Effects of Re and roughness geometry

The effects of Re and roughness geometry on F are seen in Figures 17 to 20. They are similar to those observed for the rough core annulus (Annex D, Figures 34 through 37) but of greater magnitude. The pressure losses are as expected greater than in the rough core annulus, by a factor of almost two. The only difference is the effect of U^*, which is seen to be minimal (for reasons explained in the above section 5.4.3.1), while its effects on the rough core annulus were found to be significant, as Section 5.3.3.2 and 5.3.3.3 explained.

5.4.4 Nusselt number Nu and Heat transfer ratio H

The annulus can be heated either from the core or the outer surface, or from both. In this study, both cases were investigated (i.e. Nuii, Nuoo, Hii and Hoo). The smooth annulus results for Nuii have already been presented in Annex D, Figures 38, 39 and 40. Nuoo results are found in Annex E, Figures 21 through 24. They are well within the published data of previous workers such as Kays and Leung [31] and Shigechi and Lee [11]. For the rough annulus, the results indicate higher values of Hii/F, compared with Hoo/F.

5.4.4.1 Effects of U^*

U^* is investigated in Figures 25 through 30. The effects are similar to those observed for the rough core annulus (Annex D, Figures 41, 42 and 43), except that their magnitude is less pronounced than for the rough core case. The new data for Hoo (Figures 26, 28 and 30) also indicate a similar response of Hoo to increasing U^*. The values of Hii are consistently larger than for the rough core case, an expected result since the entire flow is turbulent and more conducing to greater momentum and heat exchanges. That fact also explains why the reduction in Hii and Hoo, with increased U^*, is less severe than in the rough core annulus: the outer surface maintains a higher rate of mixing within the flow than in the smooth outer surface annulus. All other observations made at Section 5.3.4.1 are applicable to this Section.

5.4.4.2 Effects of Re and roughness geometry

Figures 31 through 40 illustrate that Hii and Hoo in the rough annulus respond to Re, roughness geometry and Pr in a fashion similar to that explained for the rough core annulus, at

Section 5.3.4.2 and 5.3.4.3. The only difference is in the magnitude of the effects: the rough annulus produces greater heat transfer gains than the rough core annulus.

5.4.5 Efficiency ratio H/F

The dramatic increase in F, discussed in Section 5.4.3, conveys with it some unexpected results in the overall efficiency ratios Hii/F and Hoo/F. An outcome of the rough core analysis was a recommendation to utilize the most severe roughness geometry to achieve the best H/F ratio (S/e = 30, P/e = 16). In Figures 41 through 56, that recommendation no longer holds; least severe roughness geometry produces the best H/F ratios, both for Hii and Hoo, which is in agreement with the predictions of Lee *et al* [21]. However, the rates of change in Hii/F and Hoo/F are seen to be dramatically different for those of Lee [21], owing principally to the new method of modelling z with Eq [3.30].

5.4.5.1 Effects of U^*

U^* imparts on the energy transfer process changes that are different from the rough core annulus flow. Figures 41 through 46 illustrate how. Both Hii/F and Hoo/F tend to decrease with increasing U^*, which is indicative of the effects of increasing F with U^* while Hii and Hoo decrease with U^*. Values of Hii/F or Hoo/F superior to unity can only be achieved by a combination of low roughness geometry and low U^*. Figures 43 and 44 reveal that high values of α will enhance the efficiency of the process. Finally, the impact of Pr on Hii/F and Hoo/F is significant and positive with large Pr (illustrated in Figures 45 and 46).

5.4.5.2. Effects of Re

Figures 47 through 56 demonstrate how Re impacts on Hii/F and Hoo/F. At low Re numbers (Re < 50 000), the ratio Hii/F is greatly influenced by Re, dropping rapidly to a stable plateau. Hoo/F is also subjected to the same drop, but in a smoother transition. Beyond Re > 60 000, the effects of Re vanish, as was the case for the rough core annulus.

5.4.5.3 Effects of roughness geometry

The benefits of using low roughness geometry geometry ($S/e >> 1$, $P/e < 2$) is seen to apply to the entire spectrum of combinations of α, U^*, Re and Pr. As the roughness geometry increases, the friction loss component, F, increases faster than the heat transfer components, Hii or Hoo, such that there is a loss of efficiency in the energy transfer process. Higher values of α will improve the efficiency ratio. In fact, at high α, the ratio Hii/F will always be superior to unity for any given combination of S/e, P/e, Re and U^* (for $Pr > 0.72$). The ratio Hoo/F is consistently lower than Hii/F, and remains superior to unity for U^* values nearing zero. Finally, Figures 55 and 56 show how the combined effects of Pr and U^* work as antagonists in the outcome of the Hii/F and Hoo/F ratios.

5.4.6 Comparison with other workers

The only data published in the literature for the case of a fully rough annulus with static core were published by Lee *et al* [21]. The results obtained during this study compared favourably for the velocity profiles and R_M^*. Different results were obtained however for F and H/F. For F, the differences lay in the magnitude of the ratio, whereas H/F saw differences both in the magnitude and the trends of the results. These differences are explained in part by the use of the new Eq [3.30], for calculating R_M and z, and by the possible variations in the predictions caused by the use of different computer algorithms. These variations can amount to major differences. Unfortunately, the results of Lee and co-workers [19], [20], [21], Bhuiyan [22] and Ahn [26] did not present actual values of z predicted, such that a comparison of the results of this study for z could not be performed.

From the foregoing discussion are drawn these recommendations, for achieving the best H/F results as design constraints of a heat exchanger systems, for any value of U^*:

a) increase S/e and decrease P/e
b) increase α and Pr
c) decrease Re

Chapter 6
Conclusion

The preceding discussion, on the effects of α, U^*, Re, Pr, S/e and P/e on the momentum and heat transfer mechanisms involved in the flow of a fluid inside an annulus, leads to the following conclusions:

1. The computer model produced very good predictions of velocity profiles, f, F, Nu, H and H/F for the variety of geometric, dynamic and thermal conditions given. The predictions were particularly accurate for the known case of a smooth annulus with a static core.

2. The effects of U^*, α, Re, S/e and P/e have been identified with reasonable accuracy.

3. New empirical formulations were found in excellent agreement with published data, for predicting R_M^* for the smooth annulus with moving core, Eq [5.1] and [5.2]), R_M^* for the rough core annulus with static core, Eq [3.30], the location of zero shear stress, Eq [5.4], and the effect of U^* on z , Eq [3.32].

For the rough core annulus

4. The friction ratio F decreases with increasing U^*, α and Re. High roughness geometry (S/e > 1, P/e > 1) produce the largest F values. Low roughness geometry (S/e > 1, P/e < 2) produce the lowest F. F can be inferior to unity for high U^*, low Re and low roughness geometry.

5. The heat transfer ratio Hii is generally superior to unity and increases with high roughness geometry, low U^* and high Re and Pr. Hii will decrease to near unity

as U^* increases toward 1.0, and will be lower than unity for low roughness geometry geometries.

6. The efficiency ratio Hii/F will react to U^*, Re, α, Pr, S/e and P/e in similar fashion to Hii. High α and U^*, in combination with low S/e and P/e will produce Hii/F values below unity. Increasing Re and Pr will increase Hii/F, with enhanced results with high roughness geometry.

<u>For the rough annulus</u>

7. The new empirical equations for R_M^*, Eq [3.30] and y_{os}, Eq [5.4] do not give good predictions. Eq [3.32] remains applicable with believed high accuracy.

8. The friction factor F will increase with U^* and Re, and decreasing α. High roughness geometry geometries produce the highest values of F. In most combinations of α, U^*, Re, S/e and P/e, F will be superior to unity.

9. The heat transfer ratios Hii and Hoo are influenced in the same manner by α, U^*, Re S/e and P/e, with Hii experiencing the largest influence. Hii is always superior to Hoo. Increasing α will reduce Hii and Hoo. Increasing Pr or Re will enhance Hii and Hoo.

10. The efficiency ratios Hii/F and Hoo/F react to increased U^* the same way Hii and Hoo do. The best values of Hii/F and Hoo/f are achieved with low roughness geometry geometries. The worst values are achieved with high roughness geometry geometries. Low U^* values will increase the ratios, as well as high α. Beyond Re $>$ 60 000, Re has no noticeable effect of the ratios. Hii/F and Hoo/F can be inferior to unity when α, Re and Pr are low and roughness geometry is high.

11. The effects of S/e and P/e are demonstrated to be local, near the roughness

surface. The effects of P/e are greater than those of S/e.

12. The effects of U^* are explained through the relative momentum analogy and corroborated by the computer predictions.

Bibliography

(By order of appearance in the text)

1. Barrow H. and Pope, C.W., *Theoretical Global Energy Analysis for a Railway Tunnel and its Environment, with Special Reference to periodic Temperature Changes*, Aerodynamics and Ventilation of Vehicle Tunnels, Brit. Rail. Board, PP. 267-280 (1991)

2. Dunn, P. and Reay, D.A., Heat Pipes, 2nd Ed., Pergamon Press, Oxford, U.K., (1978)

3. Kays, W.M. and Crawford, M.E, Convective Heat and Mass Transfer, McGraw Hill Book Company Inc., U.S.A., (1980)

4. Chapman, A.J., Heat Transfer 4th ed., MacMillan Publishing Co., New York, (1984)

5. Kays, W.M. and London, A.L., Compact Heat Exchangers 2nd ed., McGraw Hill Book Company Inc., New York (1964)

6. Rothfus, R.R., Startory, W.K. and Kermode, R.I., Flow in Concentric Annuli at High Reynolds Numbers, A.I.Ch.E Journal, 12, 1086-1091, (1966)

7. Sleicher Jr., C.A. and Tribus, M.,*Heat Transfer in a Pipe with Turbulent Flow and Arbitrary Wall Temperature Distribution*, Heat Transfer and Fluid Mechanics, Stanford University, pp. 58-78 (1956)

8. Shigechi, T.. Kawae, N. and Lee, Y., *Turbulent Fluid Flow and Heat Transfer in Concentric Annuli with moving cores,* International Journal of Heat and Mass Transfer, 33, pp.2029-2037 (1990)

9. Shigechi, T. and Lee, Y., *An Analysis on Fully Developed Laminar Fluid Flow and Heat Transfer in Concentric Annuli with moving cores*, International Journal of Heat and Mass Transfer, 34, pp.2593-2601 (1991)

10. Shigechi, and Lee, Y., *Laminar Heat Transfer in the Thermal Entrance Regions of Concentric Annuli with moving heated cores*, The Proceeding of the 2nd KSME-JSME Fluids Engineering Conference, 2, pp. 281-286, Seoul, Oct 10-12 1990

11. Lee, Y. and Shigechi, *Heat Transfer in Concentric Annuli with moving cores - Fully Developed Turbulent Flow with Arbitrarily Prescribed Heat Flux*, International Journal of Heat and Mass Transfer, 35, No. 12, pp. 3488-3493, (1992)

12. Nikuradse, J., *Laws of Flows in Rough Pipes - Technical Memorandum 1292*, National Advisory Committee for Aeronautics (NACA), Washington (1950).

13. Schlichting, H., Boundary Layer Theory, 6th ed., Mcgraw Hill Book Company Inc., U.S.A., pp.578-589, (1968)

14. Launder, B.E., Turbulent Models and their Experimental Verification - II, Imperial College of Science and Technology, Department of Mechanical Engineering, London, U.K. (1973)

15. Tanaka, H. and Yabuki, H., *Laminarization and Reversion to Turbulence of low Reynolds Number Flows Through a Converging to Constant Aera Duct*, Journal of Fluids Engineering, Vol. 108, pp. 325-330 (1986)

16. Jones. W.P. and Launder, B.E., *The Prediction of Laminarization with a Two Equation Model of Turbulence*, Int. J. of Heat and Mass Transfer, Vol. 15, pp.301-314 (1972)

17. Clauser, F.H., *Turbulent Boundary Layers in Adverse Pressure Gradients*, Journal of Aerospace Science, Vol. 21, pp. 91-108 (1954)

18. Hama, F.R. *Boundary Layer Characteristics for smooth and Rough Surfaces*, Trans. of Soc. of Naval Arch. and Marine Eng., Vol. 62, pp. 333-358 (1954)

19. Lee, Y, *An Analysis on the Enhanced Heat Transfer induced by square-ribbed surface roughness*, Heat Transfer Science and Technology, Hemisphere Publications Company, New York, U.S.A, pp. 781-788 (1987)

20. Lee, Y.P., Ahn, S.W. and Lee Y., *Turbulent Fluid Flow and Heat Transfer induced by square-ribbed surface roughness in concentric annuli*, Ninth International Heat Transfer Conference, 1990, 4-MC-20, Jerusalem, August 19-24

21. Lee, Y.P., Ahn, S.W. and Lee Y., *Enhanced Turbulent Heat Transfer induced by square-ribbed surface roughness in concentric annuli*, The Proceeding of the 2nd KSME-JSME Fluids Engineering Conference, 2, pp. 293-298, Seoul, Oct 10-12 1990

22. Bhuiyan, A., *An Asymmetric Turbulent Fluid Flow Induced by Rectangular Ribbed Surface Roughness*, M.A. Sc. Thesis, Dept of Mechanical Engineering, University of Ottawa, Canada (1977)

23. Lee Y. and Kim, K.H., *Inverted Annular Flow Boiling*, International Journal of Multiphase Flow, Vol. 13, No.3, pp.345-355 (1990)

24. Perry, A.F. and Joubert, P.N., *Rough wall Boundary Layers in adverse Pressure Gradients*, Journal of Fluid Mechanics, Vol. 17, pp.193-211 (1963)

25. Wu, J., *Flow in Turbulent Wall Layer Over Uniform Roughness*, Journal of Applied Mechanics, Vol. 40, pp. 863-867 (1973)

26. Ahn, S.W., *Turbulent Fluid Flow and heat Transfer Induced by Square-Ribbed Surface Roughness in Concentric Annuli* ,M.A. Sc. Thesis, Dept of Mechanical Engineering, University of Ottawa, Canada (1990)

27. Lee, Y., *Turbulent Heat Transfer from the Core Tube in Thermal Entrance Regions of Concentric Annuli*, Int. Journal of Heat and Mass Transfer, 11, pp.509-522 (1968)

28. Cebeci, T. and Smith, A.M.O., Analysis of Turbulent Boundary Layers, Academic Press, New York, U.S.A., pp. 47-56, 62-77, 106, 191 (1974)

29. Van Driest, E.R., Journal of Aeronautical Sciences, 23, p. 1007 (1956)

30. Reichardt, H., *Vollstandige Darstellung der turbulenten Geschwindigekeitsverterilung in glatten Leitungen*, Angew. Math. Mech., 31, pp.208-219 (1951)

31. Kays, W.M., and Leung, E.Y., *Heat Transfer in Annular Passages - Hydrodynamically Developed Turbulent Flow with Arbitrarily prescribed Heat Flux*, International Journal of Heat and Mass Transfer 6, pp.537-557 (1963)

32. Brighton, J.A. and Jones, J.B., *Fully Developed Turbulent Flow in Annuli*, Transactions ASME, Journal of Basic Engineering, 86, pp.835-844 (1964)

33. Barrow, H., Lee, Y. and Roberts, A., *The Similarity Hypothesis Applied to Turbulent Flows in an Annulus*, Int. Journal of Heat and Mass Transfer, 8, pp.1499-1505 (1965)

34. Anderson, P.S., Kays, W.M. and Moffat, R.J., *Experimental Results for the transpired turbulent Boundary Layer in an adverse pressure gradient*, Journal of Fluid Mechanics, Vol. 69, pp. 353-375 (1975)

35. Allan, W.K. and Sharma, V., *An Investigation of Low Turbulence Flows over Smooth and Rough Surface*, Journal of Mechanical Engineering Science, 16, pp.71-78 (1974)

36. Harlow, F.H. and Nakayama, P., *Turbulence Transport Equations*, The physics of Fluids, Vol 10, 323-2332 (1967)

37. Hinze, J.O., Turbulence 2nd ed., McGraw Hill Book Co. Inc., New York, (1975)

38. Jones, W.P. and Launder, B.E., *The Prediction of Laminarization with a* Two-Equation model of Turbulence, Int. Journal of Heat and Mass Transfer, 15, pp.301-314 (1972)

39. Jones, W.P. and Launder, B.E., *The Calculation of Low Reynolds number phenomena with a* Two-Equation model of Turbulence, International Journal of Heat and Mass Transfer, 16, pp. 1119-1130 (1973)

40. Lam, C.K.G. and Bremhorst, K., *A modified form of the K-ϵ Model for Predicting Wall Turbulence*, Trans. ASME, 103, pp. 456-459 (1981)

41. Monin, A.S. and Yeaglom, A.M., Statistical Fluid Mechanics II, M.I.T. Press (1975)

42. Stănisic, M.M., The Mathematical Theory of Turbulence, Springer Verlag Inc, New York (1985)

43. Launder, B.E., *Second Moment Closure: Methodology and Practise*, Turbulence Models and their Applications, Vol. II, Editions Eyrolles, Saint-Germain, Paris, (1984)

44. Hanjalic, K. and Launder, B.E., *Fully Developed Asymmetrical Flow in a Plane Channel*, Journal of Fluid Mechanics, 51 pp. 301-350 (1972)

45. Randhave, S.S., An Analysis of Turbulent Flow in Concentric Annuli, A.I.Ch.E Journal, 15, 132-133, (1969)

46. Park, S.D., *developing Turbulent Flow and Heat Transfer in Concentric Annuli: an Analytical and Experimental Study*, PH.D. Thesis, Department of Mechanical Engineering, University of Ottawa, Ottawa, Ontario Canada (1971)

47. Moody, L.F., Transactions ASME, 66, p.671 (1944)

48. Pfaffenberger, R. and Patterson, J.H., Statistical Methods for Business and Economics, Revised Ed., Richard D. Irwin Inc., Homewood, IL, U.S.A. pp. 38-40 (1981)

49. LaFara, R.L., Computer Methods for Science and Engineering, Hayden Book Company Inc., new jersey, pp. 145-155 (1973)

50. Jenkins, R., *Variation of the Eddy Conductivity with Prandtl Modulus and its Use in Predictions of Turbulent Heat Transfer Coefficients*, Heat Transfer and Fluid Mechanics, Stanford University, pp.147-158 (1951)

Other references
(in alphabetical order)

51. Batchelor, B.K., F.R.S, The Scientific Papers of Sir Geoffrey Ingram Taylor, Vol. II, Cambridge University Press, (1960)

52. Carlson, L.W. and Irvine Jr., T.F., Journal of Heat Transfer, 83, pp.441-444 (1961)

53. Giedt, W.H., *Investigation of the Variation of Point Unit Heat\ Transfer Coefficient Around a Cylinder Normal to an Air Stream*, Transactions ASME, 71, p.375 (1949)

54. Kirchhoff, R.H., Potential Flows, Marcel Dekker Inc., New York, U.S.A., (1985).

55. Mikhailov, M.D. and Özisik, M.N., Unified Analysis and Solutions of Heat and Mass Diffusion, John Wiley and Sons Publications Inc., U.S.A., (1984).

56. Offen, G.R., and Kline, S.J., Journal of Fluids Mechanics, 70, pp.209-228, (1975)

57. Shames, I.H., Mechanics of Fluids 2nd ed., McGraw Hill Book Co. Inc., USA, (1982)

58. *Turbulence and Chaotic Phenomena in Fluids*, Proceedings International Symposium on Turbulence and Chaotic Phenomena in Fluids, Kyoto, Japan, (1983)

59. Zhukauskas, A., *Heat Transfer from Tubes in Cross Flows*, Advanced in Heat Transfer, 8, p. 93 (1972)

Appendix A
Development of model equations

Appendix A.1
Force Balance Analysis of Annulus Geometry

The basic geometry of a smooth surface annulus is shown in Figure A1-1 below. The distribution of the fluid velocity across the channel section is influenced by the necessary condition of zero velocity at both wall, such that the velocity profile evolves from zero velocity at the wall to a maximum velocity at a location R_M, where $R_{Ri} < R_M < R_{Ro}$, to zero velocity again at the opposite wall. This characteristic profile allows the analysis to be divided into two regions, inner and outer, separated at the location of maximum velocity.

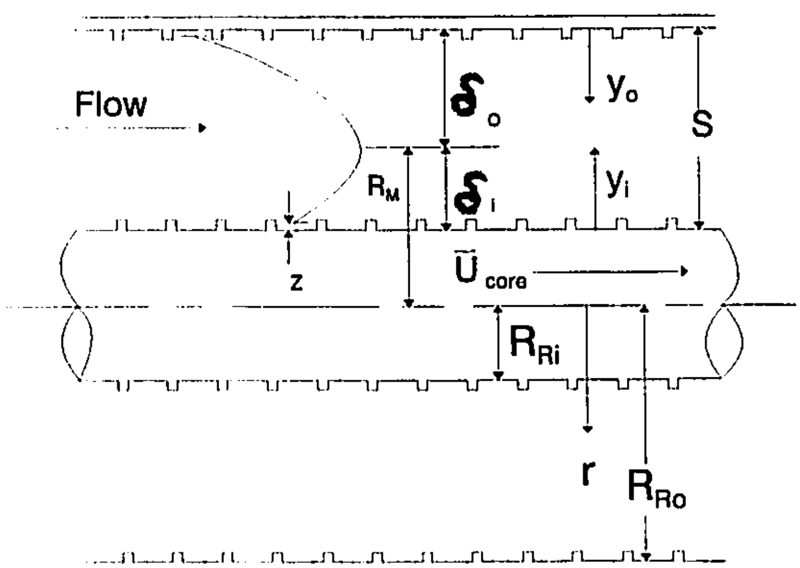

Figure A1-1: Annulus geometry and nomenclature

To perform an analysis of the force balance in each region, a control volume (C.V.) is taken on an element of the fluid:

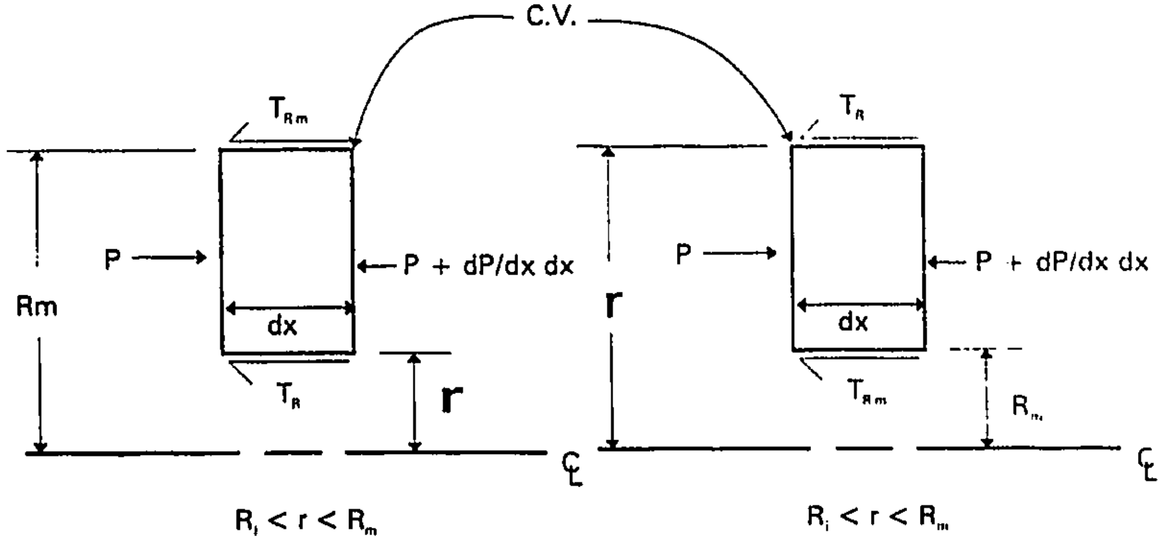

Figure A1-2: Control Volume for Inner Region

Figure A1-3: Control volume for Outer Region

ΣF_x for Inner Region

The forces applied to the control volume shown at Figure A1-2 yield the Force balance equation:

$$-\tau_r (2\pi r dx) - \tau_{R_M} (2\pi R_m dx) + \pi P (R_m^2 - r^2) - \left(P + \frac{\partial P}{\partial x}dx\right) \pi (R_m^2 - r^2) = 0$$

The pressure term is readily eliminated, with the pressure gradient term only remaining. The equation can be further simplified by dividing both sides by 2πdx. The result is:

$$-\tau_r r - \tau_m R_M = \frac{1}{2}\frac{\partial P}{\partial x}(R_M^2 - r^2) \qquad [A1.1]$$

The boundary conditions applicable to the inner region are $\tau_r = 0.0$ at $r = R_M$. Inserting these conditions in Eq [A1.1] yields the expression for τ_{Ri} and τ_r:

$$\tau_{Ri} = -\frac{1}{2}\frac{\partial p}{\partial x}\left(\frac{R_m^2 - R_{Ri}^2}{R_{Ri}}\right) \qquad [A1.2]$$

$$\tau_r = -\frac{1}{2}\frac{\partial p}{\partial x}\left(\frac{R_m^2 - r^2}{R_{Ri}}\right) \qquad [A1.3]$$

Finally, dividing Eq [A1.3] by Eq [A1.2] yields:

$$\frac{\tau_r}{\tau_{Ri}} = \frac{R_{Ri}}{r}\left(\frac{R_m^2 - r^2}{R_m^2 - R_{Ri}^2}\right) \qquad [A1.4]$$

$\sum F_x$ for the Outer Region

The force analysis for the outer region is done in the same manner, using the control volume shown at Figure A1-3. The force balance equation is in this case:

$$-\tau_{R_M}(2\pi R_m dx) - \tau_r(2\pi r dx) + \pi P(r^2 - R_m^2) - \left(P + \frac{\partial P}{\partial x}dx\right)\pi(r^2 - R_m^2) = 0 \qquad [A1.5]$$

By applying the boundary conditions to Eq [A1.5], $\tau_{Rm} = 0.0$ at $r = R_m$, the following equations can be obtained:

$$\tau_r = -\frac{1}{2}\frac{\partial P}{\partial x}\left(\frac{r^2 - R_m^2}{r}\right) \qquad [A1.6]$$

$$\tau_{Ro} = -\frac{1}{2}\frac{\partial P}{\partial x}\left(\frac{R_{Ro}^2 - R_m^2}{R_{Ro}}\right) \qquad [A1.7]$$

$$\frac{\tau_r}{\tau_{Ro}} = \frac{R_{Ro}}{r}\left(\frac{r^2 - R_m^2}{R_{Ro}^2 - R_m^2}\right) \qquad [A1.8]$$

Finally, the combination of Eq [A1.2] and [A1.7] gives:

$$\frac{\tau_{Ri}}{\tau_{Ro}} = \frac{R_{Ro}}{R_{Ri}}\left(\frac{R_m^2 - R_{Ri}^2}{R_{Ro}^2 - R_m^2}\right) \qquad [A1.9]$$

Appendix A.2

Heat Balance Analysis of Inner/Outer Surfaces Heated

In an annulus, three heating conditions may be encountered: 1) the core surface is heated with the outer surface insulated; 2) the outer surface is heated with the core surface insulated; and 3) both surfaces are heated. The heat analysis can be performed by calculating the heat balance for the first and the second conditions independently. The solution to the third condition can be obtained by applying the principle of superimposition whereby the solution to a homogeneous linear differential equation can be expressed as the sum of two particular solutions. Since the differential equation governing the heat transfer of the annulus satisfies the condition of linearity and homogeneity, the principle can be applied. In this study, however, only the first two conditions were investigated.

First Condition: Core Heating

The control volume shown in Figure A1-2 can be utilized again in this analysis. The heat exchange process is illustrated in Figure A2-1.

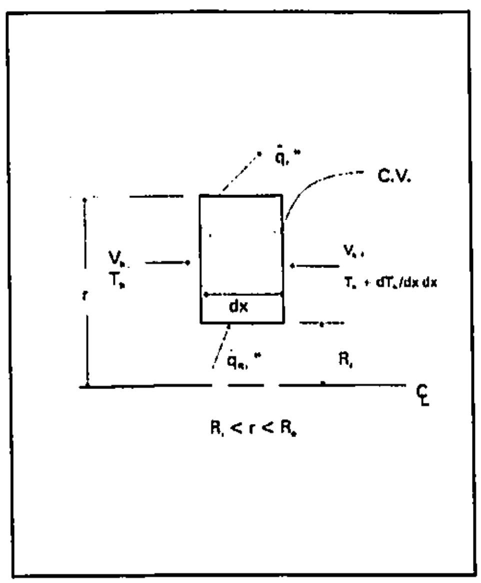

Figure A2-1: Control Volume for core heating

Neglecting viscous dissipation (an acceptable assumption for flows with a Mach number $<<0.3$, see [7]), the law of conservation of energy requires that:

Thermal Energy in = Thermal Energy out

That law may be expressed for the control volume by the equation:

$$\rho c_p T_b V_b \pi (r^2 - R_{Ri}^2) + \dot{q}_{Ri}'' 2\pi R_{Ri} dx =$$

$$\dot{q}_r'' 2\pi r dr + \pi \rho c_p V_b (r^2 - R_{Ri}^2)\left(T_b + \frac{\partial T_b}{\partial x} dx\right)$$

The first term on the left side of the equation appears on both sides of the equation, and can be eliminated. Dividing the equation by $2\pi dx$ and re-arranging, one obtains:

$$\rho c_p (r^2 - R_{Ri}^2)\left(\frac{V_b}{2}\right)\left(\frac{\partial T_b}{\partial x}\right) = \dot{q}''_{Ri} R_{Ri} - \dot{q}''_r r \qquad [A2.1]$$

The boundary condition is zero heat transfer at $r = R_{Ro}$ (the outer wall is assumed to be insulated). When applied to Eq [A2.1], the expression for the core heat flux thus becomes:

$$\dot{q}''_{Ri} = \rho c_p \frac{R_{Ro}}{R_{Ri}} \frac{V_b}{2} \frac{\partial T_b}{\partial x}\left(\frac{R_{Ro}^2 - R_{Ri}^2}{R_{Ro}}\right) \qquad [A2.2]$$

Eq [A2.1] and [A2.2] can be combined to eliminate the terms V_b, T_b, ρ and c_p. The resulting expression is:

$$\frac{\dot{q}''_r}{\dot{q}''_{Ri}} = \frac{R_{Ri}}{r}\left(\frac{R_{Ro}^2 - r^2}{R_{Ro}^2 - R_{Ri}^2}\right) \qquad [A2.3]$$

Second Condition: Outer Surface Heating

The development of the expressions for this condition is akin to that of the core condition and is not detailed here. The equation of interest that can be derived is:

$$\frac{\dot{q}''_r}{\dot{q}''_{Ro}} = \frac{R_{Ro}}{r}\left(\frac{r^2 - R_{Ri}^2}{R_{Ro}^2 - R_{Ri}^2}\right) \qquad [A2.4]$$

Appendix A.3

Non-dimensionalized Forms of the Momentum and Heat Balance Equations - Smooth Surfaces

I. Defined Parameters

The following Table A3.1 provides the list of parameters used to transform the momentum and heat equations into non-dimensionalized forms.

Table A3.1 - Independent Parameters

Inner Region	**Outer Region**
($R_{Ri} < r < R_m$)	($R_m < r < R_{Ro}$)
$\alpha = R_{Ri}/R_{Ro}$	$\alpha = R_{Ri}/R_{Ro}$
$Pr_t = \epsilon_M/\epsilon_H$	$Pr_t = \epsilon_M/\epsilon_H$
$y_i = r - R_{Ri}$	$y_o = R_{Ro} - r$
$\delta_i = R_m - R_{Ri}$	$\delta_o = R_{Ro} - R_m$
$\mu_{\tau i} = (\tau_{Ri}/\rho)^{1/2}$	$\mu_{\tau o} = (\tau_{Ro}/\rho)^{1/2}$
$y_i^+ = y_i\, \mu_{\tau i}/\nu$	$y_o^+ = y_o\, \mu_{\tau o}/\rho$
$\delta_i^+ = \delta_i\, \mu_{\tau i}/\nu$	$\delta_o^+ = \delta_o\, \mu_{\tau o}/\rho$
$R_i^+ = R_{Ri}\, \mu_{\tau i}/\nu$	$R_o^+ = R_{Ro}\, \mu_{\tau o}/\rho$
$u_i^+ = u_i/\mu_{\tau i}$	$u_o^+ = u_o/\mu_{\tau o}$
$U^+ = U_{core}/\mu_{\tau i}$	
$U^* = U_{core}/u_{bulk}$	
$\Delta_i = \delta_i^+/R_i^+$	$\Delta_o = \delta_o^+/R_o^+$
$\zeta_i = y_i^+/\delta_i^+$	$\zeta_o = y_o^+/\delta_o^+$
$T_i^+ = (T_{Ri} - T_i)\rho\, c_p\, \mu_{\tau i}/\mathring{q}_{Ri}''$	$T_o^+ = (T_{Ro} - T_o)\rho\, c_p\, \mu_{\tau o}/\mathring{q}_{Ro}''$

II. Shear Stress Ratio

Eq [A1.4] was derived in Appendix A1 as:

$$\frac{\tau_r}{\tau_{Ri}} = \frac{R_{Ri}}{r}\left(\frac{R_m^2 - r^2}{R_m^2 - R_{Ri}^2}\right) \qquad [A1.4]$$

which can be re-arranged as follows, by extracting the term R_{Ri}^2 and replacing r by $y_i + R_{Ri}$:

$$\frac{\tau_r}{\tau_{Ri}} = \frac{R_{Ri}}{(y_i + R_{Ri})}\left(\frac{R_{Ri}^2}{R_{Ri}^2}\right)\left[\frac{\left(\frac{R_M}{R_{Ri}}\right)^2 - \left(\frac{r}{R_{Ri}}\right)^2}{\left(\frac{R_M}{R_{Ri}}\right)^2 - 1}\right]$$

That expression can be further reduced to:

$$\frac{\tau_r}{\tau_{Ri}} = \frac{1}{\left(\frac{y_i}{R_{Ri}} + 1\right)}\left[\frac{\left(\frac{R_M}{R_{Ri}}\right)^2 - \left(\frac{r}{R_{Ri}}\right)^2}{\left(\frac{R_M}{R_{Ri}}\right)^2 - 1}\right]$$

Here, $R_M/R_{Ri} = (\delta_i + R_{Ri})/R_{Ri} = \Delta_i + 1$, and $r/R_{Ri} = (y_i + R_{Ri})/R_{Ri} = \Delta_i\zeta_i + 1$

Substitute these two equivalences into the expression above to obtain:

$$\frac{\tau_r}{\tau_{Ri}} = \frac{1}{\Delta_i\zeta_i + 1}\left[\frac{(\Delta_i + 1)^2 - (\Delta_i\zeta_i + 1)^2}{(\Delta_i + 1)^2 - 1}\right]$$

$$= \frac{1}{\Delta_i\zeta_i + 1}\left[\frac{\Delta_i^2 + 2\Delta_i - (\Delta_i\zeta_i)^2 - 2\Delta_i\zeta_i}{\Delta_i^2 + 2\Delta_i}\right]$$

$$= \frac{1}{\Delta_i\zeta_i + 1}\left[\frac{(1 - \zeta_i)(\Delta_i\zeta_i + 2 + \Delta_i)}{\Delta_i + 2}\right]$$

$$= \frac{1 - \zeta_i}{\Delta_i\zeta_i + 1}\left[1 + \frac{\Delta_i\zeta_i}{\Delta_i + 2}\right] \qquad [A3.1]$$

The form of Eq [A3.1] is obtained by extracting the roots of the polynomial of the right hand side numerator.

The corresponding equation for the shear stress ratio in the outer region of the flow is obtained in a similar fashion, starting with equ [A1.8]. Applying the equivalences

$$\frac{r}{R_{Ro}} = \frac{R_{Ro} - y_o}{R_{Ro}} = 1 - \zeta_o$$

$$\frac{R_M}{R_{Ro}} = \frac{R_{Ro} - \zeta_o}{R_{Ro}} = 1 - \Delta_o \zeta_o$$

to Eq [A1.8] yields the following expression:

$$\frac{\tau_r}{\tau_{Ri}} = \frac{\zeta_o - 1}{1 - \Delta_o \zeta_o}\left[\frac{\zeta_o - \dfrac{(2 - \Delta_o)}{\Delta_o}}{2 - \Delta_o}\right] \qquad [A3.2]$$

III. Heat Ratios - Inner surface heating

For this condition, the applicable equation is [A2.3]:

$$\frac{\dot{q}_r''}{\dot{q}_{Ri}''} = \frac{R_{Ri}}{r}\left(\frac{R_{Ro}^2 - r^2}{R_{Ro}^2 - R_{Ri}^2}\right) \qquad [A2.3]$$

which, by extracting R_{Ri}^2, reduces to:

$$\frac{\dot{q}_r''}{\dot{q}_{Ri}''} = \frac{R_{Ri}}{r}\left[\frac{\left(\dfrac{R_{Ro}}{R_{Ri}}\right)^2 - \left(\dfrac{r}{R_{Ri}}\right)^2}{\left(\dfrac{R_{Ro}}{R_{Ri}}\right)^2 - 1}\right]$$

Here, $R_{Ro}/R_{Ri} = 1/\alpha$.

For the inner region, the ratio $r/R_{Ri} = \Delta_i\zeta_i + 1$, such that the last equation can be re-written as:

$$\frac{\dot{q}_r''}{\dot{q}_{Ri}''} = \frac{1}{(\Delta_i\zeta_i + 1)}\left[\frac{\frac{1}{\alpha^2} - (1 + \Delta_i\zeta_i)^2}{\frac{1}{\alpha^2} - 1}\right]$$

and, finally,

$$\frac{\dot{q}_r''}{\dot{q}_{Ri}''} = \frac{1}{(\Delta_i\zeta_i + 1)}\left[\frac{1 - \alpha^2(1 + \Delta_i\zeta_i)^2}{1 - \alpha^2}\right] \qquad [A3.3]$$

For the outer region, Eq [A2.3] can be re-arranged by extracting R_{Ro}^2:

$$\frac{\dot{q}_r''}{\dot{q}_{Ri}''} = \frac{\left(\frac{R_{Ri}}{R_{Ro}}\right)\left[1 - \left(\frac{r}{R_{Ro}}\right)^2\right]}{\left(\frac{r}{R_{Ro}}\right)\left[1 - \left(\frac{R_{Ri}}{R_{Ro}}\right)^2\right]}$$

Again substituting $R_{Ri}/R_{Ro} = \alpha$ and $r/R_{Ro} = 1 - \Delta_o\zeta_o$ in the last expression yields:

$$\frac{\dot{q}_r''}{\dot{q}_{Ri}''} = \frac{\alpha}{1 - \Delta_o\zeta_o}\left[\frac{1 - (1 - (\Delta_o\zeta_o)^2}{1 - \alpha^2}\right]$$

and, finally

$$\frac{\dot{q}_r''}{\dot{q}_{Ri}''} = \frac{\alpha}{1 - \Delta_o\zeta_o}\left[\frac{2\Delta_o\zeta_o - (\Delta_o\zeta_o)^2}{1 - \alpha^2}\right] \qquad [A3.4]$$

IV. Heat Ratio - Outer surface heating

The development of the expressions for the condition of outer surface heating is similar to the development for the first heating condition. Starting with Eq [A2.4], the heat ratios for the regions are given below, without development details:

$R_M \le r \le R_{Ro}$,

$$\frac{\dot{q}_r''}{\dot{q}_{Ro}''} = \frac{1}{1 - \Delta_o \zeta_o} \left[\frac{(1 - \Delta_o \zeta_o)^2 - \alpha^2}{1 - \alpha^2} \right] \qquad [A3.5]$$

$R_{Ri} \le r \le R_M$,

$$\frac{\dot{q}_r''}{\dot{q}_{Ro}''} = \frac{\alpha}{1 + \Delta_i \zeta_i} \left[\frac{(\Delta_o \zeta_o)^2 + 2\Delta_i \zeta_i}{1 - \alpha^2} \right] \qquad [A3.6]$$

Appendix A.4

Non-dimensionalized Forms of the Momentum and Heat Balance Equations - Rough Surfaces

The general equations of the stress and heat ratios, derived in Appendices A1 through A3, can be modified to include the special case of rough surfaces. The modelling of surface roughness borrows from the concept of surface roughness developed by Bhuiyan [22] and Lee [27]. The effect of a rough surface is reflected by the variable z_{or}, which defines the location of zero fluid velocity above the root of the rough surface, shown here in Figure A4-1.

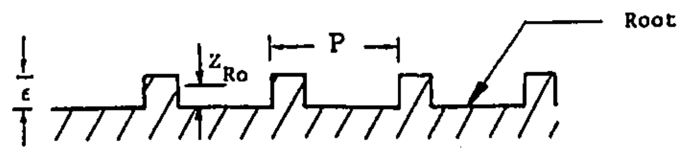

Figure A4-1: Geometry of core roughness

I. Shear Stress Ratios

The effective domain of application for r in a roughened annulus will necessarily shrink by z_{or} near the rough surface. The new domain becomes:

$$R_{Bi} < r < R_{Bo}$$

At the inner surface, R_{Bi} is the sum $R_{Ri} + (z_{or})_i$. At the outer surface, R_{Bo} is the sum $R_{Ro} + (z_{or})_o$. For simplicity, the z terms will be written as z_{Ri} and z_{Ro}. The shear stress equations [A1.4], [A1.8] and [A1.9] can be modified by inserting the variables R_{Bi} and R_{Bo} in lieu of R_{Ri} and R_{Ro}. After manipulating the equations , by isolating either R_{Ri} or R_{Ro}, the following equations are obtained for [A1.4] and [A1.8]:

$R_{Bi} \le r \le R_M,$

$$\frac{\tau_R}{\tau_{R_{Ri}}} = \frac{1 + \frac{z_{Ri}}{R_{Ri}}}{1 + \Delta_i \zeta_i} \left[\frac{(1 + \Delta_i)^2 - (1 + \Delta_i \zeta_i)^2}{(1 + \Delta_i)^2 - \left(1 + \frac{z_{Ri}}{R_{Ri}}\right)^2} \right] \qquad [A4.1]$$

$R_M \le r \le R_{Bo},$

$$\frac{\tau_r}{\tau_{R_{Ro}}} = \frac{1 - \frac{z_{Ro}}{R_{Ro}}}{1 - \Delta_o \zeta_o} \left[\frac{(1 - \Delta_o \zeta_o)^2 - (1 - \Delta_o)^2}{\left(1 - \frac{z_{Ro}}{R_{Ro}}\right)^2 - (1 - \Delta_o)^2} \right] \qquad [A4.2]$$

For Eq [A1.9], the expression is derived as follows:

$$\frac{\tau_{Bi}}{\tau_{Bo}} = \left(\frac{R_{Ro} - z_{Ro}}{R_{Ri} + z_{Ri}}\right) \left(\frac{R_{Ri}}{R_{Ro}}\right)^2 \left[\frac{\left(\frac{R_m}{R_{Ri}}\right)^2 - \left(1 + \frac{z_{Ri}}{R_{Ri}}\right)^2}{\left(1 - \frac{z_{Ro}}{R_{Ro}}\right)^2 - \left(\frac{R_m}{R_{Ro}}\right)^2} \right]$$

Substituting the R_M/R_{Ri} and R_M/R_{Ro} with the expressions $(1 + \Delta_i)$ and $(1 - \Delta_o)$ respectively, the above equation is transformed to:

$$\frac{\tau_{Bi}}{\tau_{Bo}} = \frac{R_{Ro}}{R_{Ri}} \left(\frac{1 - \frac{z_{Ro}}{R_{Ro}}}{1 + \frac{z_{Ri}}{R_{Ri}}} \right) \left(\frac{R_{Ri}}{R_{Ro}}\right)^2 \left[\frac{(1 + \Delta_i)^2 - \left(1 + \frac{z_{Ri}}{R_{Ri}}\right)^2}{\left(1 - \frac{z_{Ro}}{R_{Ro}}\right)^2 - (1 - \Delta_o)^2} \right]$$

And, after substituting R_{Ri}/R_{Ro} by α, the equation takes the final form:

$$\frac{\tau_{Bi}}{\tau_{Bo}} = \alpha \left(\frac{1 - \frac{z_{Ro}}{R_{Ro}}}{1 + \frac{z_{Ri}}{R_{Ri}}} \right) \left[\frac{(1 + \Delta_i)^2 - \left(1 + \frac{z_{Ri}}{R_{Ri}}\right)^2}{\left(1 - \frac{z_{Ro}}{R_{Ro}}\right)^2 - (1 - \Delta_o)^2} \right] \qquad [A4.3]$$

II. Heat Ratios

A. Inner Surface Heating - Inner Region

For the inner surface heated only, Eq [A2.3] is applicable, with the substitution of R_{Ri} by $(R_{Ri} + z_{Ri})$ and R_{Ro} by $(R_{Ro} - Z_{Ro})$, as was done for the shear stress equations. With these substitutions and re-arranging, Eq [A2.3] is transformed as follows:

$$\frac{\dot{q}_r''}{\dot{q}_{Ri}''} = \frac{R_{Ri} + z_{Ri}}{r}\left[\frac{(R_{Ro} - z_{Ro})^2 - r^2}{(R_{Ro} - z_{Ro})^2 - (R_{Ri} + z_{Ri})^2}\right]$$

$$= \frac{R_{Ri}}{r}(1 + \frac{z_{Ri}}{R_{Ri}})\left[\frac{R_{Ro}^2(1 - \frac{z_{Ro}}{R_{Ro}})^2 \; - \; R_{Ri}^2(\frac{r}{R_{Ri}})^2}{R_{Ro}^2(1 - \frac{z_{Ro}}{R_{Ro}})^2 \; - \; R_{Ri}^2(1 + \frac{z_{Ri}}{R_{Ri}})^2}\right]$$

$$= \frac{R_{Ri}}{r}(1 + \frac{z_{Ri}}{R_{Ri}})\left[\frac{(1 - \frac{z_{Ro}}{R_{Ro}})^2 \; - \; \alpha^2(1 + \frac{z_{ri}}{R_{Ri}})^2}{(1 - \frac{z_{Ro}}{R_{Ro}})^2 \; - \; \alpha^2(1 + \frac{z_{Ri}}{R_{Ri}})^2}\right]$$

Finally, the term R_{Ri}/r can be replaced by its non-dimensional equivalent:

$$\frac{\dot{q}_r''}{\dot{q}_{Ri}''} = \frac{1 + \frac{z_{Ri}}{R_{Ri}}}{1 + \Delta_i\zeta_i}\left[\frac{(1 - \frac{z_{Ro}}{R_{Ro}})^2 \; - \; \alpha^2(1 + \Delta_i\zeta_i)^2}{(1 - \frac{z_{Ro}}{R_{Ro}})^2 \; - \; \alpha^2(1 + \frac{z_{Ri}}{R_{Ri}})^2}\right] \qquad [A4.4]$$

B. Inner Surface Heating - Outer Region

The development of the heat ratio for the outer region is similar and will not be reproduced here. Only the resulting equation will be given:

$$\frac{\dot{q}_r''}{\dot{q}_{Ri}''} = \alpha\frac{1 + \frac{z_{Ri}}{R_{Ri}}}{1 - \Delta_o\zeta_o}\left[\frac{(1 - \frac{z_{Ro}}{R_{Ro}})^2 \; - \; (1 - \Delta_o\zeta_o)^2}{(1 - \frac{z_{Ro}}{R_{Ro}})^2 \; - \; \alpha^2(1 + \frac{z_{Ri}}{R_{Ri}})^2}\right] \qquad [A4.5]$$

C. Outer Surface Heating - Inner Region

In this case, the applicable equation is again [A2.3], which is modified in the same manner as explained before:

$$\frac{\dot{q}_r''}{\dot{q}_{Ro}''} = \frac{R_{Ro} - z_{Ro}}{r}\left[\frac{r^2 - (R_{Ri} + z_{Ri})^2}{(R_{Ro} - z_{Ro})^2 - (R_{Ri} + z_{Ri})^2}\right]$$

$$= \frac{R_{Ro}}{r}(1 - \frac{z_{Ro}}{R_{Ro}})\left[\frac{R_{Ri}^2(\frac{r}{R_{Ri}})^2 - R_{Ri}^2(1 + \frac{z_{Ri}}{R_{Ri}})^2}{R_{Ro}^2(1 - \frac{z_{Ro}}{R_{Ro}})^2 - R_{Ri}^2(1 + \frac{z_{Ri}}{R_{Ri}})^2}\right]$$

The last equation can be further simplified by extracting the terms $(R_{Ri})^2$ and $(R_{Ro})^2$, and by replacing r/R_{Ri} by $1 + \zeta_i\Delta_i$. The result is:

$$\frac{\dot{q}_r''}{\dot{q}_{Ro}''} = \alpha\frac{1 - \frac{z_{Ro}}{R_{Ro}}}{1 + \Delta_i\zeta_i}\left[\frac{(1 + \Delta_i\zeta_i)^2 - (1 + \frac{z_{Ri}}{R_{Ri}})^2}{(1 - \frac{z_{Ro}}{R_{Ro}})^2 - \alpha^2(1 + \frac{z_{Ri}}{R_{Ri}})^2}\right] \qquad [A4.6]$$

D. Outer Surface Heating - Outer Region

Using Eq [A2.4], the development for the inner region can be applied to the outer region. The result is Eq [A2.6]:

$$\frac{\dot{q}_r''}{\dot{q}_{Ro}''} = \frac{1 - \frac{z_{Ro}}{R_{Ro}}}{1 - \Delta_o\zeta_o}\left[\frac{(1 - \Delta_o\zeta_o)^2 - \alpha^2(1 - \frac{z_{Ro}}{R_{Ro}})^2}{(1 - \frac{z_{Ro}}{R_{Ro}})^2 - \alpha^2(1 + \frac{z_{Ri}}{R_{Ri}})^2}\right] \qquad [A4.7]$$

Appendix A.5
Non-dimensionalized Forms of the Velocity and Temperature Equations

I. Velocity Profile

The definition of total shear stress can be used to derive an expression for the fluid's axial velocity u(r). In its most basic form, the total shear stress is related to the fluid velocity through the equation:

$$\frac{\tau_j}{\rho} = (\nu + \epsilon_M)\frac{\partial \overline{u_j}}{\partial x} \qquad [A5.1]$$

But the shear stress τ_j/ρ is also related to the wall velocity $\mu_{\tau j}$ by the expression defined in Appendix A.3. Based on these two equations, the following relationships can be derived:

$$\frac{\tau_j}{\rho} = \mu_{\tau_j}^2 \qquad \textit{[by definition]}$$

$$\mu_j = \mu_j^+ \cdot \mu_{\tau_j} \quad \rightarrow \quad \partial\mu_j = \mu_{\tau_j}\,\partial\mu_j^+$$

$$y_j = \frac{y_j^+ \nu}{\mu_{\tau_j}} \quad \rightarrow \quad \partial y_j = \frac{\nu}{\mu_{\tau_j}}\,\partial y_j^+$$

also,

$$y_j^+ = \delta_j^+\,\zeta_j \quad \rightarrow \quad \partial y_j = \frac{\nu}{\mu_{\tau_j}}\,\delta_j^+\,\partial\zeta_j$$

$$[A5.2]$$

Eq [A5.1] can now be re-arranged by inserting the identities developed in Eq [A5.2]:

$$\frac{\tau_j}{\rho} = \nu\left(1 + \frac{\epsilon_M}{\nu}\right)\frac{\mu_{\tau_j}^2}{\nu\,\delta_j^2}\frac{\partial u_j^+}{\partial \zeta_j^+}$$

$$= \left(1 + \frac{\epsilon_M}{\nu}\right)\frac{\mu_{\tau_j}^2}{\delta_j^+}\frac{\partial u_j^+}{\partial \zeta_j^+}$$

$$= \left(1 + \frac{\epsilon_M}{\nu}\right)\frac{\tau_{Rj}}{\rho}\frac{1}{\delta_i^+}\frac{\partial u_j^+}{\partial \zeta_j^+}$$

The last expression can be re-arranged in terms of the velocity derivative:

$$\frac{\partial u_j^+}{\partial \zeta_j} = \frac{\delta_j^+\left(\frac{\tau}{\tau_R}\right)_j}{\left(1 + \frac{\epsilon_M}{\nu}\right)} \qquad [A5.3]$$

II. Eddy viscosity modelling

The term ϵ_M/ν appears in Eq [A5.1] when the components of the flow's momentum equation [1.2] are decomposed into time average and fluctuating components. That term requires mathematical modelling in order to utilize it for computational purposes, since it cannot be determined analytically. The term will exhibit a very different behaviour, depending on the state of the boundary layer. It is a widely accepted fact that a boundary layer can be regarded as consisting of two layers. The first one, the *viscous sublayer*, is confined to a region of the flow immediately adjacent to a solid boundary, such as the annulus' internal surfaces. Beyond the viscous sublayer lays the fully turbulent layer. Both regions require distinct mathematical models (refer to Chapter 3 of this study for details).

Viscous Sublayer

In the viscous sublayer, the model proposed by Van Driest [29] is used. The equation for that model is:

$$\frac{\epsilon_M}{\nu} = (\kappa_j y_j^+)^2 \left[1 - \exp\left(-\frac{y_j^+}{A_j^+}\right)\right]^2 \left|\frac{\partial u_j^+}{\partial y_j^+}\right| \qquad [A5.4]$$

That equation can be made dimensionless by inserting the equalities derived in Eq [A5.2] and [A5.3]. Doing so, and multiplying each side of the equation by $(1 + \epsilon_M/\nu)$, one obtains:

$$\frac{\epsilon_M}{\nu} + \left(\frac{\epsilon_M}{\nu}\right)^2 = (\kappa_j \delta_j^+ \zeta_j)^2 \left[1 - \exp\left(-\frac{\delta_j^+ \zeta_j}{A_j^+}\right)\right]^2 \left|\frac{\delta_j^+ \left(\frac{\tau}{\tau_R}\right)_j}{\left(1 + \frac{\epsilon_M}{\nu}\right)}\right| \qquad [A5.5]$$

That last equation is cumbersome but can simplified by taking advantage of the fact that the equation is an incomplete square polynomial in ϵ_M/ν. Thus, by finding the roots of the polynomial using the familiar relationship

$$x = \frac{-b \pm \sqrt{b^2 - 4ac}}{2a}$$

$$\textit{where} \quad x = \frac{\epsilon_M}{\nu}, \quad a = 1, \quad b = 1, \quad c = \textit{right side of } [A5.5]$$

the positive root of the polynomial is found to be:

$$\frac{\epsilon_M}{\nu} = \frac{1}{2}\left\{-1 + \sqrt{1 + 4(\kappa_j \delta_j^+ \zeta_j)^2 \left[1 - \exp\left(-\frac{\delta_j^+ \zeta_j}{A_j^+}\right)\right]^2 \left|\delta_j^+ \left(\frac{\tau}{\tau_R}\right)_j\right|}\right\} \qquad [A5.6]$$

Fully Turbulent Layer

In the fully turbulent layer, the model originally proposed by Reichardt is used in a modified form:

$$\frac{\epsilon_M}{\nu} = \frac{\kappa_j\,\delta_j^+}{6}\left[1-\left(1-\frac{y_j^+}{\delta_j^+}\right)^2\right]\times\left[1+2\left(1-\frac{y_j^+}{\delta_j^+}\right)^2\right] \qquad [A5.7]$$

Here, the term in y_j^+ /Δ_j^+ can be replaced by the variable ζ_j. Eq [A5.7] can then be re-arranged as follows:

$$\frac{\epsilon_M}{\nu} = \frac{\kappa_j\,\delta_j^+}{6}\left[1-(1-2\zeta_j+\zeta_j^2)\right]\times\left[1+(2-4\zeta_j+2\zeta_j^2)\right]$$

$$= \frac{\kappa_j\,\delta_j^+}{6}\left[2\zeta_j-\zeta_j^2\right]\left[3-4\zeta_j+2\zeta_j^2\right]$$

$$= \frac{\kappa_j\,\delta_j^+\,\zeta_j}{6}\left[2-\zeta_j\right]\left[3-4\zeta_j+2\zeta_j^2\right] \qquad [A5.8]$$

III. Temperature profile

The equation for the temperature profile throughout the flow cross-section is derived from the basic heat transport equation:

$$-\frac{\dot{q}_r''}{\rho\,c_p} = (\alpha+\epsilon_H)\frac{\partial T}{\partial r} \qquad \textit{where } \alpha \textit{ is the thermal diffusivity}$$

The presence of the negative sign is important. It signifies that heat will flow in a positive direction along r if the temperature *diminishes* as r grows (q being positive into the fluid). The distinction is essential when the equation is applied to the case of an annulus heated from the outer surface only. In that case, the direction gradient δr is negative, which requires that the negative sign be eliminated if the heat is to flow inward, into the fluid (the temperature gradient being also negative).

The above equation can be made dimensionless by introducing a non-dimensionalized temperature T_j^+, defined at Appendix A3:

$$T_j^+ = \frac{(T_{Rj} - T_j)\ \rho\ c_p\ \mu_{\tau_j}}{\dot{q}''_{R_j}} \qquad [A5.9]$$

Using Eq [A5.9], the partial derivative for T can be transformed as follows:

$$T_j = T_{Rj} - \frac{T_j^+\ \dot{q}R_j''}{\rho\ c_p\ \mu_{\tau_j}} \quad \rightarrow \quad \partial T_j = -\frac{\dot{q}''_{R_j}}{\rho\ c_p\ \mu_{\tau_j}}\ \partial T_j^+$$

$$r_j = R_j \pm y_j \quad \rightarrow \quad \partial r_j = \pm \partial y_j \quad \rightarrow \quad \partial r_j = \pm \frac{\nu}{\mu_{\tau_j}} \partial y_j^+ \quad \rightarrow \quad = \pm \delta_j^+ \frac{\nu}{\mu_{\tau_j}} \partial \zeta_j$$

$$\text{and} \quad \frac{\partial T_j}{\partial r} = \mp \frac{\dot{q}''_{Rj}}{\rho\ c_p\ \delta_j^+\ \nu}\ \frac{\partial T_j^+}{\partial \zeta_j}$$

The + sign applies where j = i. The - sign applies where j = o.

The last expression can be inserted directly into the basic heat transport equation. The terms ρ and c_p cancel out, such that the equation can be re-arranged in terms of T_j^+ as follows:

$$\frac{\partial T_j^+}{\partial \zeta_j} = \frac{\pm \delta_j^+ \left(\dfrac{\dot{q}''_r}{\dot{q}''_{Rj}} \right)}{\left(\dfrac{1}{Pr} \right) \left(1 + \dfrac{\epsilon_H}{\alpha} \right)} \qquad \text{where} \quad Pr = \frac{\nu}{\alpha} \qquad [A5.10]$$

Eq [A5.10] can be further simplified by re-arranging the denominator as follows:

The last expression is inserted in Eq [A5.10] to yield the final expression:

$$\frac{1}{Pr}\left(1+\frac{\epsilon_H}{\alpha}\right) = \left(\frac{1}{Pr}+Pr\,\frac{\epsilon_H}{\alpha}\right)$$

$$= \left(\frac{1}{Pr}+\frac{\epsilon_H}{\nu}\right)$$

$$\text{and, from } Pr_t = \frac{\epsilon_M}{\epsilon_H},$$

$$= \frac{1}{Pr}+\frac{\epsilon_M}{\nu}\frac{1}{Pr_t}$$

$$= \frac{1}{Pr}\left(1+\frac{Pr}{Pr_t}\frac{\epsilon_M}{\nu}\right)$$

$$\frac{\partial T_j^*}{\partial \zeta_j} = \frac{\pm\delta_j^*\left(\dfrac{\dot{q}_r''}{\dot{q}_{R_j}''}\right)}{\left(\dfrac{1}{Pr}\right)\left(1+\dfrac{Pr}{Pr_t}\dfrac{\epsilon_M}{\nu}\right)} \qquad [A5.11]$$

The $\pm$ sign is allocated according to the surface heated, as shown in the table below:

SIGN	INNER	OUTER
+	j = i	j = o
-	j = o	j = i

The value of Pr_t is typically set at 1.0. However, early works on ϵ_H, by Sleicher and Tribus [7] and Jenkins [50], led to the formulation of an infinite series solution to Eq [1.1]:

$$\frac{\epsilon_H}{\epsilon_M} = Pr\,\frac{F_H}{F_M}$$

$$\text{where } F_{H\text{ or }M} = \left[\frac{2}{15}-\frac{12}{\pi^6}A\sum_{n=1}^{\infty}\frac{1}{n^6}\left(1-\frac{1}{e^{\left(\frac{n^2\pi^2}{A}\right)}}\right)\right]$$

$$\text{and } A = \frac{\kappa\, y\, u'}{\nu} \text{ for } F_M, \qquad A = \frac{\kappa\, y\, u'}{k} \text{ for } F_H$$

The theoretical distribution of Pr_t as a function of Pr, predicted by this series is shown in Figure A5.1.

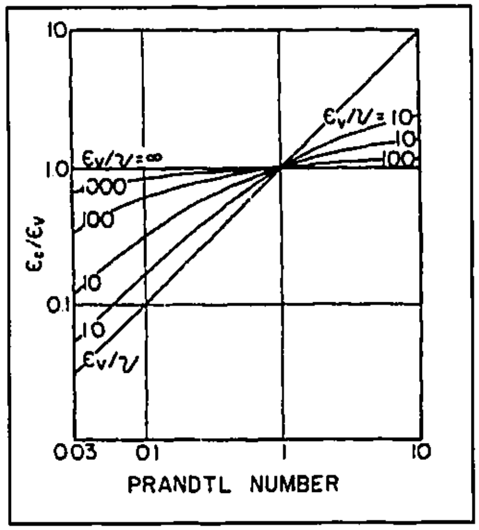

Figure A5.1 Variation of Pr_t with Pr From Jenkins [50], p.157

For Pr = 1, the formula predicts a Pr_t equal to unity, the same result obtained by the Reynolds analogy. (In the figure, the subscript "v" stands for "M" and the subscript "c", for "H").

IV. Eddy viscosity for rough surface

The presence of roughness elements on the annular surfaces has the effect of eradicating the viscous sublayer. The boundary layer immediately adjacent to the surface exhibits fully turbulent behaviour. In such an instance, the two expressions developed earlier, namely Eq [A5.6] and [A5.8], can not be applied and a new expression must be sought. The hypothesis established for that case is to assume that the eddy diffusivity concept developed by Prandtl is valid:

$$\left(\frac{\epsilon_M}{\nu}\right)_j = l_j^2 \left|\frac{\partial \overline{u_j}}{\partial y_j}\right|$$

$$\textit{with} \quad l_j = \kappa_j\, y_j$$

$$\textit{and} \quad Z_{R_j} < y_j < y_{j_{max}}$$

The last expression can be re-written using the identities developed previously for U_j and y_j. The result is:

$$\left(\frac{\epsilon_M}{\nu}\right)_j = \kappa_j^2\, \zeta_j^2\, \delta_j^+ \left|\frac{\partial \overline{u_j^+}}{\partial \zeta_j}\right| \qquad [A5.11]$$

In the fully turbulent region, the eddy viscosity is usually much larger than the viscosity. Using this simplification and Eq [A5.11], Eq [A5.3] can be re-written as follows:

$$\frac{\tau_j}{\tau_{Rj}} = \kappa_j^2 \, \zeta_j^2 \left(\frac{\partial u_j^+}{\partial \zeta_j} \right)^2 \qquad [A5.12]$$

The Prandtl hypothesis requires that the shear stress ratio be constant and close to unity. Therefore, Eq [A5.12] reduces to :

$$\frac{1}{\kappa_j \zeta_j} = \frac{\partial u_j^+}{\partial \zeta_j} \qquad [A5.13]$$

$$\textit{from which} \quad u_j^+ = \frac{1}{\kappa_j} Ln(\zeta_j) + C_1 \qquad [A5.14]$$

The integration constant C_1 can be found with the boundary condition that $u_j^+ = U^+$ at $\zeta_j = Z_{Rj}^+/\delta_j^+$. The result is

$$C_1 = -\frac{1}{\kappa_j} Ln\left(\frac{z_{R_j}^+}{\delta_j^+} \right) + U+$$

$$u_j^+ = \frac{1}{\kappa_j} Ln\left(\frac{\zeta_j}{\frac{z_{R_j}^+}{\delta_j^+}} \right) + U+ \qquad [A5.15]$$

$$\textit{and also} \quad \left(\frac{\epsilon_M}{\nu} \right)_j = \kappa_j \, \zeta_j \, \delta_j^+ \qquad [A5.16]$$

V. Matching z_{Ri} and z_{Ro}

When the core surface and the outer surface are roughened, it is possible to express z_{Ro} in terms of z_{Ri}. At the location of maximum velocity, the equality of velocity requires that both expressions for Eq [A5.14] be equal in the following proportions:

$$\left(\frac{1}{k_i}\,Ln\left(\frac{1}{\zeta_{zi}}\right) + U^{*}_{core}\right) u_{\tau_{Ri}} = \left(\frac{1}{k_o}\,Ln\left(\frac{1}{\zeta_{zo}}\right)\right) u_{\tau_{Ro}} \qquad [A5.17]$$

$$since \quad u_i = u_i^{*}\, u_{\tau_{Ri}}\,, \qquad u_o = u_o^{*}\, u_{\tau_{Ro}}$$

$$and \quad u_i = u_o \quad at \quad \zeta_i = \zeta_o = 1.0$$

The terms ζ_{zi} and ζ_{zo} are equal to z_{Ri}^{+}/δ_i^{+} and z_{Ro}^{+}/δ_o^{+}, respectively.

Eq [A5.17] can be re-arranged as follows:

$$u_{\tau_{Ri}}\, U^{*}_{core} = \frac{u_{\tau_{Ro}}}{k_o}\,Ln\left(\frac{1}{\zeta_{zo}}\right) - \frac{u_{\tau_{Ri}}}{k_i}\,Ln\left(\frac{1}{\zeta_{zi}}\right)$$

$$or \quad e^{\left(u_{\tau_{Ri}}\, U^{*}_{core}\right)} = \frac{\zeta_{zi}^{\left(\frac{u_{\tau_{Ri}}}{ki}\right)}}{\zeta_{zo}^{\left(\frac{u_{\tau_{Ro}}}{ko}\right)}} \qquad [A5.18]$$

Finaly, Eq [A5.18] is re-arranged to its final form:

$$\zeta_{zo}^{\left(\frac{u_{\tau_{Ro}}}{ko}\right)} = \frac{\zeta_{zi}^{\left(\frac{u_{\tau_{Ri}}}{ki}\right)}}{e^{\left(u_{\tau_{Ri}}\, U^{*}_{core}\right)}}$$

$$\zeta_{zo} = \frac{z^{+}_{Ro}}{\delta^{+}_{Ro}} = \frac{\zeta_{zi}^{\left(\frac{u_{\tau_{Ri}}}{u_{\tau_{Ro}}}\,\frac{ko}{ki}\right)}}{e^{\left(\frac{u_{\tau_{Ri}}}{u_{\tau_{Ro}}}\, U^{*}_{core}\, ko\right)}} \qquad [A5.19]$$

Appendix A.6

Non-dimensionalized Forms of Other Fluid Parameters

I. Bulk Velocity

The average, or bulk velocity of the fluid across the annulus section can be defined as:

$$u_b = \frac{\int_{R_{Ri}}^{R_{Ro}} 2\pi\ u(r)\ dr}{\int_{R_{Ri}}^{R_{Ro}} 2\pi\ r\ dr}$$

$$= \frac{2}{R_{Ro}^2 - R_{Ri}^2}\left[\int_{R_{Ri}}^{R_{m}} u_i\ r\ dr \quad + \quad \int_{R_{m}}^{R_{Ro}} u_o\ r\ dr\right]$$

The terms u_i, u_o, y_i and y_o can be replaced by their non-dimensional counterparts derived at Eq [A5.2]. The radius r takes either the form $R_{Ri} + y_i$ or $R_{Ro} - y_o$. The wall velocities u_i^+ and u_o^+ will cancel out. Therefore, the last expression can be re-arranged as:

$$u_b = \frac{2}{R_{Ro}^2 - R_{Ri}^2}\left[\int_0^1 u_i^+\ R_{Ri}(1 + \Delta_i\zeta_i)\nu\delta_i^+ d\zeta_i \quad + \quad \int_0^1 u_o^+\ R_{Ro}(1 - \delta_o\zeta_o)\nu\delta_o^+ d\zeta_o\right]$$

or

$$u_b = \frac{2\ \nu\ R_{Ri}}{R_{Ro}^2 - R_{Ri}^2}\left[\delta_i^+ \int_0^1 u_i^+\ (\ 1 + \Delta_i\zeta_i)\ d\zeta_i \quad + \quad \delta_o^+ \frac{R_{Ro}}{R_{Ri}} \int_0^1 u_o^+\ (\ 1 - \delta_o\zeta_o)\ d\zeta_o\right]$$

or

$$u_b = \frac{2\ \nu\ \alpha}{R_{Ro}(1 - \alpha^2)}\left[\delta_i^+ \int_0^1 u_i^+(1 + \Delta_i\zeta_i)d\zeta_i \quad + \quad \delta_o^+ \frac{1}{\alpha}\int_0^1 u_o^+(1 - \delta_o\zeta_o)\ d\zeta_o\right]$$

[A6.1]

II. Reynolds number

The Reynolds number for the annulus geometry is *defined* as:

$$Re = \frac{u_b\, D_H}{\nu} \qquad where \quad D_H = 2(R_{Ro} - R_{Ri})$$

$$= \frac{2\, u_b\, R_{Ro}\, (\,1 - \alpha)}{\nu}$$

Substituting Eq [A6.1] into the last expression yields:

$$\Upsilon = \frac{2R_{Ro}(1 - \alpha)}{\nu}$$

$$\Phi = \frac{2\nu\alpha}{R_{Ro}(1 - \alpha^2)}$$

and,

$$Re = \Upsilon\, \Phi \left[\delta_i^+ \int_0^1 u_i^+\, (1 + \Delta_i\zeta_i)d\zeta_i \; + \; \delta_o^+ \frac{1}{\alpha} \int_0^1 u_o^+\, (1 - \delta_o\zeta_o)d\zeta_o\right]$$

and finally,

$$Re = \frac{4\,\alpha}{(\,1 + \alpha)} \left[\alpha\ \delta_i^+ \int_0^1 u_i^+\, (1 + \Delta_i\zeta_i)d\zeta_i \; + \; \delta_o^+ \int_0^1 u_o^+\, (1 - \delta_o\zeta_o)d\zeta_o\right] \tag{A6.2}$$

III. Friction factor

The friction factor f is *defined* as:

$$f = \frac{R_{Ro} - R_{Ri}}{\rho\, u_b^2}\left(- \frac{\partial P}{\partial x}\right)$$

The pressure gradient can be expressed in terms of the surface shear stresses (refer to Appendix A1, Figure A1-1):

$$\tau_{R_{Ri}}\, R_{Ri} + \tau_{R_{Ro}}\, R_{Ro} = -\frac{1}{2}\,\frac{\partial P}{\partial x}\left(R_{Ro}^2 - R_{Ri}^2\right)$$

The pressure gradient in the definition equation for f is substituted with the last expression, yielding the following:

$$f = \frac{4(R_{Ro} - R_{Ri})(R_{Ro} - R_{Ri})^2}{Re^2\ \nu^2\ \rho}\left(\frac{\tau_{R_{Ri}}\ R_{Ri} + \tau_{R_{Ro}}\ R_{Ro}}{(R_{Ro}^2 - R_{Ri}^2)}\right) \times 2$$

$$= 8\frac{(R_{Ro} - R_{Ri})^3}{Re^2\ \nu^2\ \rho}\left(\frac{\tau_{R_{Ri}}\ R_{Ri} + \tau_{R_{Ro}}\ R_{Ro}}{(R_{Ro} + R_{Ri})(R_{Ro} - R_{Ri})}\right)$$

$$= \frac{8\ (R_{Ro} - R_{Ri})^2}{Re^2\ \nu^2(R_{Ro} + R_{Ri})}\ \frac{\tau_{R_{Ri}}}{\rho}\ R_{Ri}\left(1 + \frac{\tau_{R_{Ro}}}{\tau_{R_{Ri}}}\ \frac{1}{\alpha}\right)$$

Finally, the last expression can be re-arranged by expressing the radii in terms of α, and the shear stress in terms of the wall velocity, as shown here:

$$f = \frac{8(R_{Ro} - R_{Ri})^2\ \mu_{\tau_{Ri}}\ R_{Ri}^{+}}{Re^2\ \nu^2}\left(1 + \frac{\tau_{R_{Ro}}}{\tau_{R_{Ri}}}\ \frac{1}{\alpha}\right)$$

$$= \frac{8}{Re^2}\ \frac{\mu_{\tau_{R_{Ri}}}\ R_{Ri}^{+}}{\nu}\ \frac{R_{Ri}^2\ (\frac{1}{\alpha} - 1)^2}{R_{Ri}(\frac{1}{\alpha} + 1)}\left(1 + \frac{\tau_{R_{Ro}}}{\tau_{R_{Ri}}}\ \frac{1}{\alpha}\right)$$

$$= 8\left(\frac{R_{Ri}}{Re}\right)^2 \frac{(1 - \frac{1}{\alpha})^2}{(1 + \frac{1}{\alpha})}\left(1 + \frac{\tau_{R_{Ro}}}{\tau_{R_{Ri}}}\ \frac{1}{\alpha}\right) \qquad [A6.3]$$

Note that $\left(\frac{1}{\alpha} - 1\right)^2 = \left(1 - \frac{1}{\alpha}\right)^2$

IV. Nusselt number (Nu_{jj})

The Nusselt number Nu_{jj} will take on two separate forms, depending on the annulus surface being heated (Nu_{ii} for core surface heating; Nu_{oo} for outer surface heating). However, both Nu numbers are derived from the same root equation, which is defined here as:

$$N_{jj} = \frac{h_{jj}\, D_H}{k}$$

$$\text{where} \quad h_{jj} = \dot{q}''_{Rj}\,(T_{Rj} - T_b)$$

$$\text{and} \quad D_H = 2(R_{Ro} - R_{Ri})$$

replacing the heat transfer coefficient h_{jj} in the equation for Nu_{jj} gives:

$$Nu_{jj} = \frac{\dot{q}''_{Rj}\, 2(R_{Ro} - R_{Ri})}{(T_{Rj} - T_b)\, k}$$

and, from the definition of T_b^+,

$$Nu_{jj} = \frac{2\, \rho\, c_p\, (R_{Ro} - R_{Ri})}{T_b^+\, k}\, \mu_{\tau_j}$$

Therefore, for Nu_{ii}, the expression takes the form:

$$Nu_{ii} = \frac{2}{\alpha}\, \frac{\mu_{\tau_{Ri}} R_{Ri} \left(\dfrac{R_{Ro}}{R_{Ri}} - 1 \right)}{T_{b_i}^+} \qquad \text{where} \quad \alpha = \text{thermal diffusivity}$$

$$= 2\, \frac{\nu}{\alpha}\, \frac{R_{Ri}^+ \left(\dfrac{R_{Ro}}{R_{Ri}} - 1 \right)}{T_{b_i}^+}$$

$$= 2\, Pr\, R_{Ri}^+\, \frac{\left(\dfrac{1 - \alpha}{\alpha} \right)}{T_{b_i}^+} \qquad [A6.4]$$

$$\text{where} \quad \alpha = \text{radius ratio} \quad \frac{R_{Ri}}{R_{Ro}}$$

The development of the expression for Nu_{oo} is similar and yields the equation:

$$Nu_{oo} = 2\, Pr\, R_{Ro}^+\, \frac{(1 - \alpha)}{T_{b_o}^+} \qquad [A6.5]$$

V. Bulk Temperature Tb^+

A non-dimensionalized bulk temperature can be defined in a way similar to that for the bulk fluid velocity. In this case, the definition is given as:

$$t_b = \frac{\int_{R_{Ri}}^{R_{Ro}} 2\pi\ u(r)\ T(r)\ dr}{\int_{R_{Ri}}^{R_{Ro}} 2\pi\ u(r)\ r\ dr}$$

That equation can decomposed into two parts by utilizing the definition of the dimensionless temperature T_j^+ (refer to Appendix A.3):

$$T_j = T_{R_j} - \frac{T_j^+\ \dot{q}''_{Rj}}{\rho\ c_p\ \mu_{\tau_{Rj}}}$$

Thus, the definition equation can be re-written as :

$$(T_b)_j = \frac{T_{Rj} \int_{R_{Ri}}^{R_{Ro}} u(r)\ r\ dr}{\int_{R_{Ri}}^{R_{Ro}} u(r)\ r\ dr} - \frac{\dot{q}''_{Rj}}{\rho\ c_p\ \mu_{\tau_{Rj}}} \frac{\int_{R_{Ri}}^{R_{Ro}} u(r)\ r\ T(r)_j^+\ dr}{\int_{R_{Ri}}^{R_{Ro}} u(r)\ r\ dr}$$

Which reduces to:

$$(T_b)_j = T_{Rj} - \frac{\dot{q}''_{Rj}}{\rho\ c_p\ \mu_{\tau_{Rj}}} \frac{\int_{R_{Ri}}^{R_{Ro}} u(r)\ r\ T(r)_j^+\ dr}{\int_{R_{Ri}}^{R_{Ro}} u(r)\ r\ dr}$$

This last equation can be further reduced by replacing the integral at the denominator by the equivalence:

$$\int_{R_{Ri}}^{R_{Ro}} u(r)\ r\ dr = \frac{1}{4}\ \nu\ R_{Ro}\ Re\ (\ 1 + \alpha)$$

which can be easily derived from the definition of the bulk velocity and the Reynolds number.

The substitution changes the equation to:

$$(T_b)_j = T_{Rj} - \frac{4\,\dot{q}''_{Rj}}{\rho\ c_p\ \mu_{\tau_{Rj}}} \frac{\int_{R_{Ri}}^{R_{Ro}} u(r)\ r\ T(r)^+_j\ dr}{\nu\ R_{Ro}\ Re\ (\ 1 + \alpha)} \qquad [A6.6]$$

The integral at the numerator can be expanded by making substitutions similar to those made for the development of the expression for the bulk velocity

$$\int_{R_{Ri}}^{R_{Ro}} u(r) r T(r)^+_j\ dr =$$

$$R_{Ri}\nu\delta_i^+ \left[\int_0^1 u_i^+\ R_{Ri}(1 + \Delta_i\zeta_i)\ T_i^+\ d\zeta_i \ + \ \int_0^1 u_o^+\ R_{Ro}(1 - \delta_o\zeta_o)\ T_o^+\ d\zeta_o\right]$$

[A6.7]

Inserting Eq [A6.7] into [A6.6] yields the new expression:

$$Tb_j = T_{Rj} - \Lambda \times \left[\frac{\delta_i^+}{\mu_{\tau_{Ri}}}\int_0^1 u_i^+\ R_{Ri}\ (1 + \Delta_i\zeta_i)\ T_i^+\ d\zeta_i\right]$$

$$+ \ \Lambda \times \left[\frac{\delta_o^+}{\mu_{\tau_{Ro}}\ \alpha}\int_0^1 u_o^+\ R_{Ro}\ (1 - \delta_o\zeta_o)\ T_o^+\ d\zeta_o\right] \qquad [A6.8]$$

$$where \quad \Lambda = \frac{\dot{q}''_{Rj}\ 4\ R_{Ri}}{\rho\ c_p\ R_{Ro}\ Re\ (1 + \alpha)}$$

Eq [A6.8] can still be reduced to a more compact form. Multiply both sides of Eq [A6.8] by -1, add T_{Rj} and multiply by $\rho c_p \mu_{\tau k}/q_{Rj}$. The left side of Eq [A6.8] now appears as the definition of the non-dimensional bulk temperature, where the subscript k indicates the value of the subscript j (for core heating, j=k=i; for outer surface heating, j=k=o). The generic form of the new equation becomes:

$$T_{b_j} = \Omega \times \left[\alpha\ \delta_i^+ \left(\frac{\mu_{\tau_k}}{\mu_{\tau_i}}\right) \int_0^1 u_i^+\ R_{Ri}\ (1 + \Delta_i\zeta_i)\ T_i^+\ d\zeta_i\right]$$

$$+\ \Omega \times \left[\delta_o^+ \left(\frac{\mu_{\tau_k}}{\mu_{\tau_o}}\right) \int_0^1 u_o^+\ R_{Ro}\ (1 - \delta_o\zeta_o)\ T_o^+\ d\zeta_o\right]$$

$$where \quad \Omega = \frac{4}{Re\ (1 + \alpha)}$$

[A6.9]

Finally, Eq [A6.9] can be expressed specifically for the case of core heating and outer surface heating, by replacing the subscript k with the appropriate subscript i or o:

$$T_{b_i}^+ = \Omega \times \left[\alpha\ \delta_i^+ \int_0^1 u_i^+\ R_{Ri}\ (1 + \Delta_i\zeta_i)\ T_i^+\ d\zeta_i\right]$$

$$+\ \Omega \times \left[\delta_o^+ \left(\frac{\mu_{\tau_i}}{\mu_{\tau_o}}\right) \int_0^1 u_o^+\ R_{Ro}\ (1 - \delta_o\zeta_o)\ T_o^+\ d\zeta_o\right] \qquad [A6.10]$$

and

$$T_{b_o}^+ = \Omega \times \left[\alpha\ \delta_i^+ \left(\frac{\mu_{\tau_o}}{\mu_{\tau_i}}\right) \int_0^1 u_i^+\ R_{Ri}\ (1 + \Delta_i\zeta_i)\ T_i^+\ d\zeta_i\right]$$

$$+\ \Omega \times \left[\delta_o^+\ \int_0^1 u_o^+\ R_{Ro}\ (1 - \delta_o\zeta_o)\ T_o^+\ d\zeta_o\right] \qquad [A6.11]$$

Appendix B
Laminar flow analysis

The momentum characteristic of a fluid flowing in an annulus in the laminar regime in a fully developed state can be completely solved analytically. Starting from the fundamental momentum equation, Eq [1.1], the simplifications due to symmetry, constant velocity profile and constant fluid parameters causes Eq [1.1] to be reduced to the form:

$$\frac{1}{r}\frac{\partial}{\partial r}\left(\mu\, r\,\frac{\partial u(r)}{\partial r}\right) = +\frac{\partial P}{\partial x}$$

$$\textit{Integrating once yields} \quad r\,\frac{\partial u}{\partial r} = \frac{1}{2\,\mu}\frac{\partial P}{\partial x} + C_1$$

$$\textit{Integrating again yields} \quad u(r) = \frac{1}{4\,\mu}\frac{\partial P}{\partial x}\,r^2 + C_1\,Ln(r) + C_2$$

[*B1*.1]

The most general case is found when both annular surfaces are moving at different velocities V_i and V_o . Therefore, the boundary conditions applicable to Eq [B1.1} are:

$u = V_i$ at $r = R_{Ri}$

$u = V_o$ at $r = R_{Ro}$

Substitute these particular values for u and r into Eq [B1.1] to find C_1:

$$V_o = A\times R_{Ro}^2 + C_1\,Ln(R_{Ro}) + C_2 \qquad [B1.2]$$

$$-\quad V_i = A\times R_{Ri}^2 + C_1\,Ln(R_{Ri}) + C_2 \qquad [B1.3]$$

$$V_o - V_i = A\times(R_{Ro}^2 - R_{Ri}^2) + C_1\,Ln\left(\frac{R_{Ro}}{R_{Ri}}\right)$$

$$\textit{thus}\ C_1 = \frac{(V_o - V_i) - A\times(R_{Ro}^2 - R_{Ri}^2)}{B}$$

$$\textit{with}\ A = \frac{1}{4\,\mu}\frac{\partial P}{\partial x} \qquad \textit{and} \qquad B = Ln\left(\frac{R_{Ro}}{R_{Ri}}\right)$$

By adding Eq [B1.2] and [B1.3], the expression for C_2 is directly obtained:

$$C_2 = \frac{(V_o + V_i)}{2} - A\frac{(R_{Ro}^2 + R_{RI})}{2} - \frac{C_1}{2} Ln\ (R_{RI} \cdot R_{Ro})$$

Eq [B1.1] can now be re-written by direct substitution of C_1 and C_2:

$$u(r) = A\left[r^2 - \left(\frac{R_{Ro}^2 - R_{RI}^2}{2}\right)\right] + C_1\left[Ln\ (r) - \frac{1}{2} Ln\ (R_{Ro} \cdot R_{RI})\right] + \left(\frac{V_o + V_i}{2}\right)$$

Note that the terms in the brackets following C_1 can be re-written as:

$$Ln\left(\frac{r}{\sqrt{R_{Ro} \cdot R_{RI}}}\right)$$

Now, substitute the expression for C_1 into the equation for u(r) and introduce a new parameter R_M, such that:

$$2\ R_M^2 = \frac{R_{Ro}^2 - R_{RI}^2}{Ln\left(\frac{R_{Ro}}{R_{RI}}\right)}$$

Then, with some re-arranging, the expression for u(r) can be written in its final form:

$$u(r) = A\left[r^2 - \left(\frac{R_{Ro}^2 - R_{RI}^2}{2}\right) - 2\ R_M^2\ Ln\left(\frac{r}{\sqrt{R_{Ro}\ R_{RI}}}\right)\right]$$
$$+ \left(\frac{V_o - V_i}{Ln\left(\frac{R_{Ro}}{R_{RI}}\right)}\right) Ln\left(\frac{r}{\sqrt{R_{RI}\ R_{Ro}}}\right) + \frac{V_o + V_i}{2}$$

The special case where $V_i = V_o = 0$ yields the familiar expression for the static annulus: The meaning of R_M becomes apparent when the position of maximum velocity is sought

$$u(r) = \frac{1}{4\mu}\frac{\partial P}{\partial x}\left[r^2 - \left(\frac{R_{Ro}^2 - R_{Ri}^2}{2}\right) - 2\,R_M^2\,Ln\left(\frac{r}{\sqrt{R_{Ro}\,R_{Ri}}}\right)\right] \qquad [B1.4]$$

($\delta u/\delta r = 0$). Taking the derivative of Eq [B1.4] and equating to zero gives:

$$\frac{\partial u(r)}{\partial r} = 0 = \frac{1}{4\mu}\frac{\partial P}{\partial x}\left[2r - 2\,R_M^2 \times \frac{\sqrt{R_{Ri}\,R_{Ro}}}{r} \times \frac{1}{\sqrt{R_{Ro}\,R_{Ri}}}\right]$$

The terms inside the square brackets reduce to

$$2r - 2\,\frac{R_M^2}{r} = 0$$

$$or\ r^2 = R_M^2$$

Hence, the term R_M represents the location of maximum fluid velocity within the annular passage. When it is re-inserted into the derivative equation above, the expression obtained is readily seen to be:

$$R_M^2 = \frac{R_{Ro}^2 - R_{Ri}^2}{2\,Ln\left(\frac{R_{Ro}}{R_{Ri}}\right)} = R_{lam}^2 \qquad [B1.5]$$

which is the expression set in the development of Eq [B1.4].

Another version of Eq [B1.4] can be derived by extracting R_{Ro} from the right hand side of the equation and replacing R_M^2 by Eq [B1.5}:

$$u(r) = \frac{1}{4\mu}\frac{\partial P}{\partial x}R_{Ro}^2\left[\left(\frac{r}{R_{Ro}}\right)^2 - \left(\frac{1-\alpha^2}{2}\right) - \frac{1-\alpha^2}{Ln\,(\alpha)}\left(\frac{\frac{r}{R_{Ro}}}{\sqrt{\alpha}}\right)\right]$$

$$= \frac{1}{4\mu}\frac{\partial P}{\partial x} R_{Ro}^2 \left[\left(\frac{r}{R_{Ro}}\right)^2 - \frac{1}{2} - \frac{\alpha^2}{2} - \left(\frac{\alpha^2 - 1}{Ln\,(\alpha)}\right)\left(Ln\left(\frac{r}{R_{Ro}}\right) - \frac{1}{2} Ln\,(\alpha) \right) \right]$$

Now, let $B = \dfrac{\alpha^2 - 1}{Ln\,(\alpha)}$ *and re-arrange the previous expression:*

$$= \frac{1}{4\mu}\frac{\partial P}{\partial x} R_{Ro}^2 \left[\left(\frac{r}{R_{Ro}}\right)^2 - \frac{1}{2} - \frac{\alpha^2}{2} - B\,Ln\left(\frac{r}{R_{Ro}}\right) - \left(\frac{1 - \alpha^2}{2}\right) \right]$$

$$\longrightarrow \quad u(r) = -\frac{1}{4\mu}\frac{\partial P}{\partial x} R_{Ro}^2 \left[1 - \left(\frac{r}{R_{Ro}}\right)^2 + B\,Ln\left(\frac{r}{R_{Ro}}\right) \right] \qquad [B1.6]$$

The bulk velocity can be easily found using the definition given at Appendix A.6. Substituting the expression for u(r) from Eq [B1.6] then integrating directly, one obtains:

$$V_b = -\frac{2A}{1 - \alpha^2}\left[\frac{R_{Ro}^2}{4}(1 - \alpha^2)^2 + \frac{B\,R_{Ro}^2}{2}\left(\frac{r}{R_{Ro}}\right)^2 \left(Ln\left(\frac{r}{R_{Ro}}\right) - \frac{1}{2} \right) \right] \Bigg|_{\alpha}^{1}$$

Note that the limits of integration are from R_{Ri} to r_{Ro}, or equivalently, from R_{Ri}/R_{Ro} to R_{Ro}/R_{Ro} (hence, from α to 1). The above expression reduces to:

$$V_b = -\frac{2A\,R_{Ro}^2}{4}\left[(1 - \alpha^2) + \frac{1}{(1 - \alpha^2)}\{- B + B\,\alpha^2 - 2B\alpha^2\,Ln(\alpha)\} \right]$$

Note that the logarithmic term can be replaced by:

$$2B\alpha^2\,Ln\,(\alpha) = 2\,(1 - \alpha^2)\,\alpha^2$$

by direct substitution of the term B defined in Eq [B1.6].

With that last substitution, the expression for the bulk velocity is readily obtained by simple manipulations:

$$V_b = -\frac{A\,R_{Ro}^2}{2}\left[\,1 + \alpha^2 - B\right] \qquad [B1.7]$$

Finally, by dividing Eq [B1.4] by [B1.7], one obtains the immediate result:

$$\frac{u(r)}{V_b} = +\frac{2}{M}\left[1 - \left(\frac{r}{R_{Ro}}\right)^2 + B\,Ln\left(\frac{r}{R_{Ro}}\right)\right]$$

$$where\ M = 1 + \alpha^2 - B$$

Appendix C
Numerical curve fitting - fundamentals

The process of developing an empirical formula based on a set of inter-related data is called *curve fitting*[1]. If y is the output variable (dependent) and x_1, x_2, ...x_n the n control variables (independent), the process can be reduced to finding a formula of the form[2]:

$$y = f(x_1, x_2, ..., x_n) \;=\; a_1\, g(x_1) \;+\; a_2\, g(x_2) \;+ ... +\; a_n\, g(x_n)$$

where a_i are coefficients and $g(x_i)$ are single valued functions. The traditional approach to finding the values of a_i and $g(x_i)$ is the *least square* fitting method, whereby an error ϵ is defined as:

$$\epsilon_i \;=\; \{y_i \;-\; f(x_1, x_2, ..., x_n)\}^2$$

$$and \;\sum_{i=1}^{n} \epsilon_i \;=\; 0$$

This method requires, as a working hypothesis, that the coefficients a_i be independent of each other. Furthermore, the function f must be linear. The error term ϵ can be found by taking its derivative:

$$\frac{\partial \epsilon_i}{\partial a_i} \;=\; \frac{\partial (y_i - f)^2}{\partial a_i} \;=\; -2 \sum_{i=1}^{n} g(x_i)\, [y_i - a_1\, g(x_1) \;+\; a_2\, g(x_2) \;+ ... +\; a_n\, g(x_n)\,]$$

The n derivative expressions produce a set of linear equations, which can be expressed in a matrix form:

---

1 The methodology was borrowed from concepts presented by Pfaffenberger and Peterson [48].

2 See LaFara [49] pp.145-155

$$\begin{vmatrix} g(x_1)\sum g(x_1) & g(x_1)\sum g(x_2) & \dots & g(x_1)\sum g(x_n) \\ g(x_2)\sum g(x_1) & g(x_2)\sum g(x_2) & \dots & g(x_2)\sum g(x_n) \\ \dots & & & \\ g(x_n)\sum g(x_1) & g(x_n)\sum g(x_2) & \dots & g(x_n)\sum g(x)n \end{vmatrix} \times \begin{vmatrix} a_1 \\ a_2 \\ \dots \\ a_n \end{vmatrix} = \begin{vmatrix} y_1 \\ y_2 \\ \dots \\ y_n \end{vmatrix}$$

This matrix equation can then easily solved for the a_i.

The functions $g(x_i)$ must be established as control variables, with known form. The best known form of the function $g(x_i)$ is the polynomial, where $g(x_i) = x^i$.

If the function f is not linear, the procedure can still be applied by linearizing it. For example, if

$$f(\alpha) = C_1 \times \alpha^{C_2}$$

$$\textit{where} \quad \alpha = \textit{control variable} \quad \textit{and} \quad C_1, C_2 \quad \textit{are constant}$$

the expression can linearized by taking the logarithm on each side:

$$\log [\, f(\alpha) \,] = \log [C_1] + C_2 \, Log \, [\, \alpha \,]$$

This latter expression lends itself readily to the matrix procedure described above.

The faithfulness of the empirical expression (how close the predicted value of the function f is to the real value y) can be assessed by measuring its *correlation factor*. Let *SSE* be the sum of the errors ϵ_i, *SST be the sum of the point deviations and* CORR, the correlation coefficient. Then CORR can be shown to be[3]:

---

3 Pfaffenberger and Patterson [48]

$$CORR = \sqrt{\frac{SST - SSE}{SST}}$$

$$\text{with} \quad SSE = \sum_{k=1}^{n\ points} \epsilon_k \qquad \text{and} \qquad SST = \sum_{k=1}^{n\ points} (y_k - y_{mean})^2$$

A perfect fit to a set of datum points is given by CORR = 1.0. A complete absence of relationship between the curve fit and the datum points is given by CORR = 0.0.

Appendix D

Graphical results

Annulus with rough core

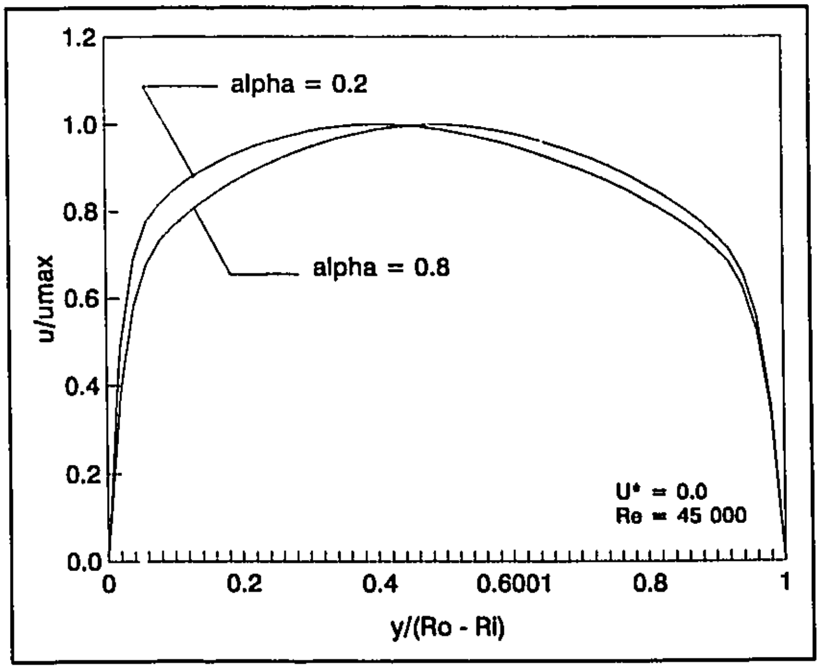

Figure 1: Velocity profile in smooth annulus - static core

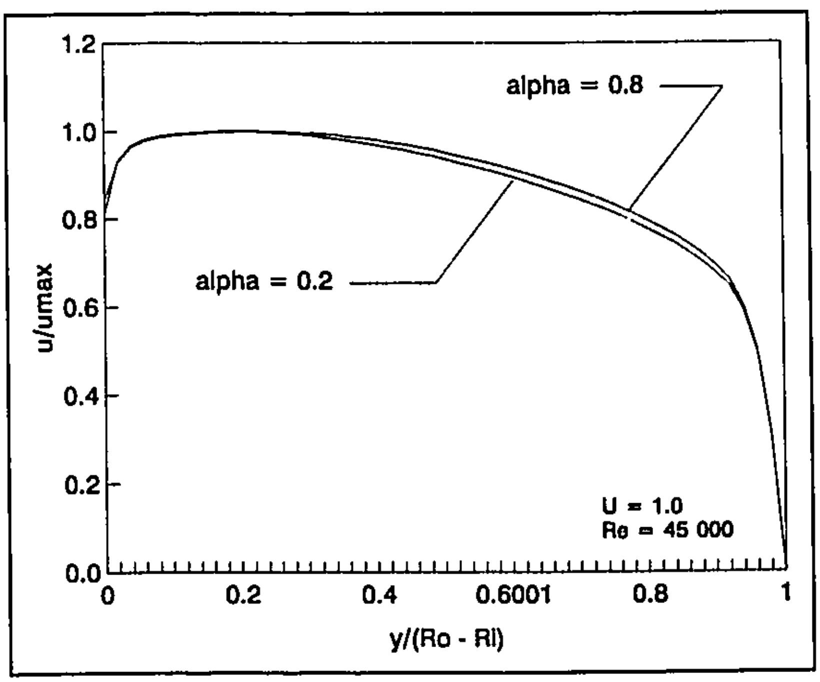

Figure 2: Velocity profile in smooth annulus - moving core

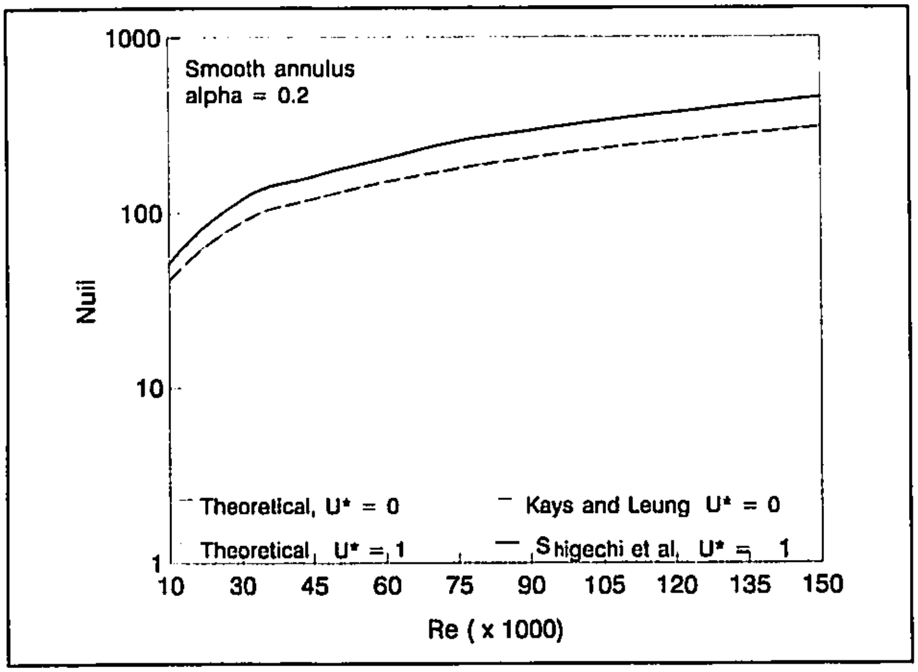

Figure 3: Nu vs Re in smooth annulus

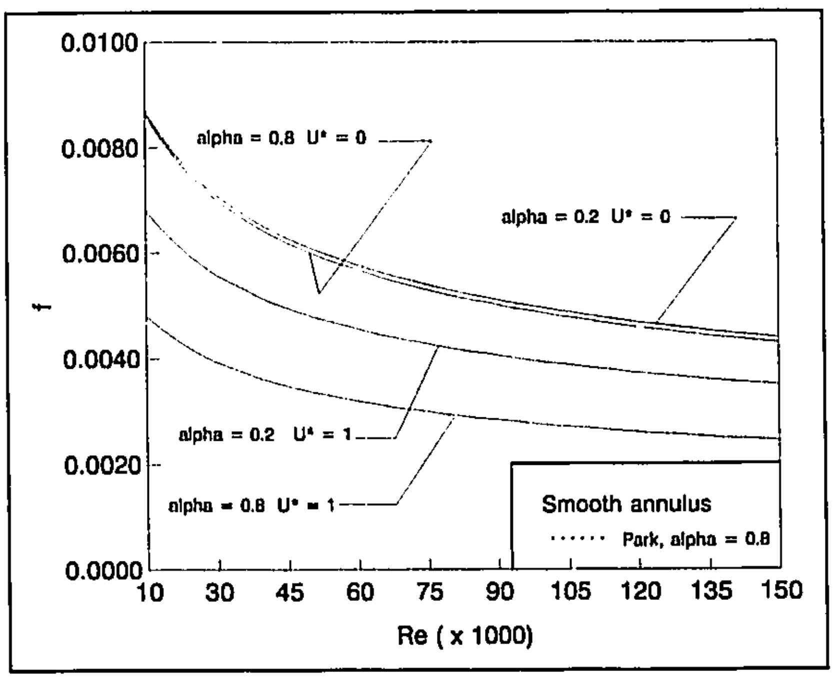

Figure 4: Friction factor f in smooth annulus

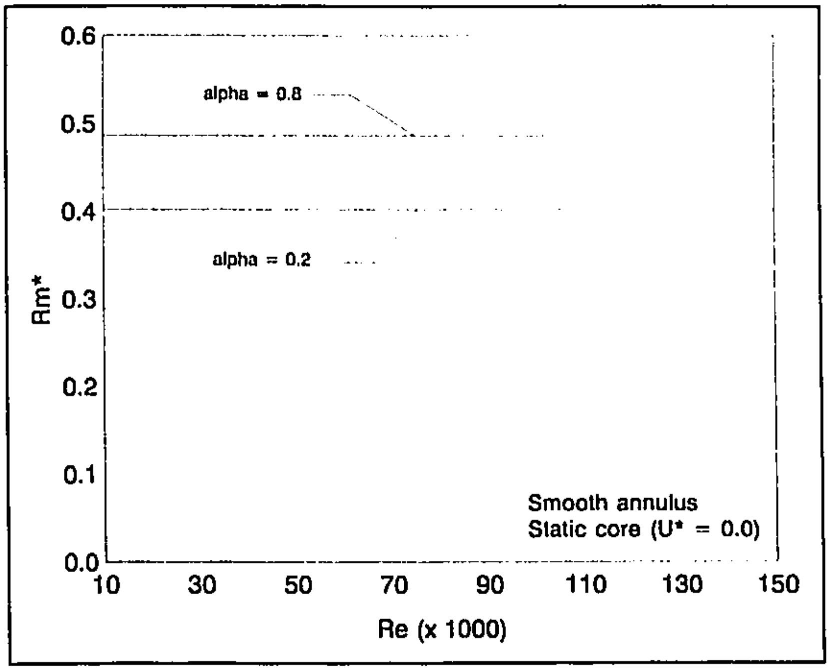

Figure 5: R_M^* vs Re - smooth annulus

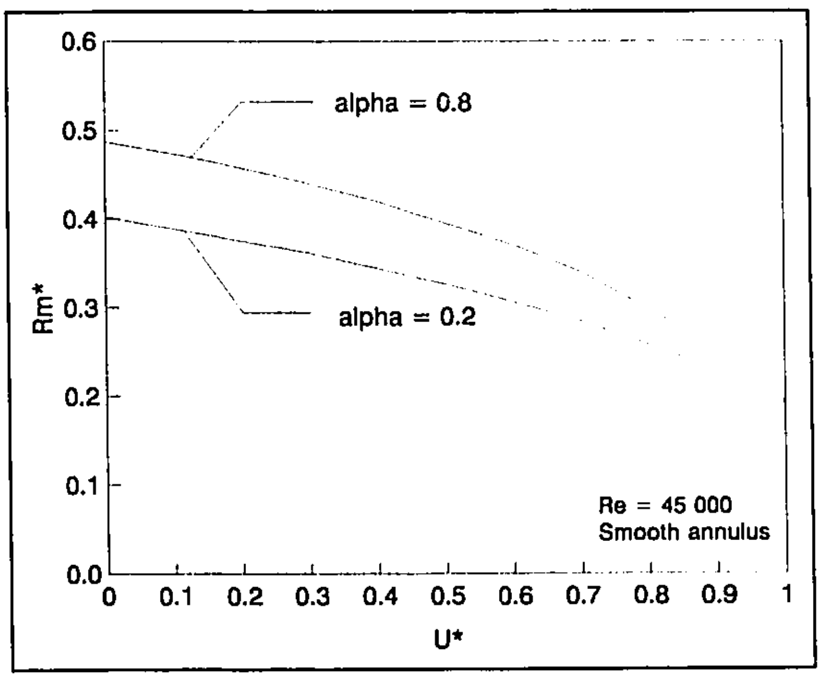

Figure 6: R_M^* vs U^* in smooth annulus

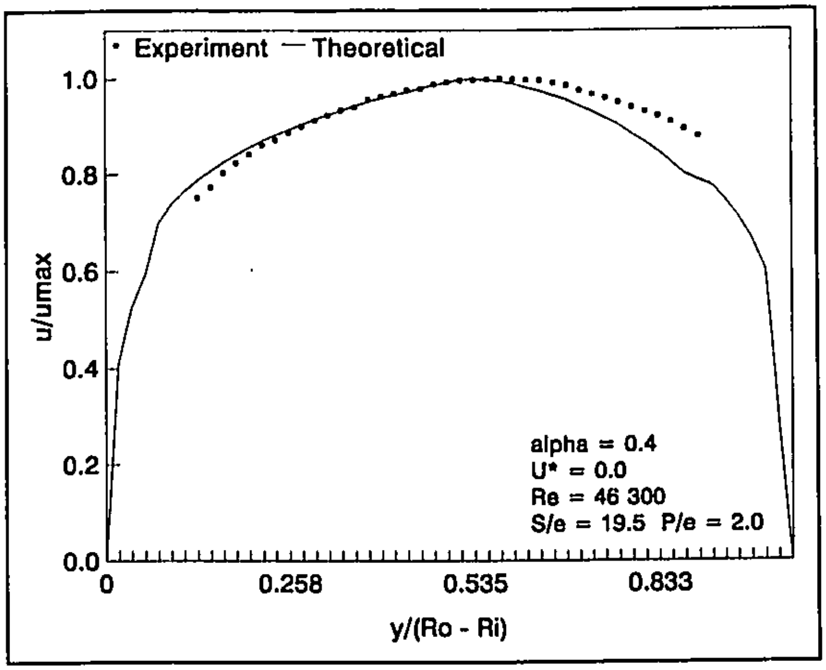

Figure 7: Velocity profile, rough core, compared to data of Ahn [26]

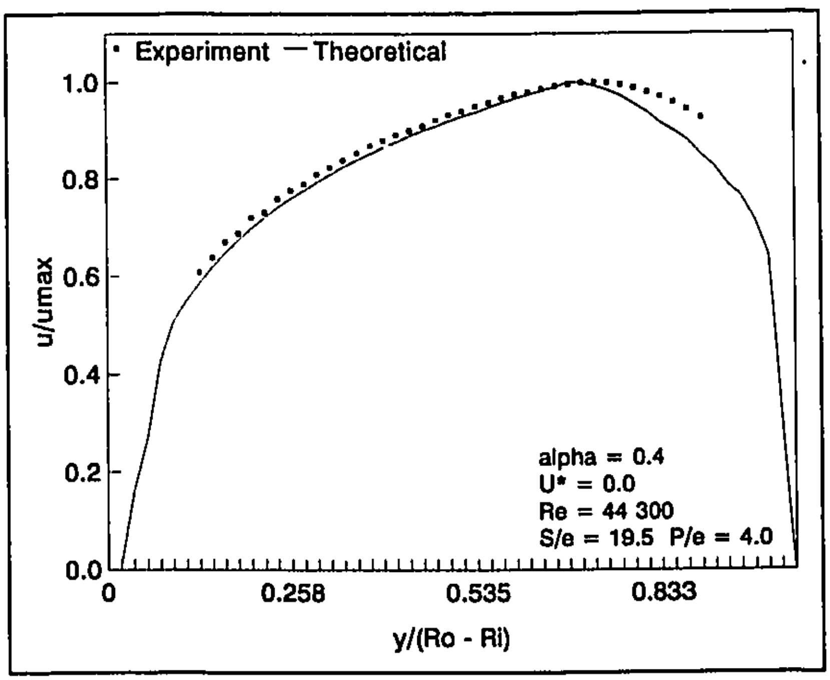

Figure 8: Velocity profile, rough core, compared to data of Ahn [26]

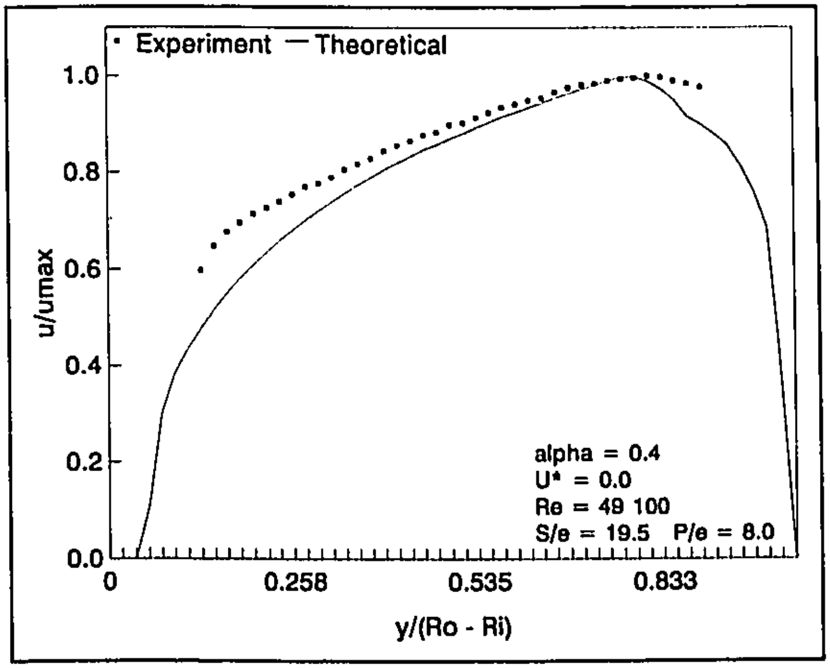

Figure 9: Velocity profile, rough core, compared to data of Ahn [26]

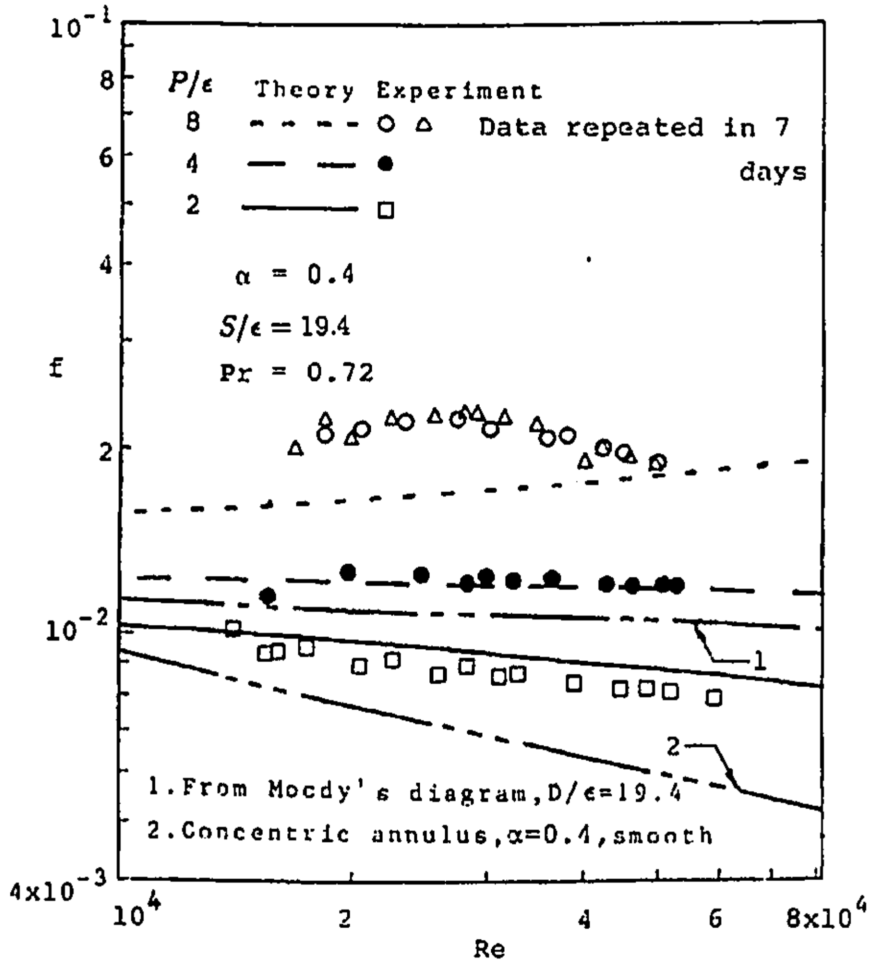

Figure 10: Friction factor - experimental results (From Ahn [26])

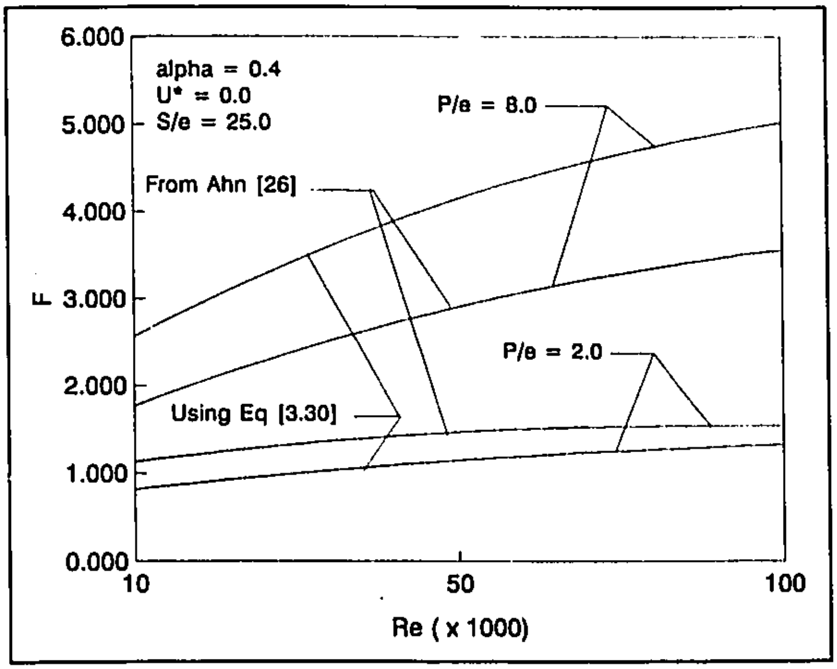

Figure 11: Comparison of predictions from Ahn [26] with present study

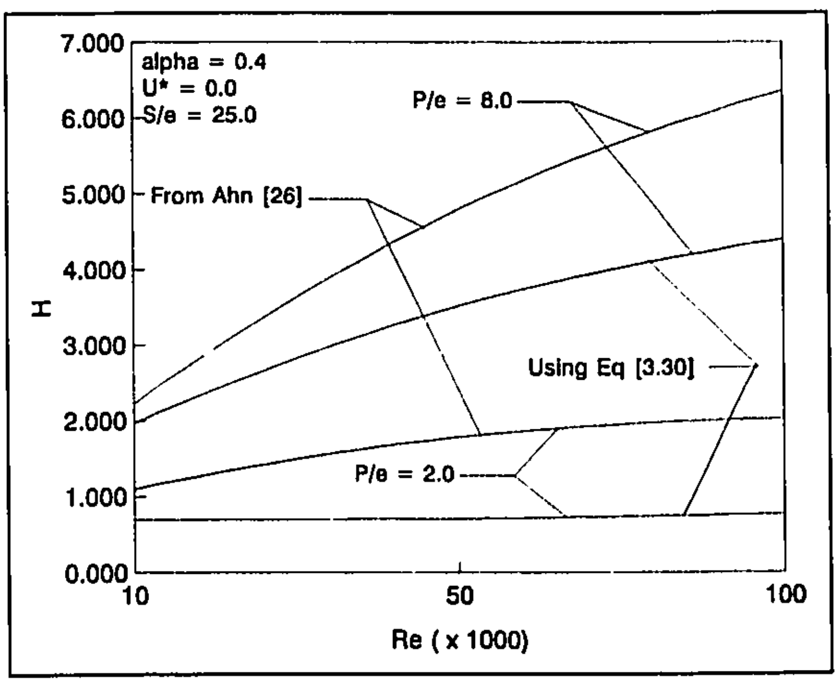

Figure 12: Comparison of predictions of Ahn [26] with present study

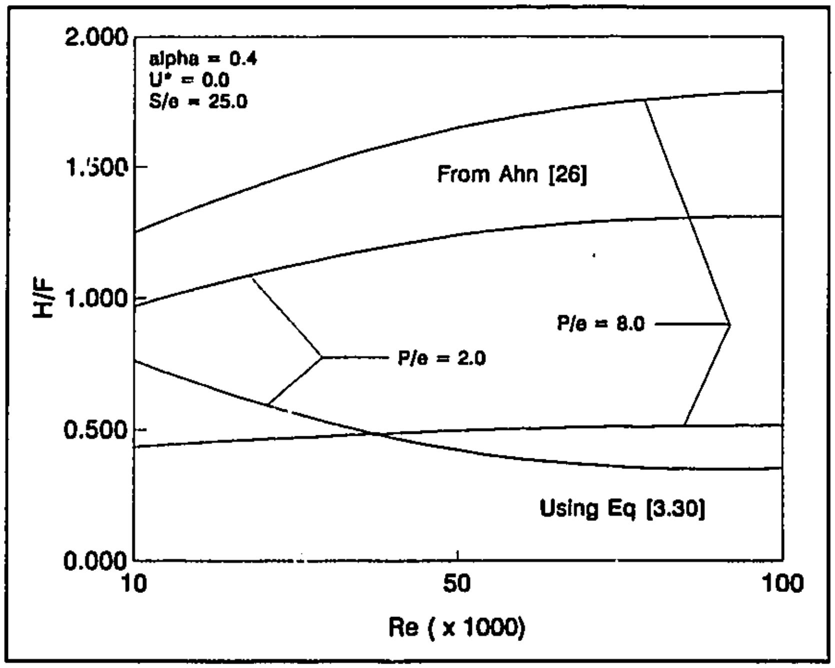

Figure 13: Comparison of predictions of Ahn [26] with present study

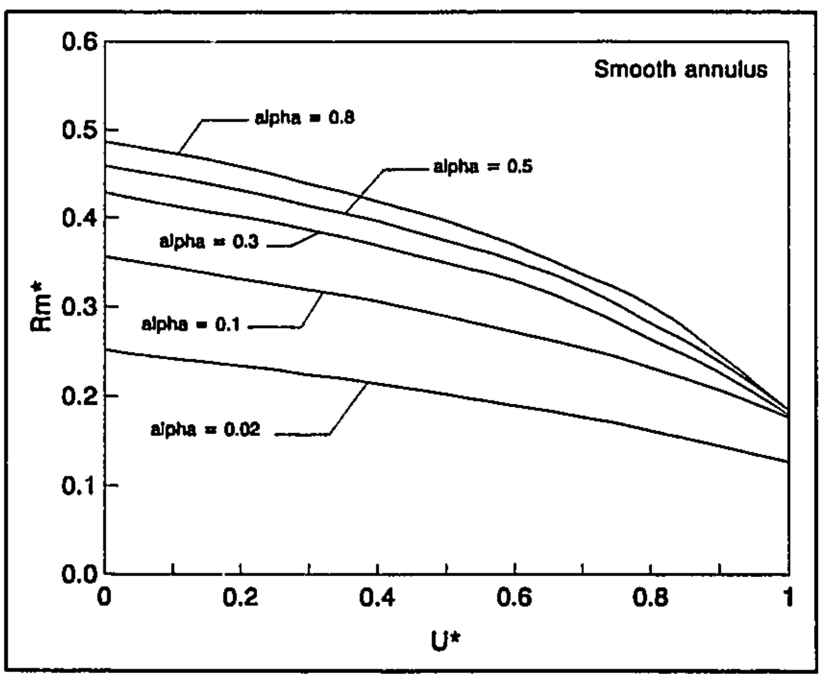

Figure 14: Predicted R_M^* vs U^* using Eq [5.1] and [5.2]

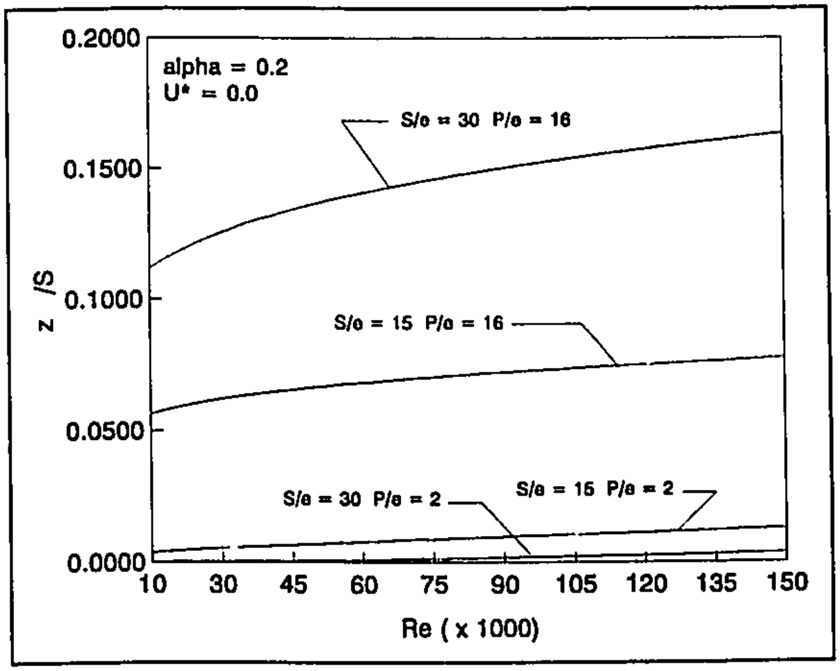

Figure 15: z_{or}/S vs Re using Eq [3.32]

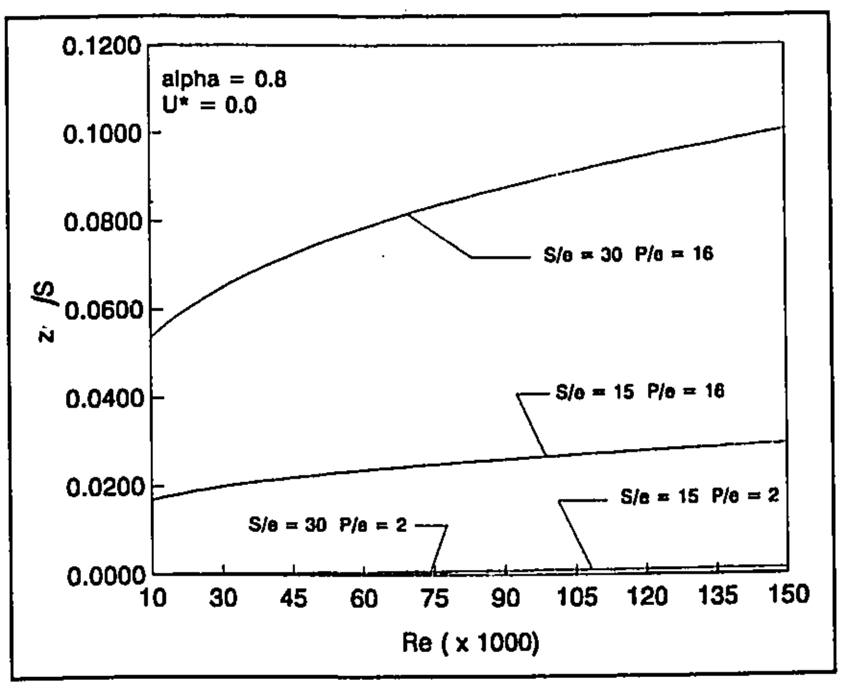

Figure 16: z_{or}/S vs Re using Eq [3.32]

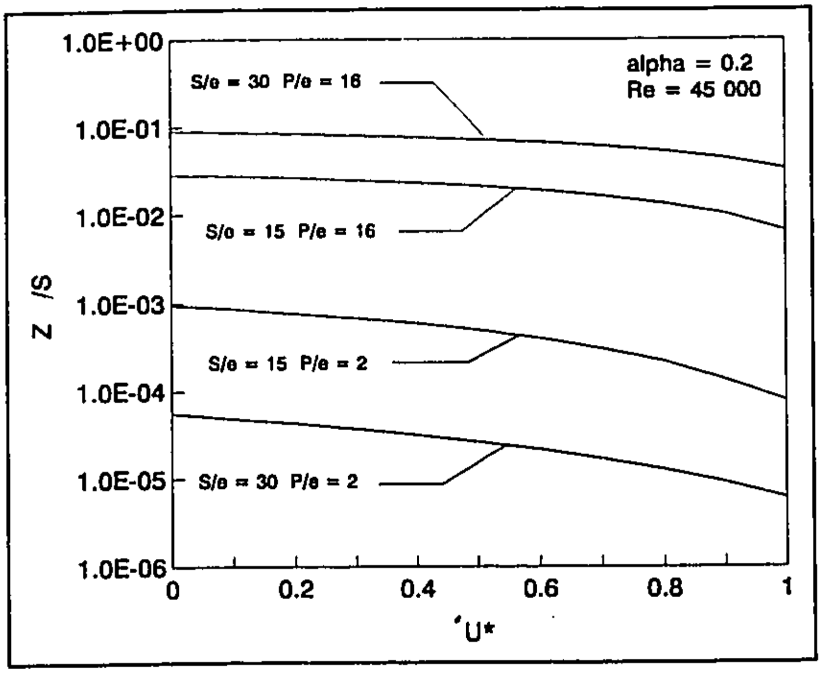

Figure 17: Effects of U* on z_{or}/S using Eq [3.32]

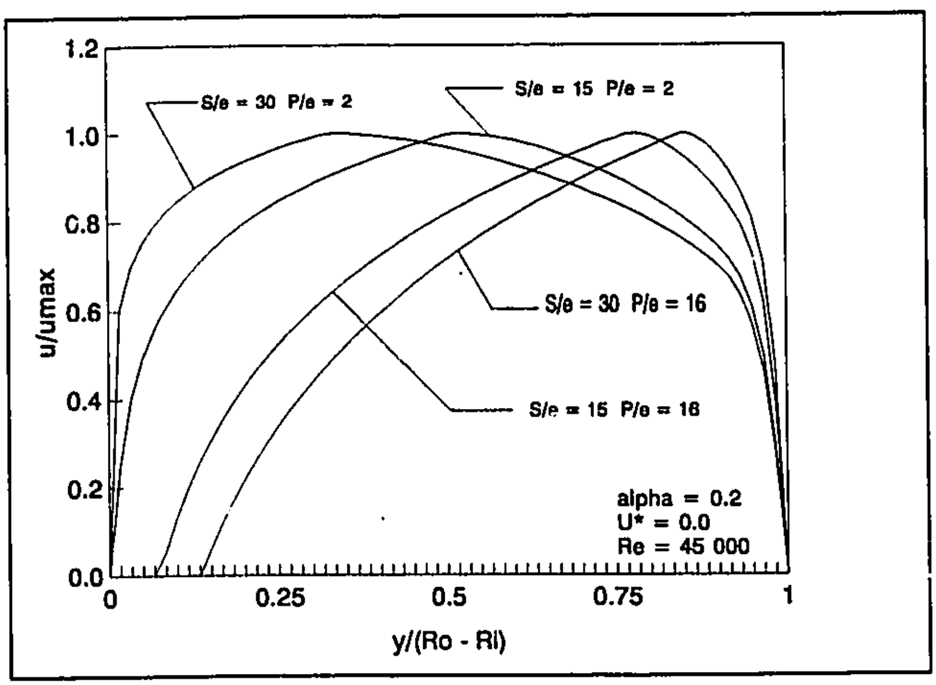

Figure 18: Effects of roughness on the velocity profiles

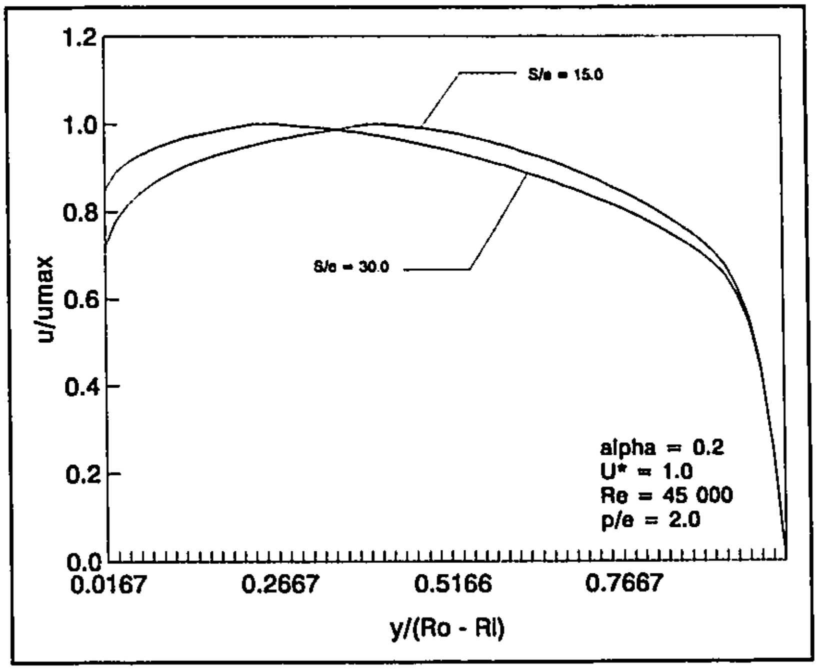

Figure 19: Effects of roughness and core motion on velocity profiles

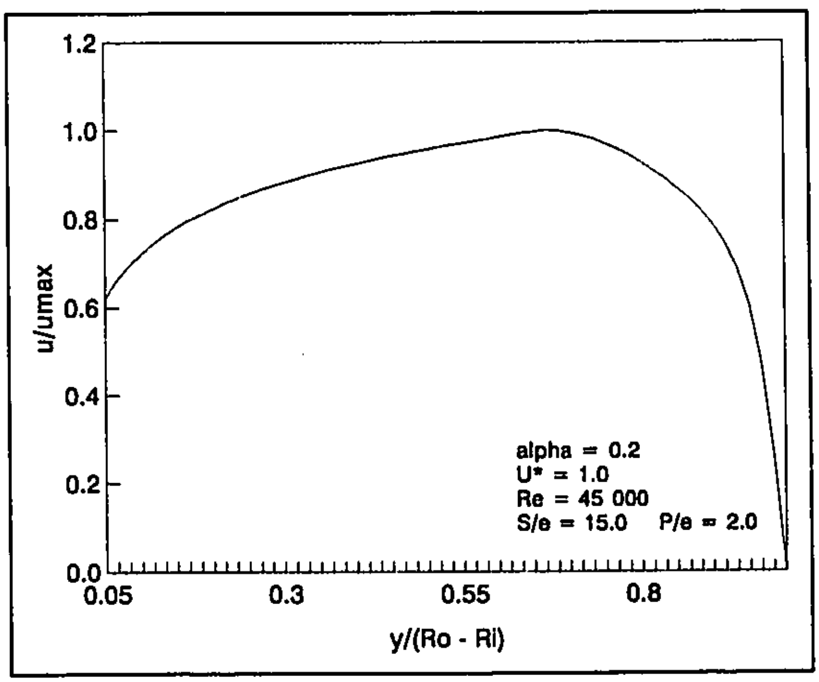

Figure 20: Effects of roughness and core motion on velocity profile

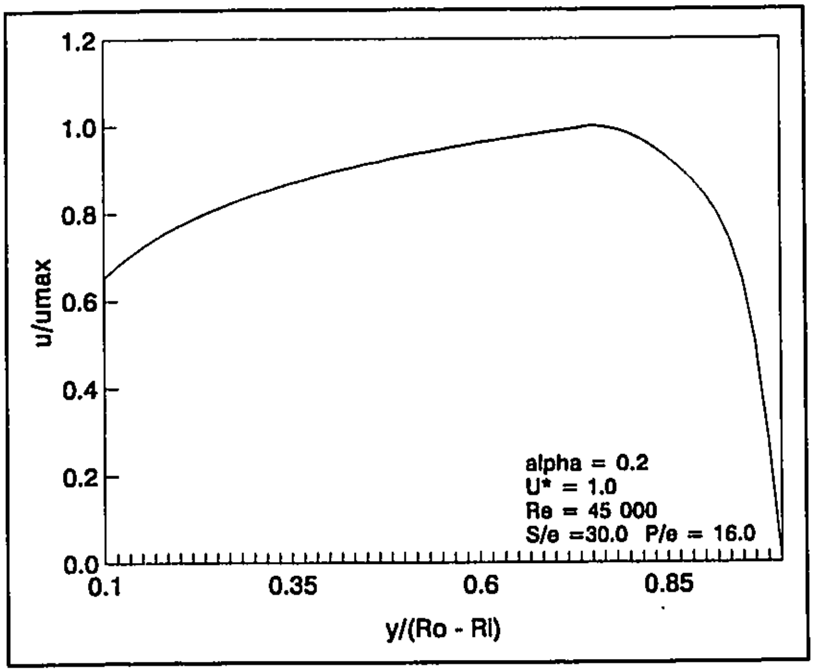

Figure 21: Effects of roughness and core motion on velocity profiles

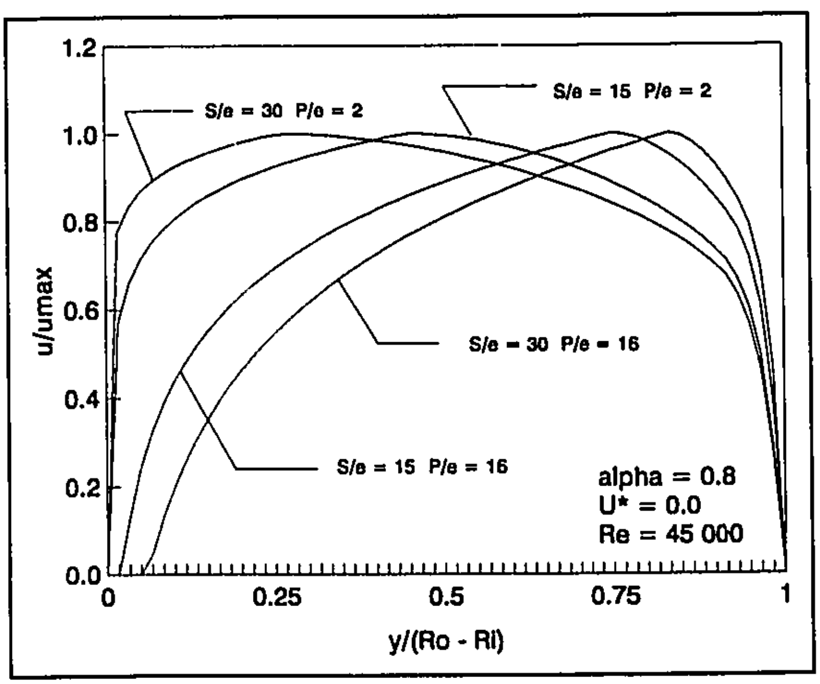

Figure 22: Effects of roughness on velocity profiles, static core

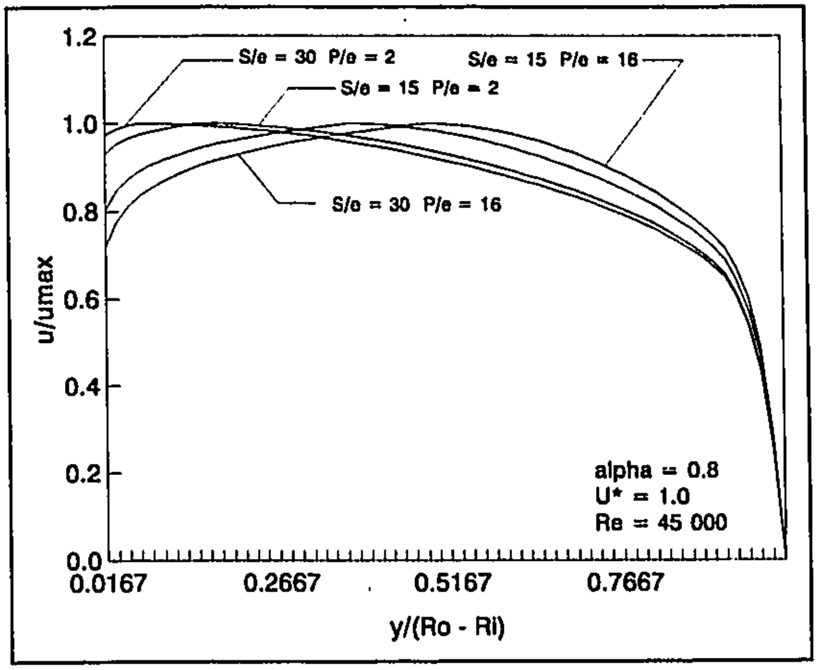

Figure 23: Effects of roughness and core motion on velocity profiles

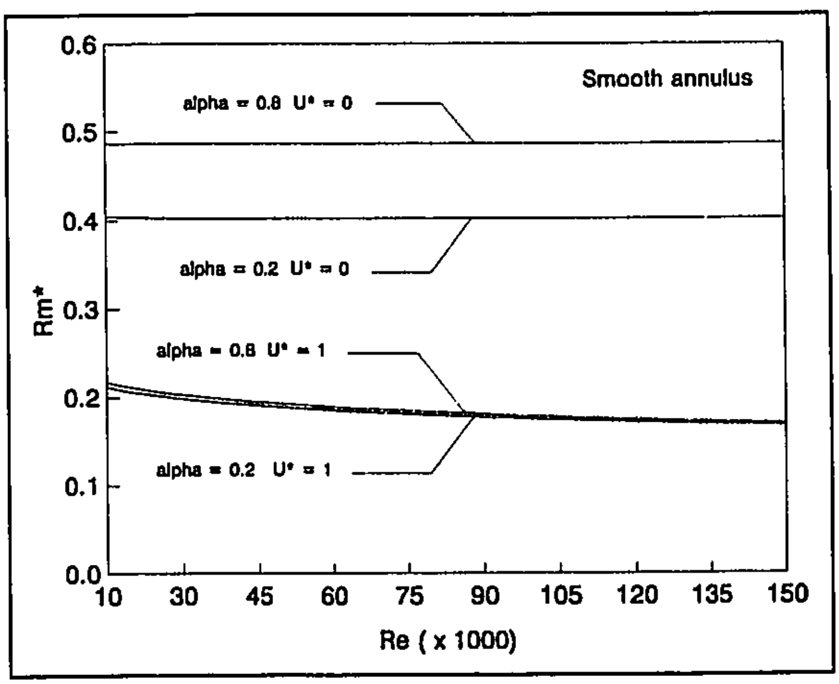

Figure 24: R_M^* vs Re in smooth annulus

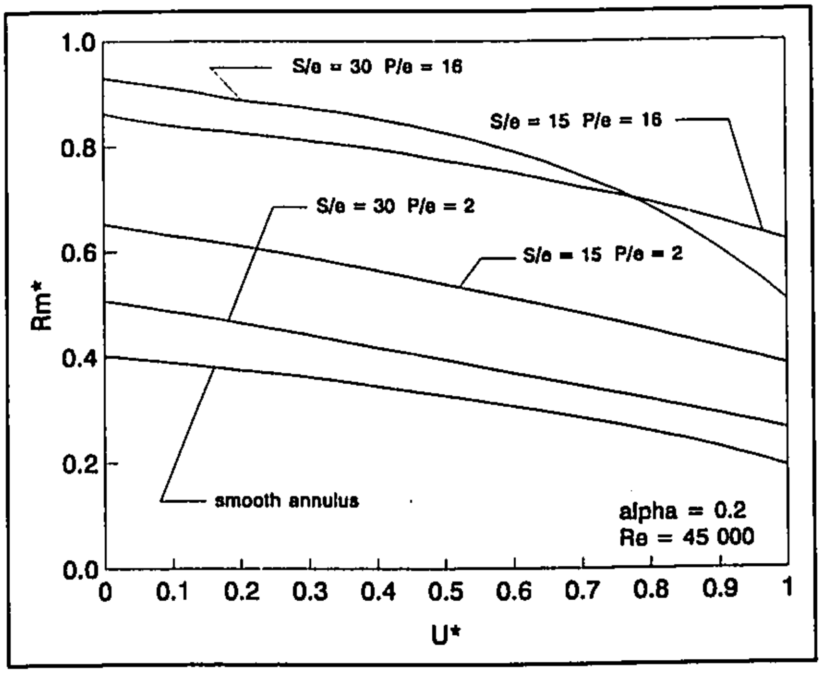

Figure 25: R_M^* vs U^* in rough annulus

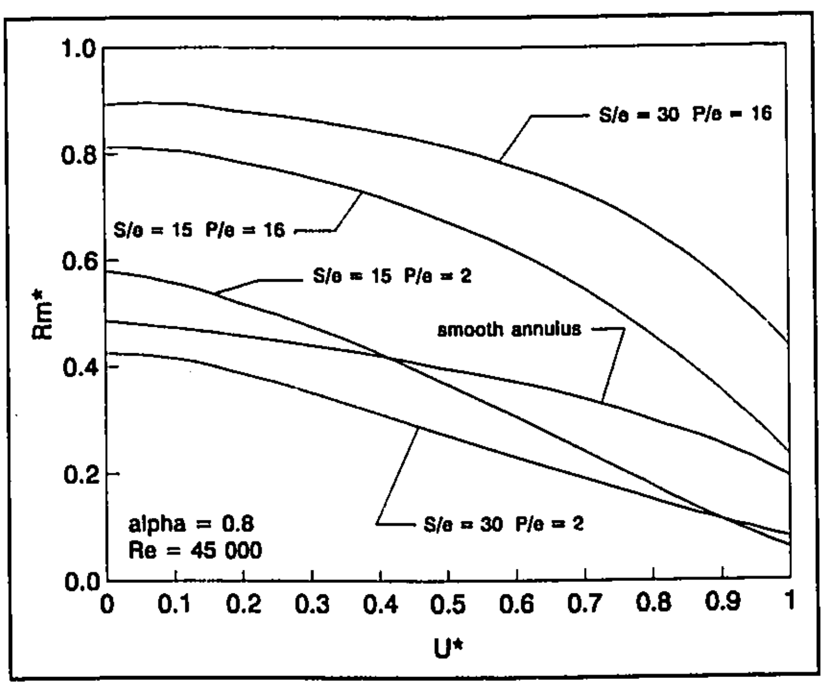

Figure 26: R_M^* vs U^* in rough annulus

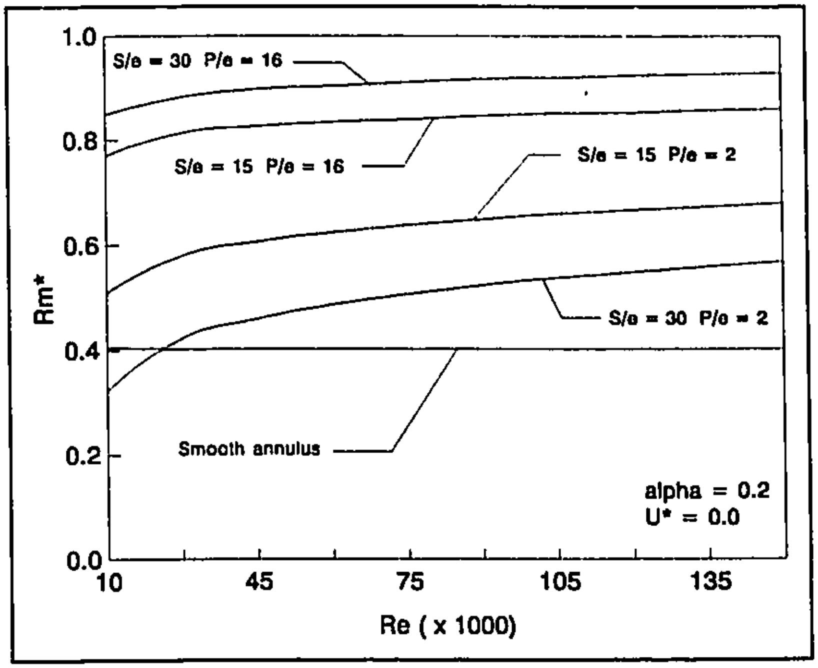

Figure 27: Effects of roughness on R_M^* (vs Re)

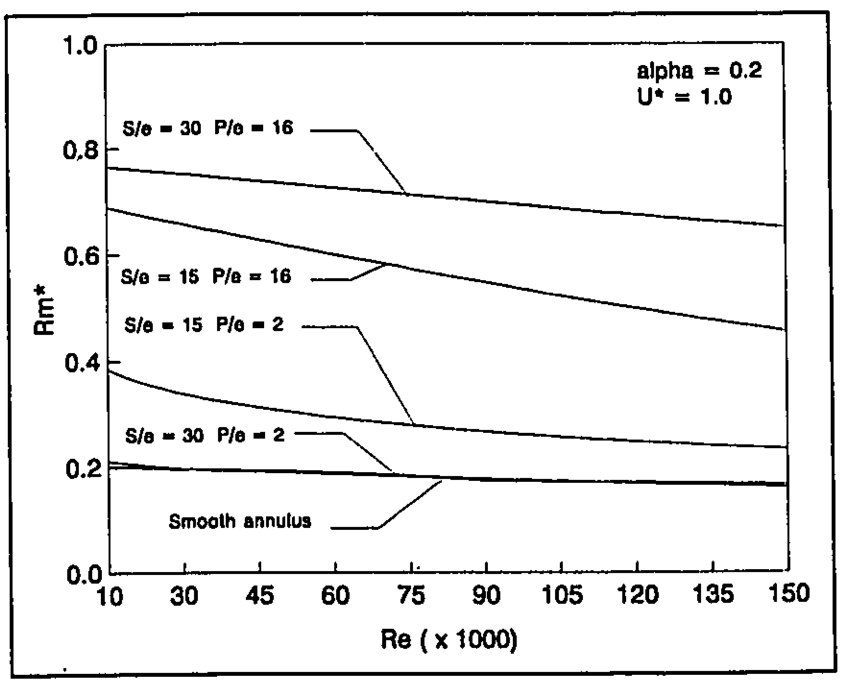

Figure 28: Effects of roughness and core motion on R_M^* (vs Re)

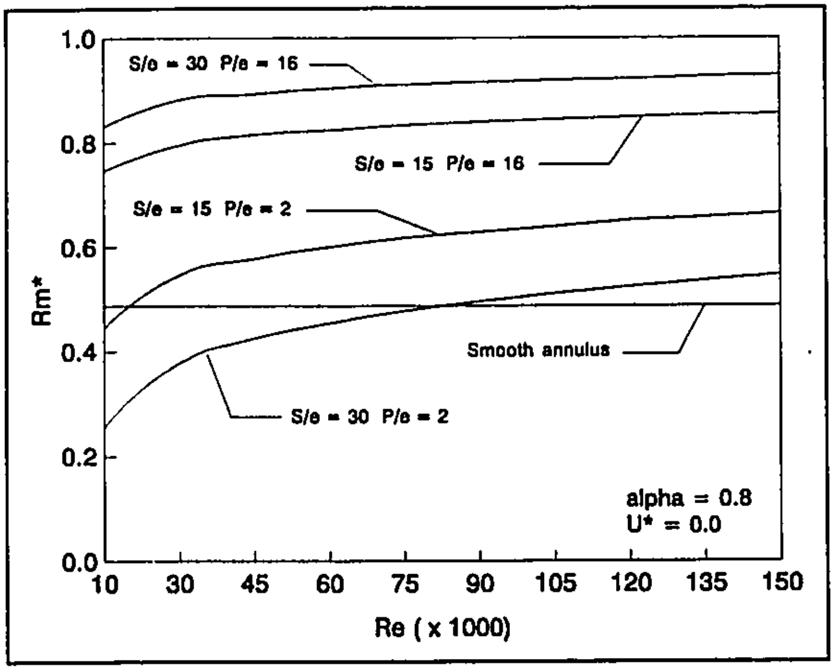

Figure 29: Effects of roughness on R_M^* (vs Re)

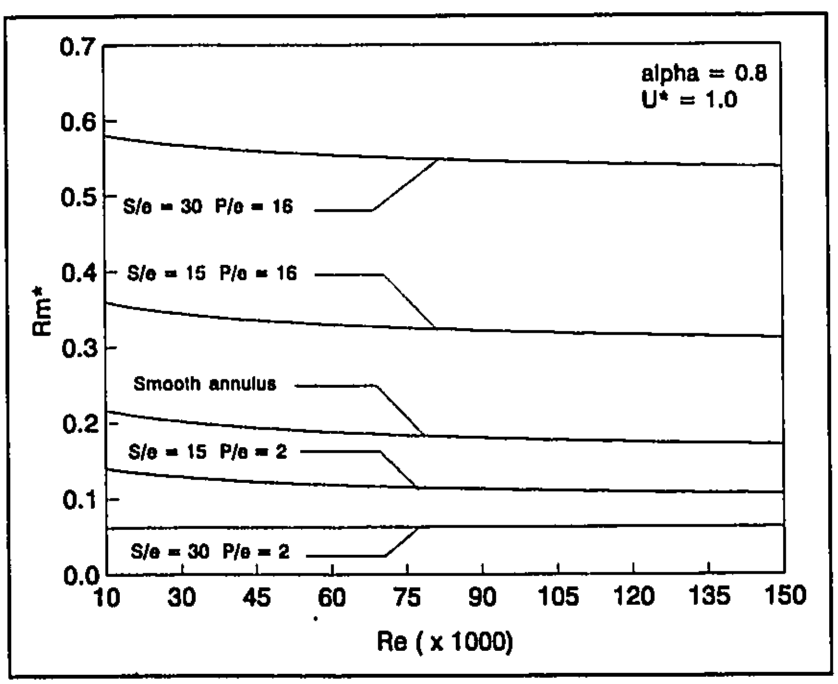

Figure 30: Effects of roughness and core motion on R_M^* (vs Re)

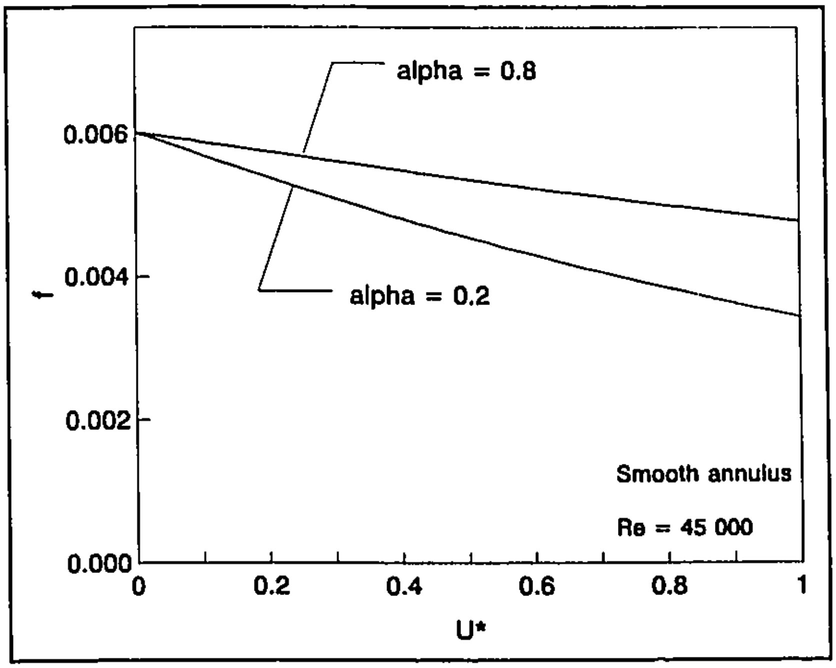

Figure 31: f vs U* in smooth annulus

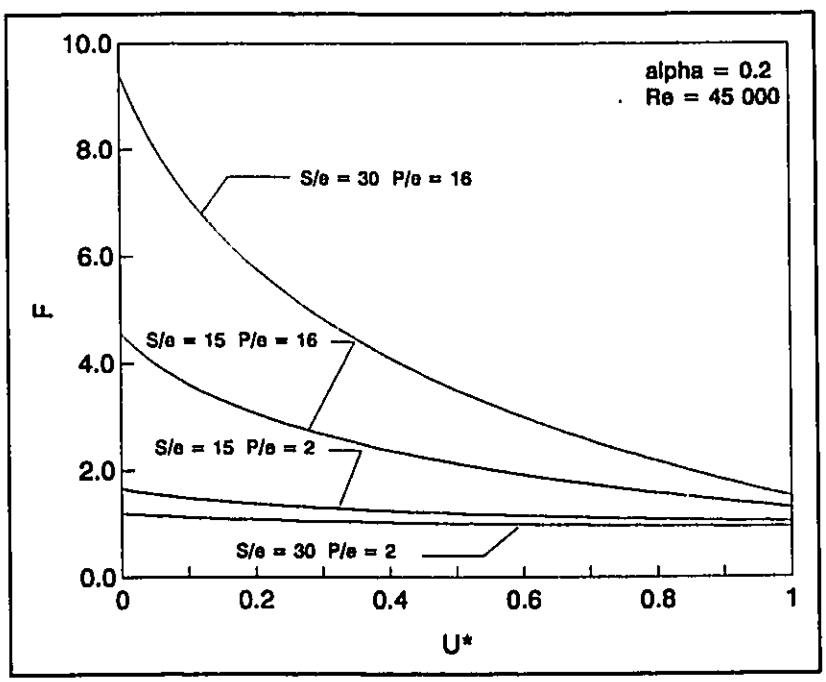

Figure 32: Effects of roughness on F (vs U*)

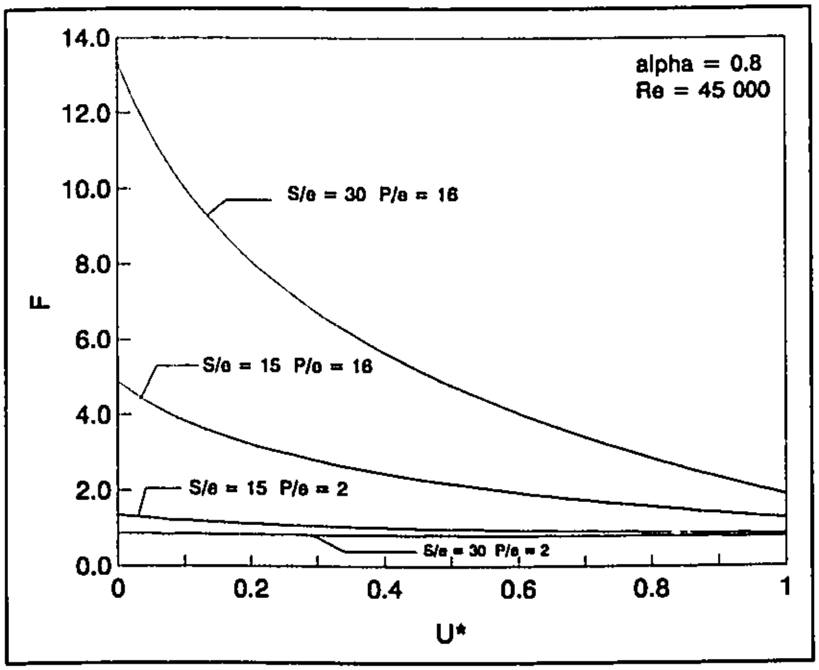

Figure 33: Effects of roughness on F (vs U*)

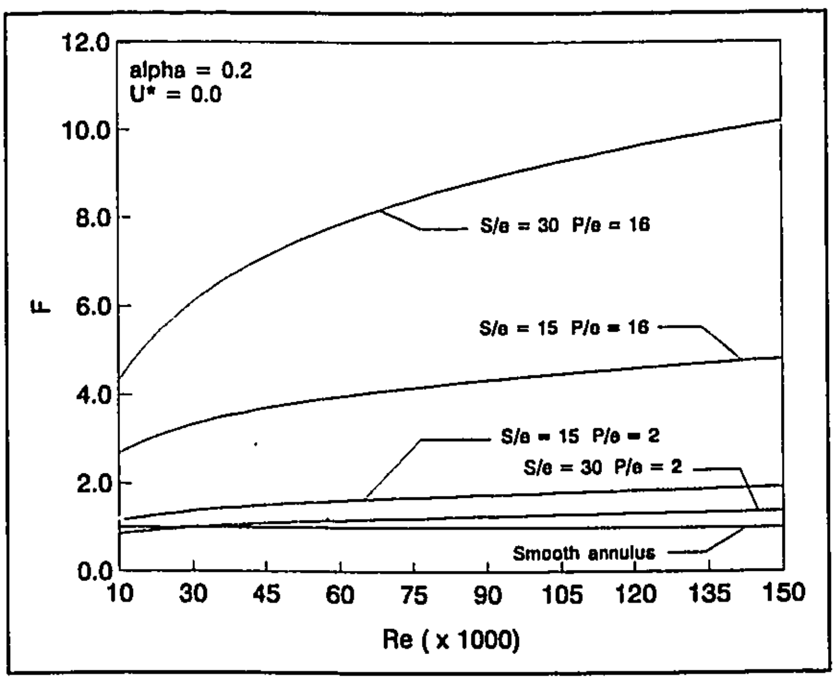

Figure 34: F vs Re in rough core annulus - static core

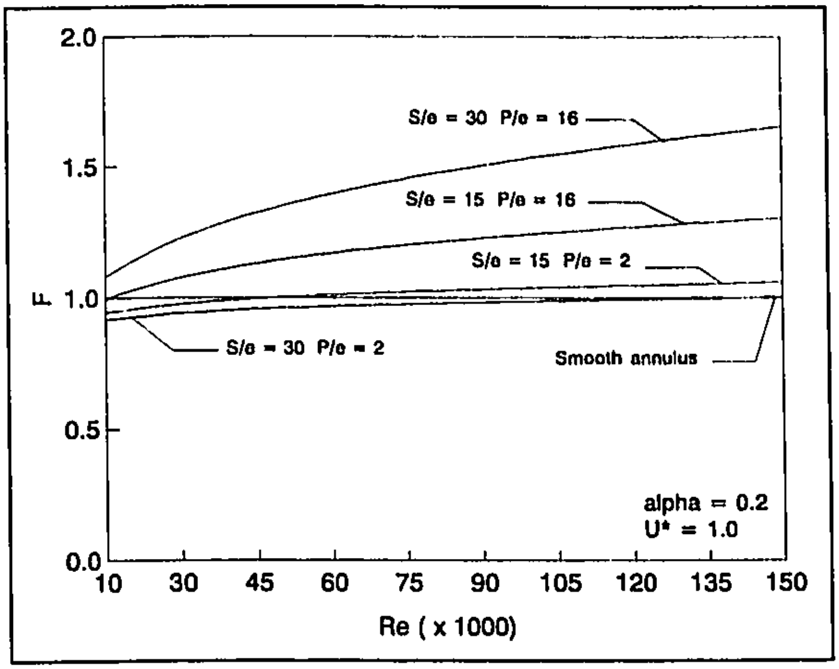

Figure 35: F vs Re in rough core annulus - moving core

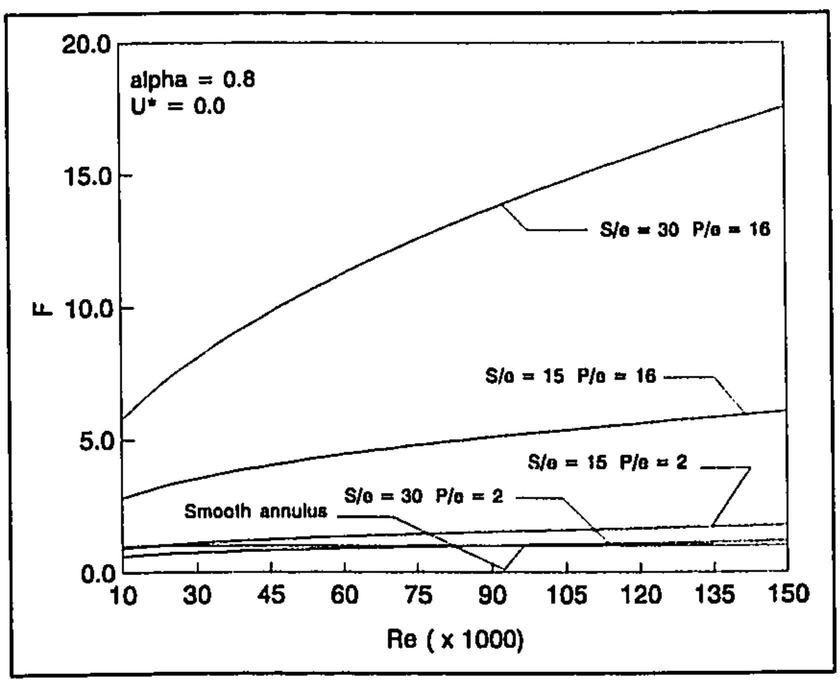

Figure 36: F vs Re in rough core annulus - static core

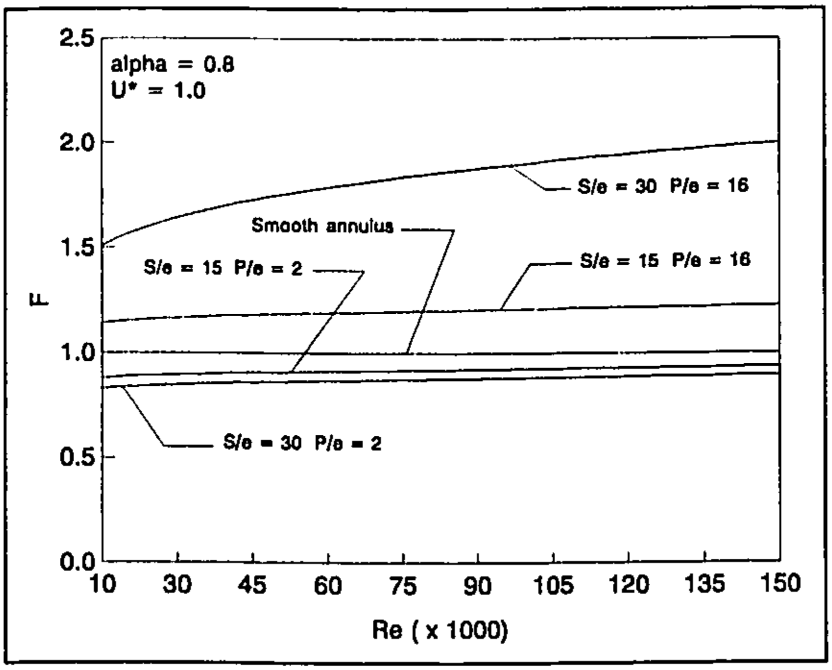

Figure 37: F vs Re in rough core annulus - moving core

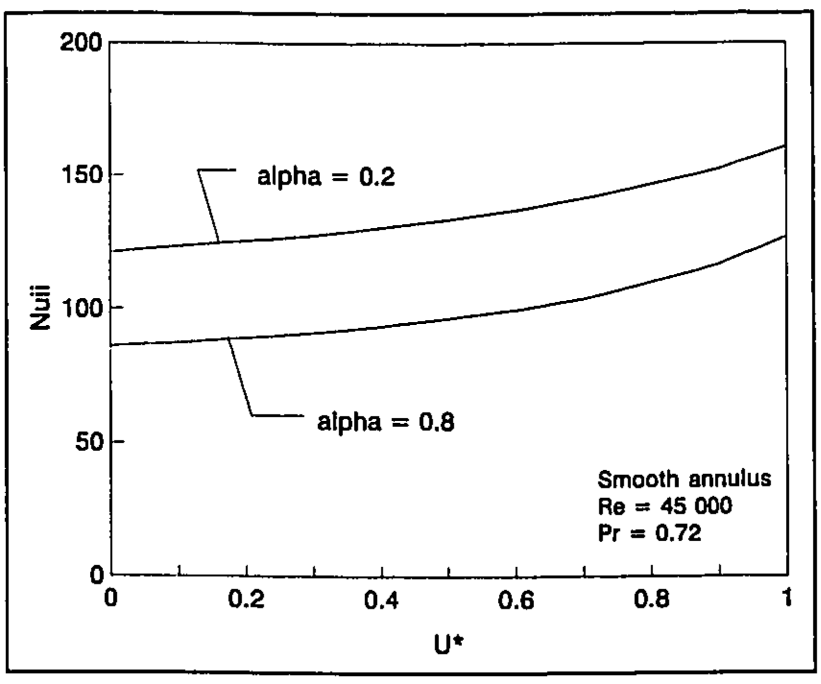

Figure 38: Nu vs U* in smooth annulus

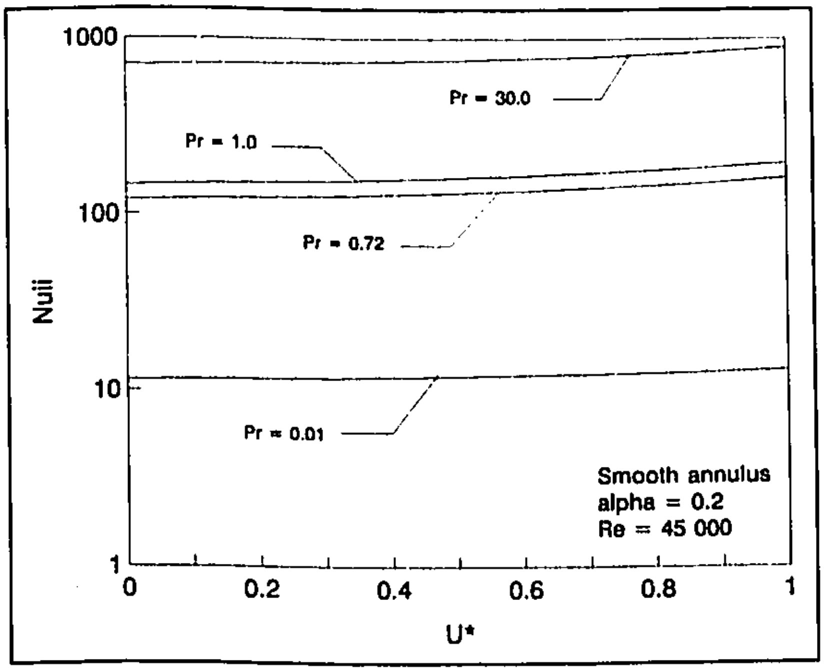

Figure 39: Nu vs U^* in smooth annulus

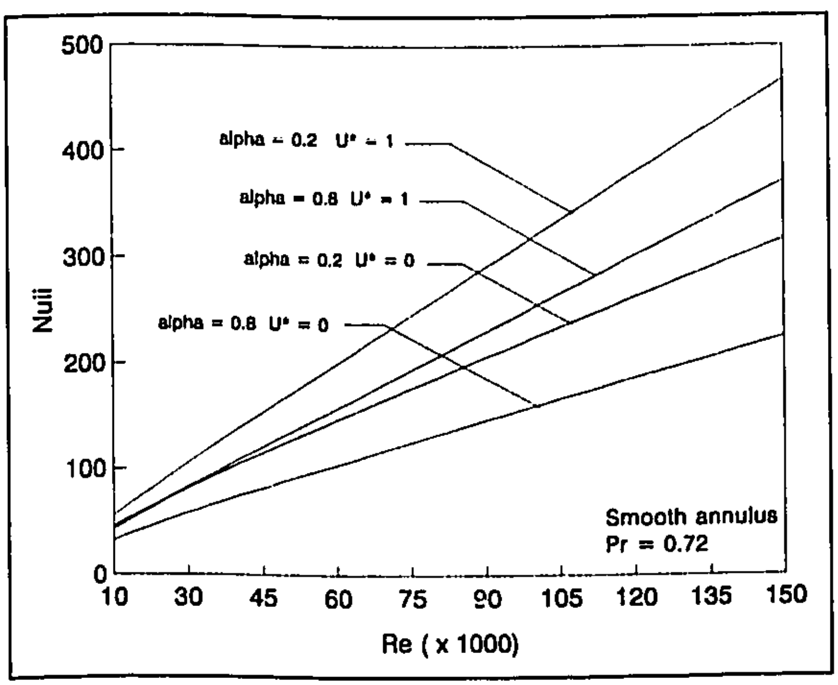

Figure 40: Effects of α and U^* on Nu - smooth annulus

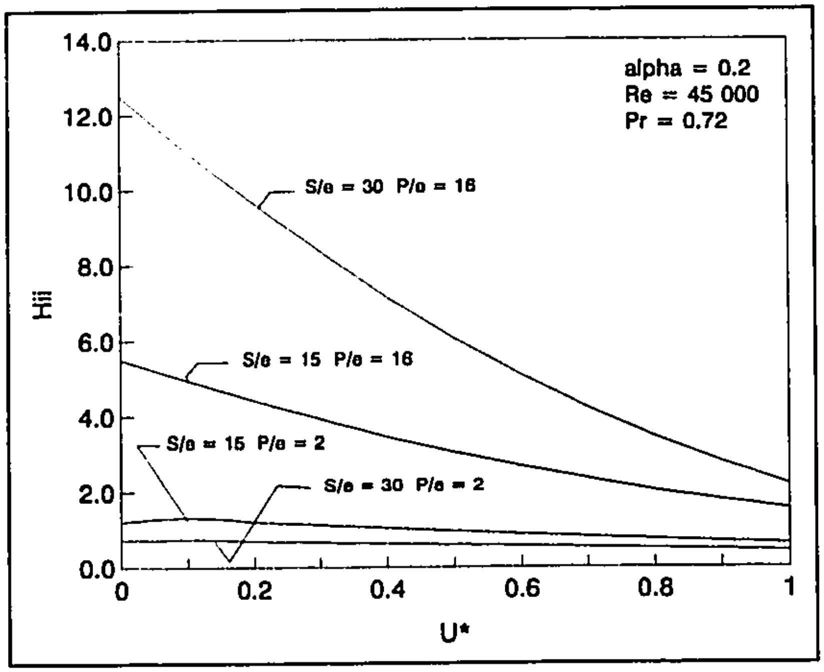

Figure 41: Effects of roughness on Hii (vs U*)

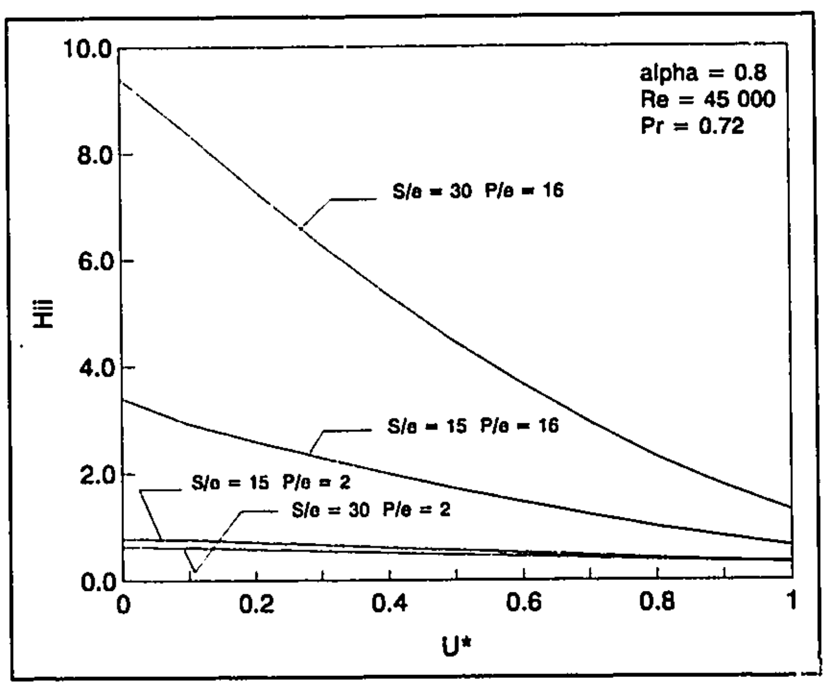

Figure 42: Effects of roughness on Hii (vs U*)

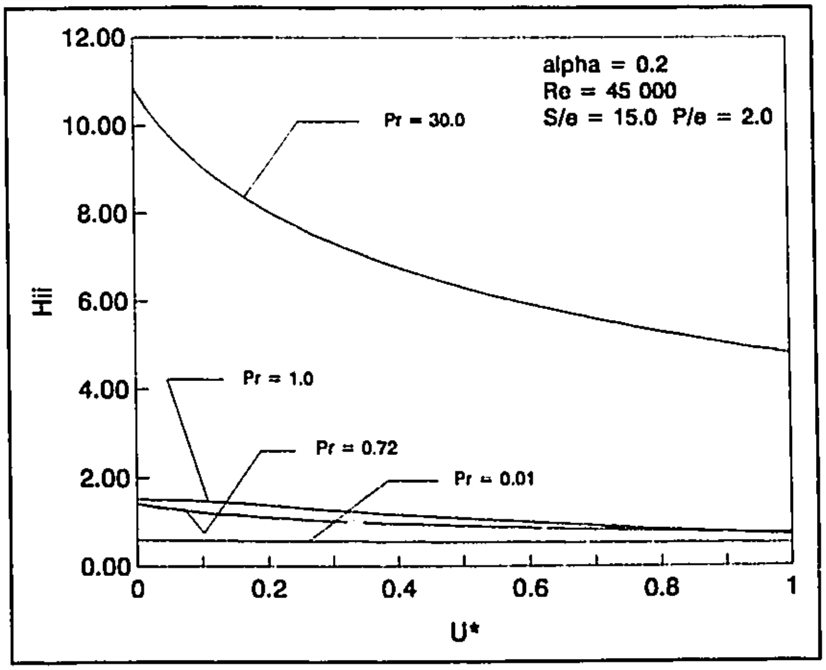

Figure 43: Effects of Pr on Hii (vs U*)

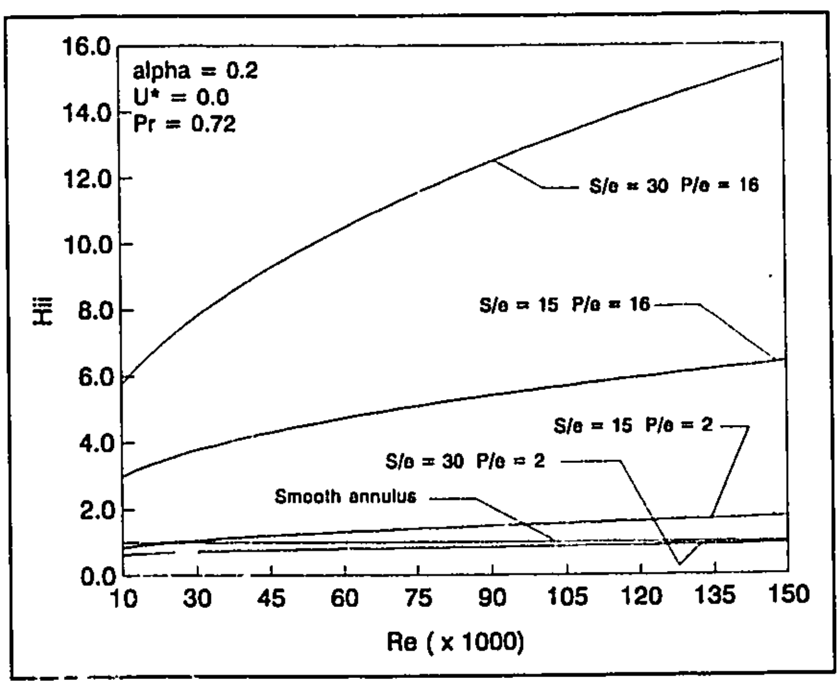

Figure 44: Effects of roughness on Hii (vs Re) - static core

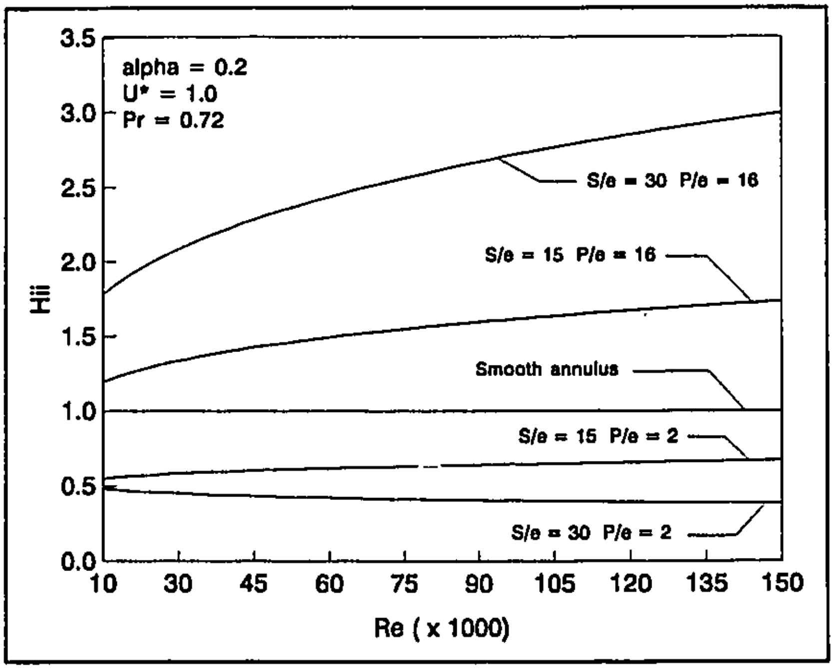

Figure 45: Effects of roughness on Hii (vs Re) - moving core

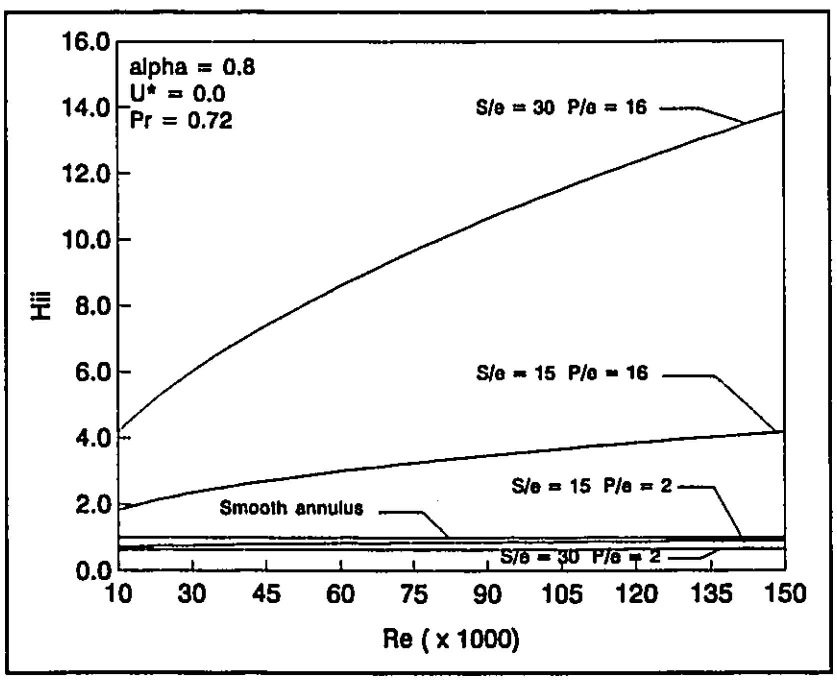

Figure 46: Effects of roughness on Hii (vs Re) - static core

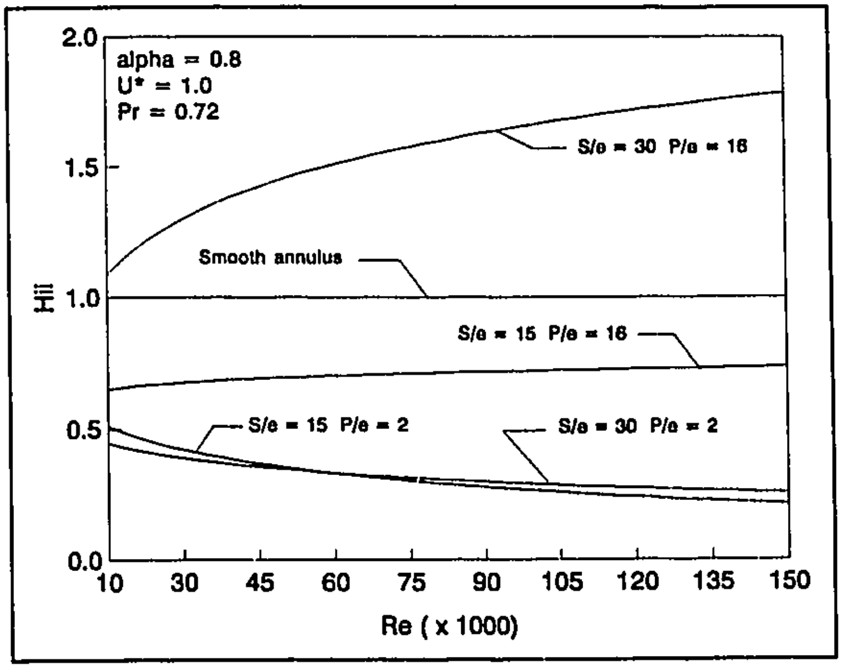

Figure 47: Effects of roughness on Hii (vs Re) - moving core

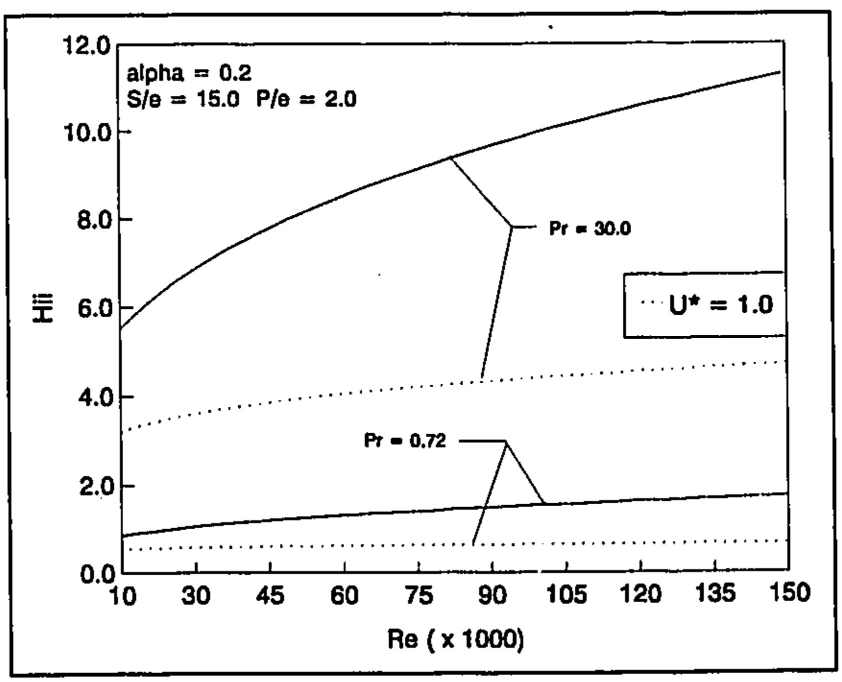

Figure 48: Effects of Pr on Hii (vs Re)

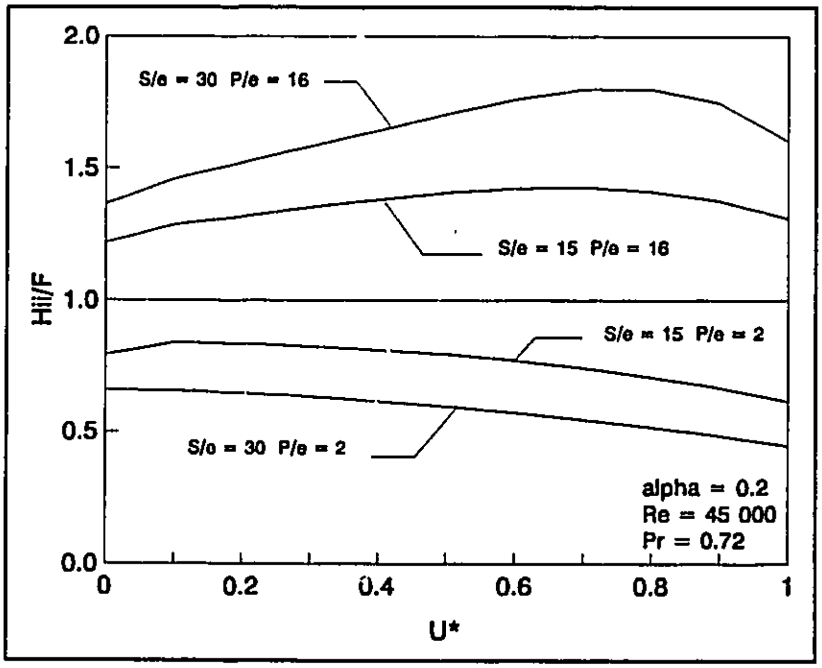

Figure 49: Effects of roughness on Hii/F (vs U*)

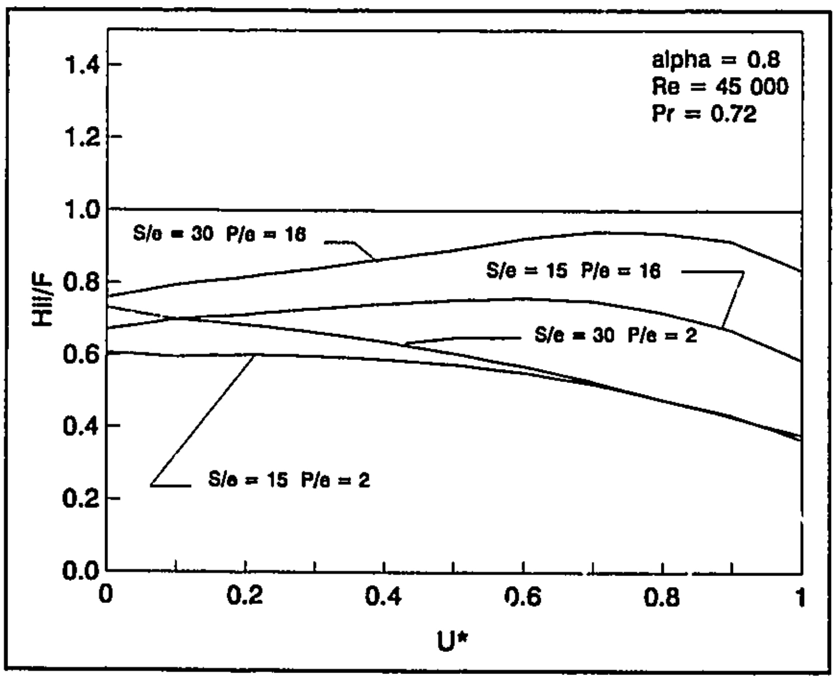

Figure 50: Effects of roughness on Hii/F (vs U*)

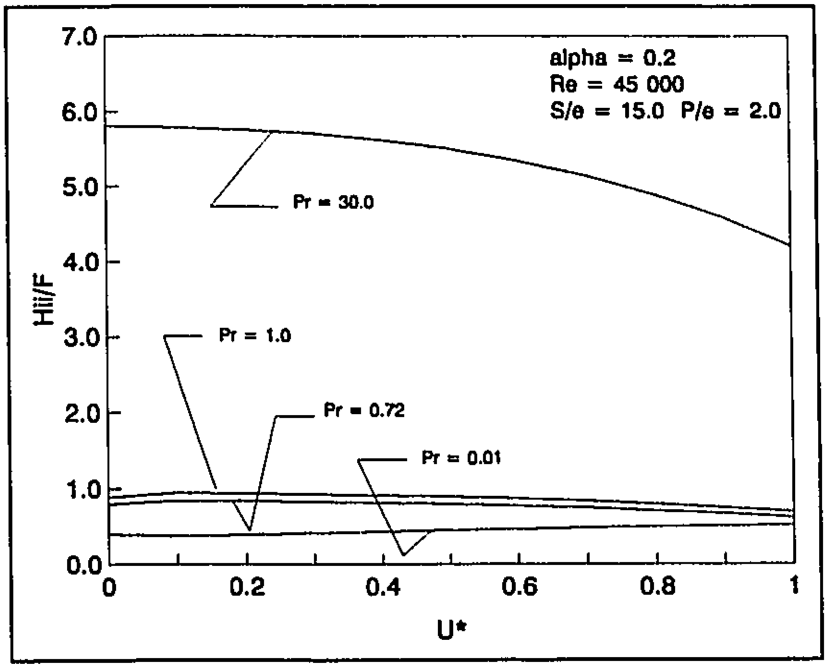

Figure 51: Effects of Pr on Hii/F (vs U*)

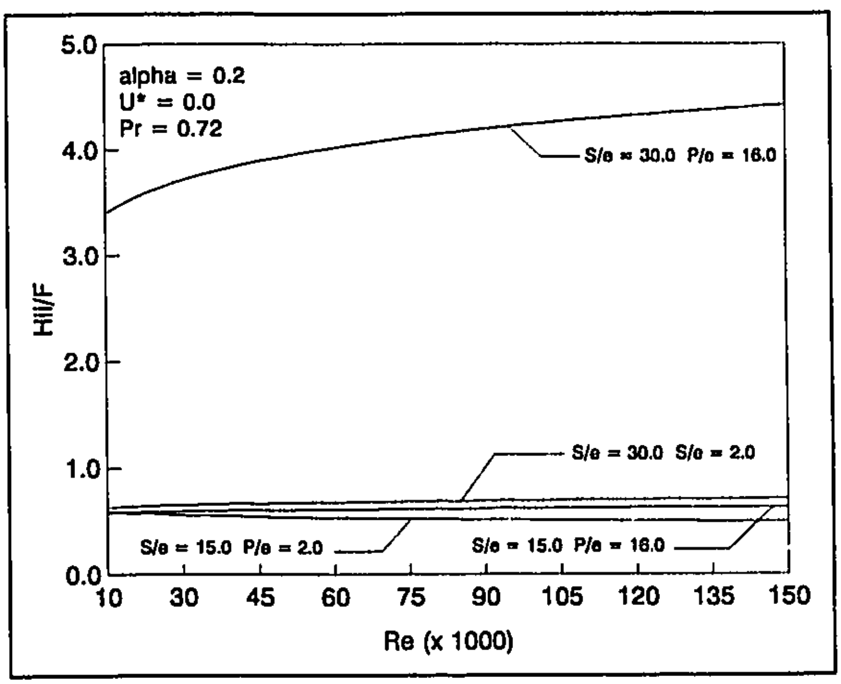

Figure 52: Effects of roughness on Hii/F (vs Re) - static core

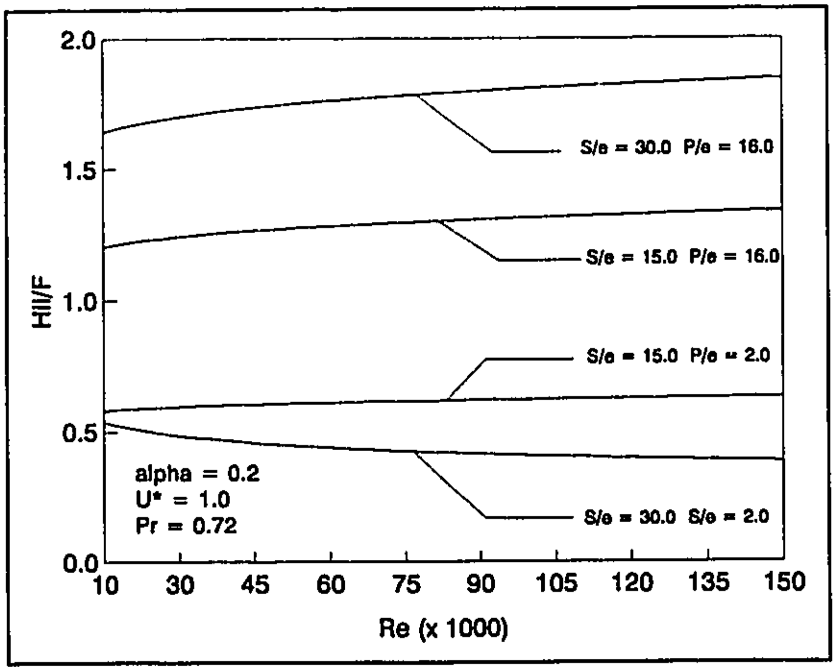

Figure 53: Effects of roughness on Hii/F (vs Re) - moving core

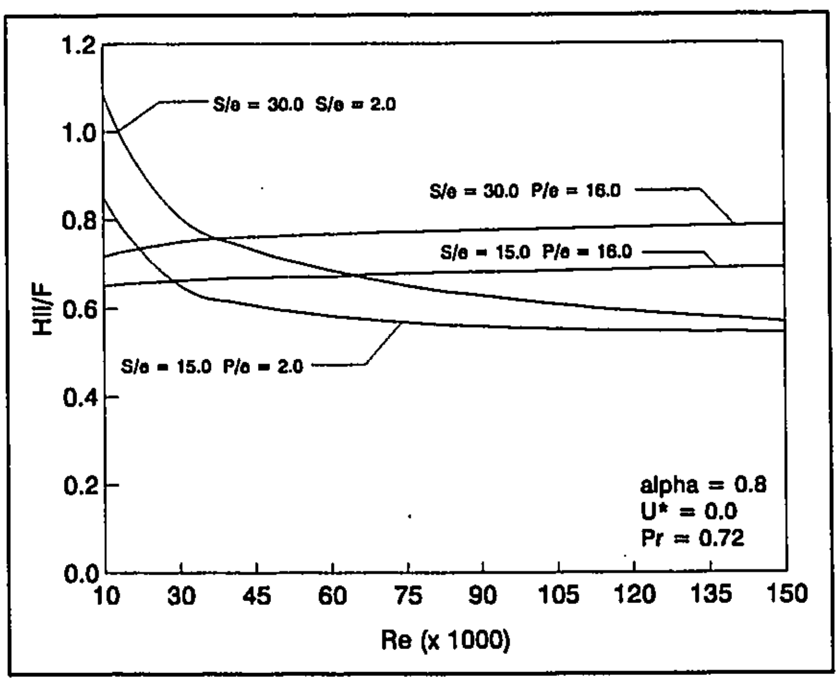

Figure 54: Effects of roughness on Hii/F (vs Re) - static core

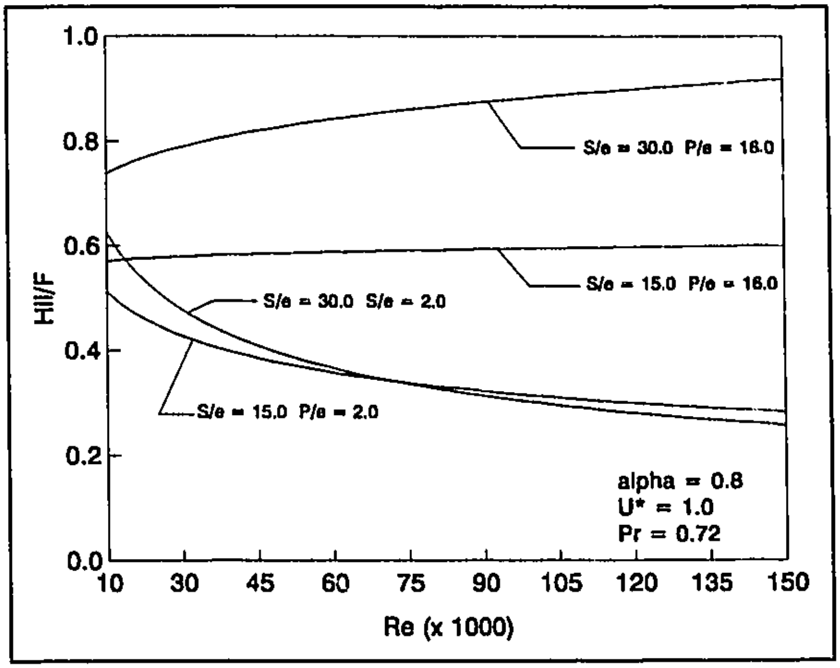

Figure 55: Effects of roughness on Hii/F (vs Re) - moving core

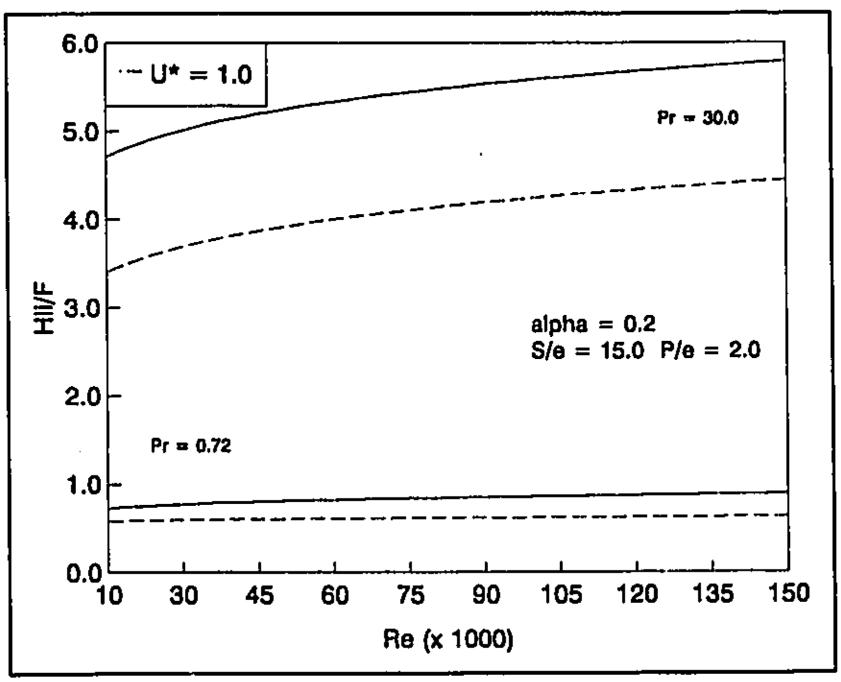

Figure 56: Effects of Pr on Hii/F (vs Re) - moving core

Appendix E

Graphical results

Annulus with rough core and casing

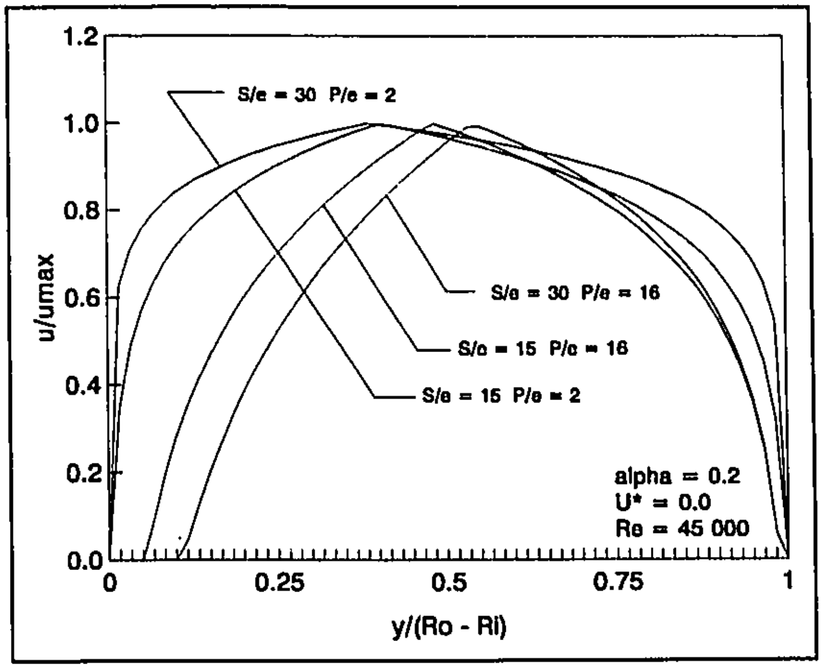

Figure 1: Effects of roughness on the velocity profiles - static core

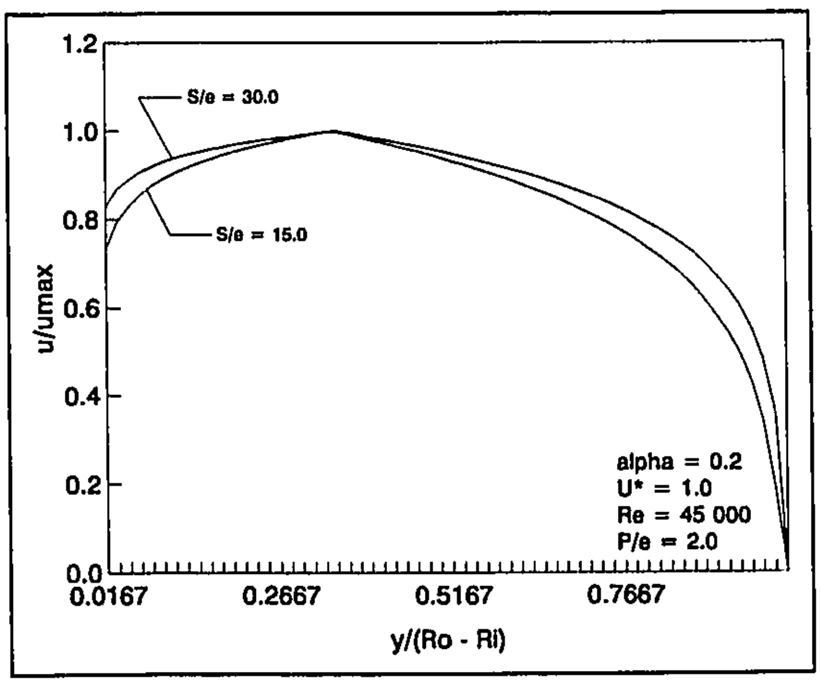

Figure 2: Effects of roughness on velocity profiles - moving core

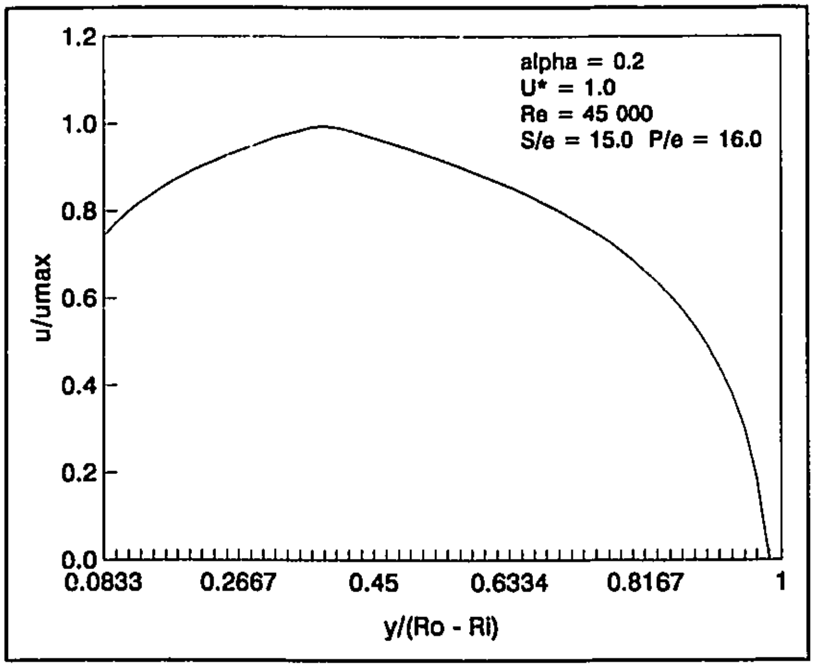

Figure 3: Effects of roughness on velocity profiles - moving core

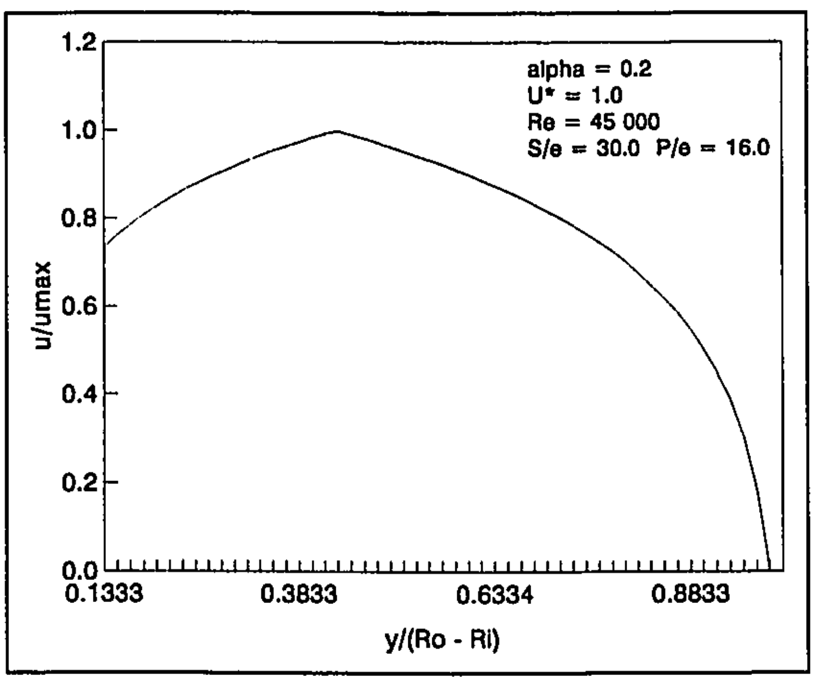

Figure 4: Effects of roughness on velocity profile - moving core

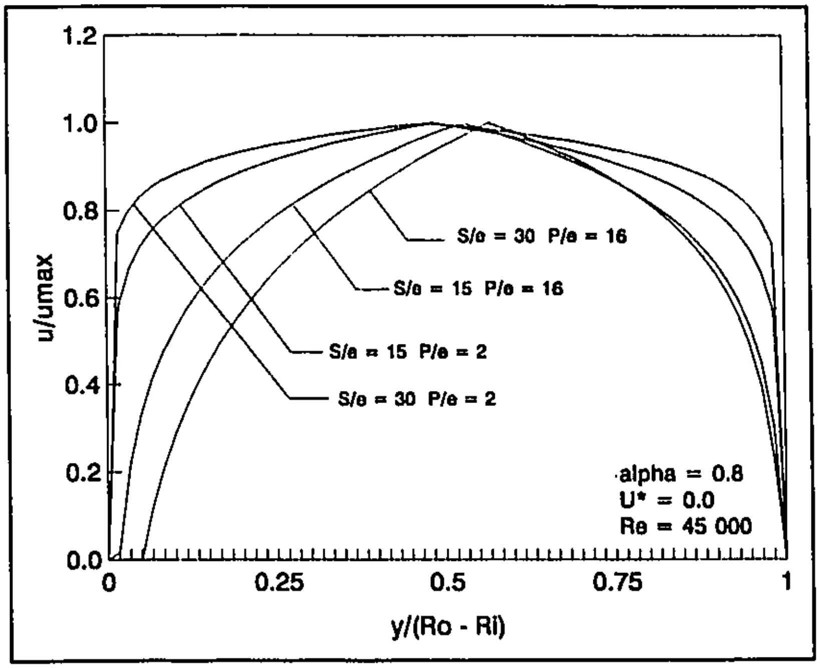

Figure 5: Effects of roughness on velocity profiles - static core

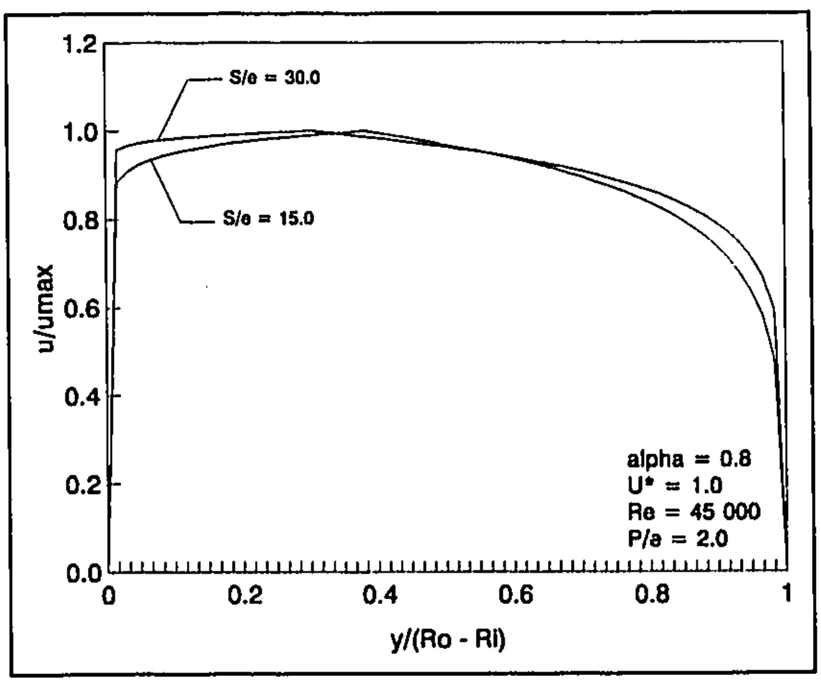

Figure 6: Effects of roughness on velocity profiles - moving core

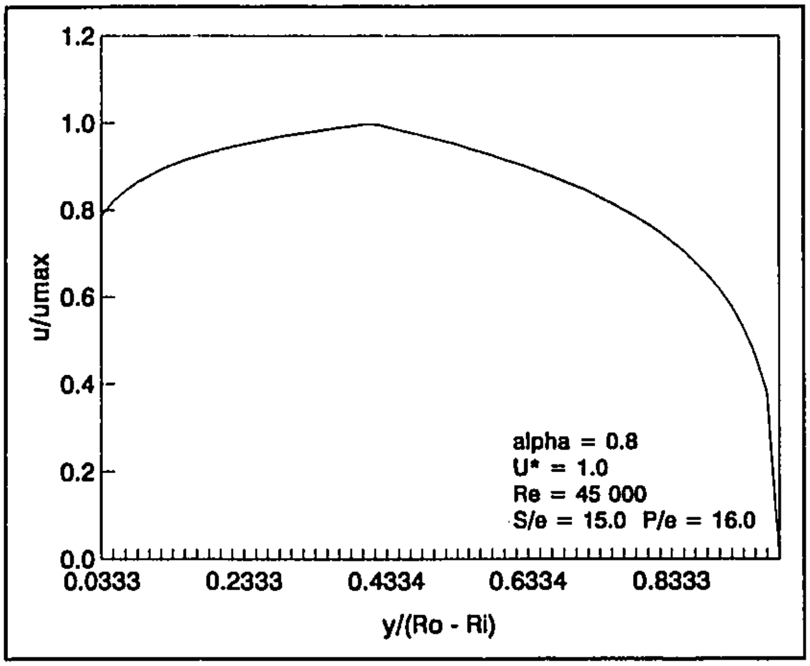

Figure 7: Effects of roughness on velocity profile - moving core

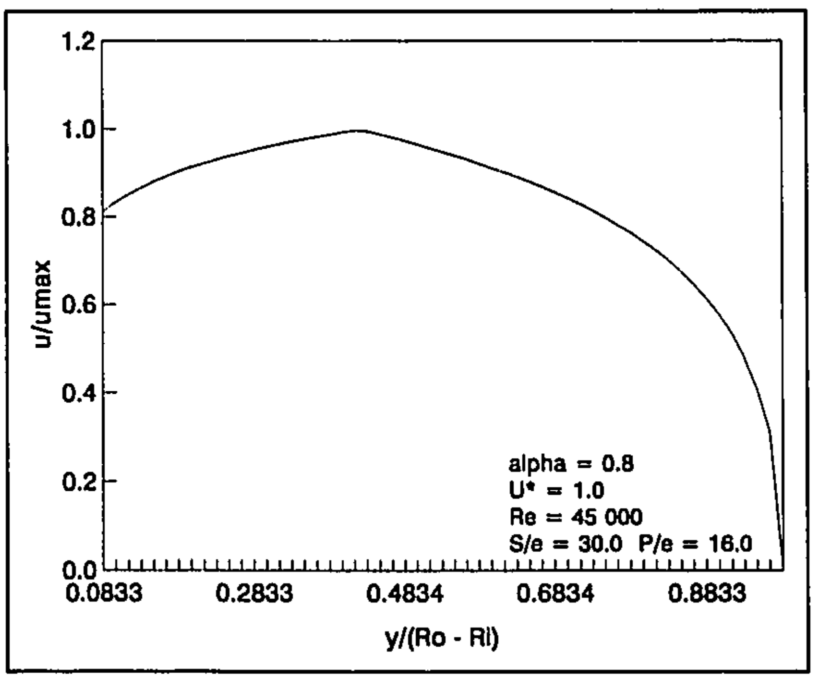

Figure 8: Effects of roughness velocity profile - moving core

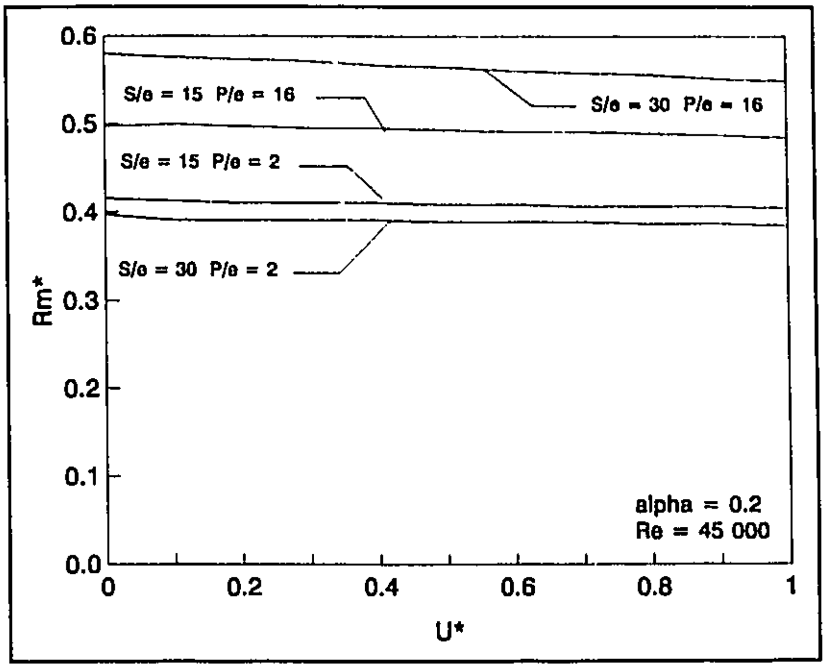

Figure 9: R_M^* vs U^* in rough annulus

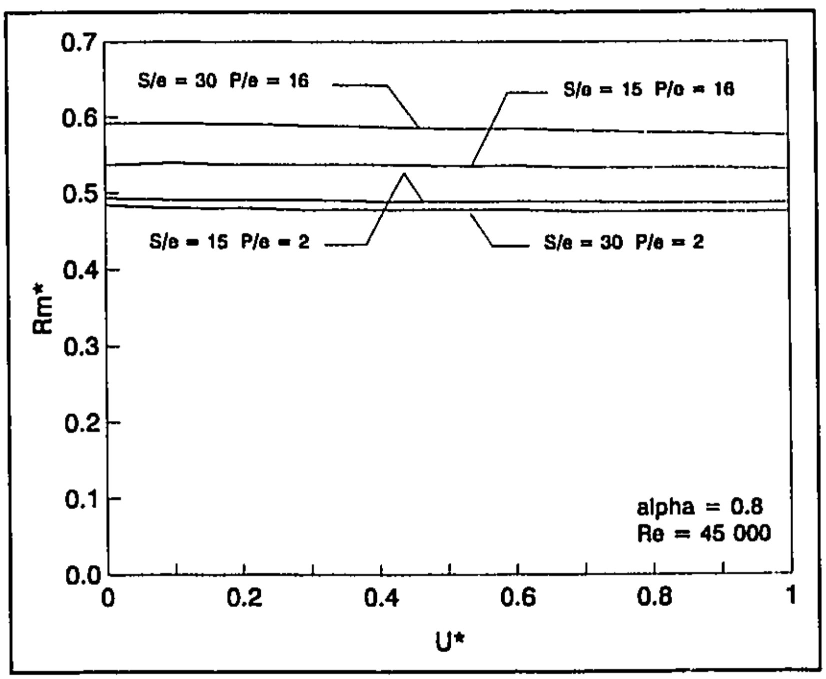

Figure 10 R_M^* vs U^* in rough annulus

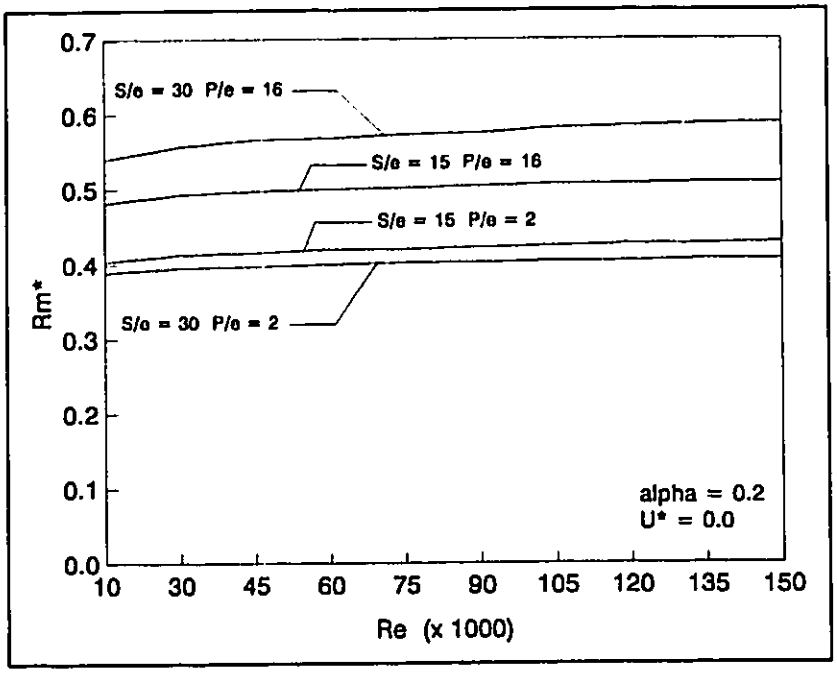

Figure 11: Effects of roughness on R_M^* (vs Re) - static moving

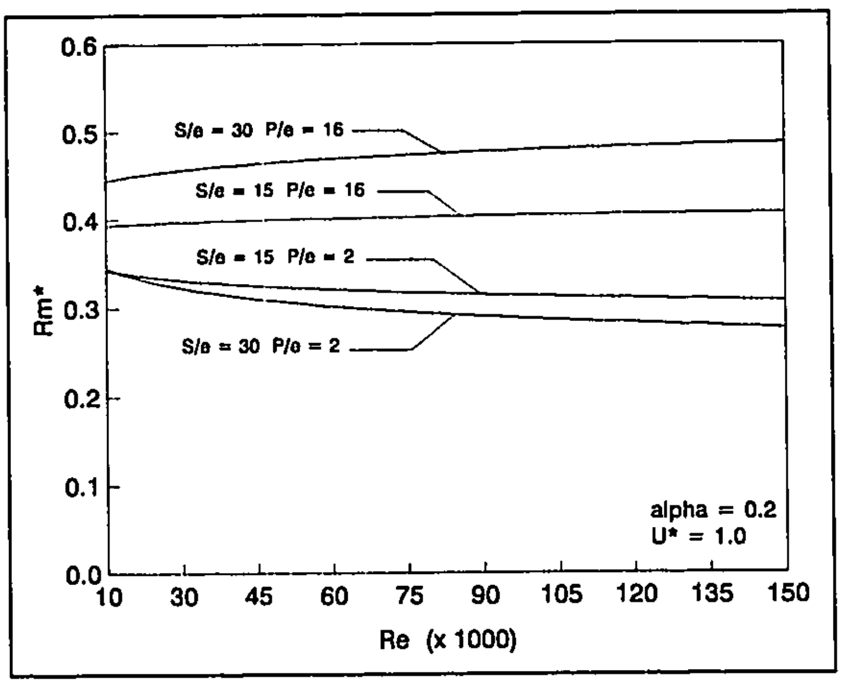

Figure 12: Effects of roughness on R_M^* (vs Re) - moving core

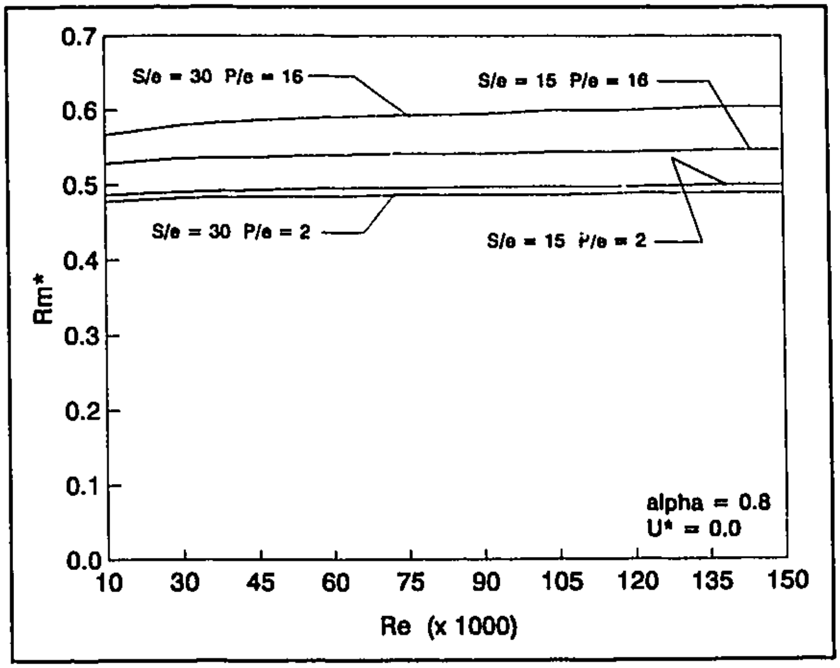

Figure 13: Effects of roughness on R_M^* (vs Re) - static core

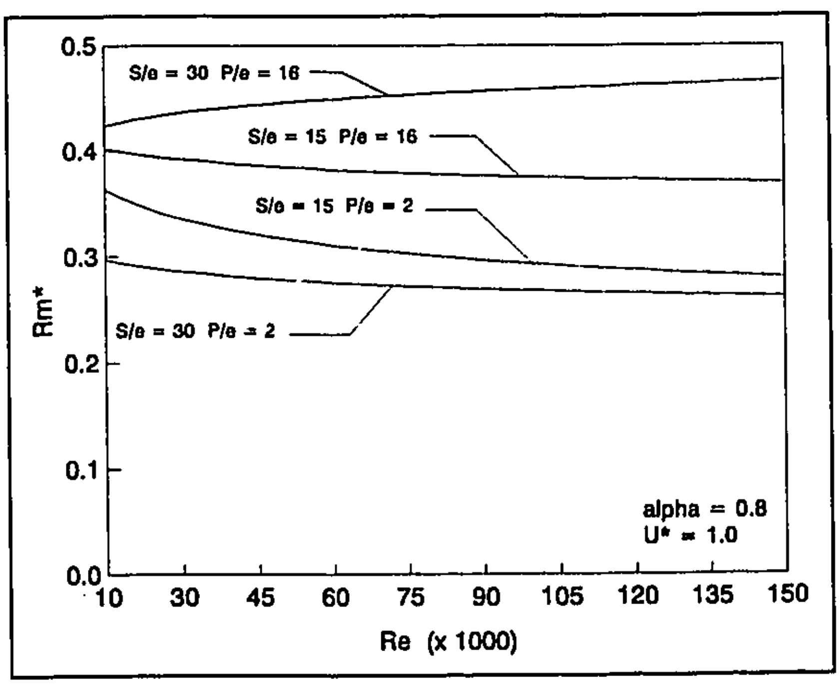

Figure 14: Effects of roughness on R_M^* (vs Re) - moving core

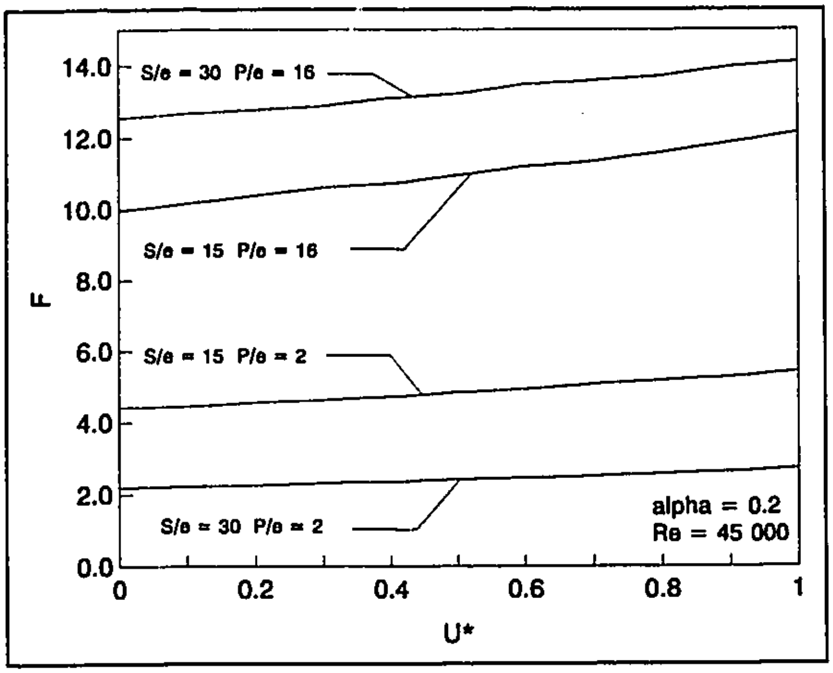

Figure 15: Effects of roughness on F (vs U*)

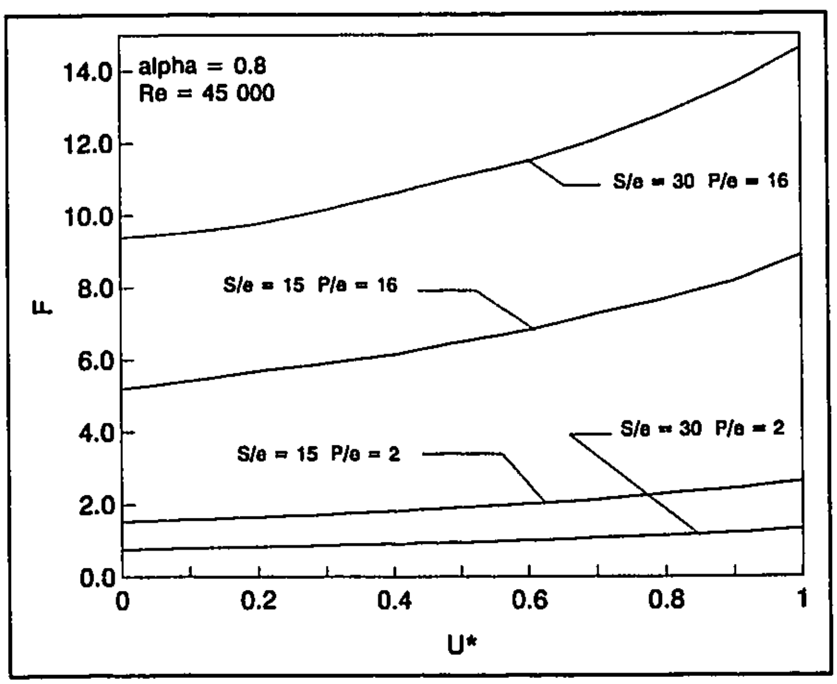

Figure 16: Effects of roughness on F (vs (U*)

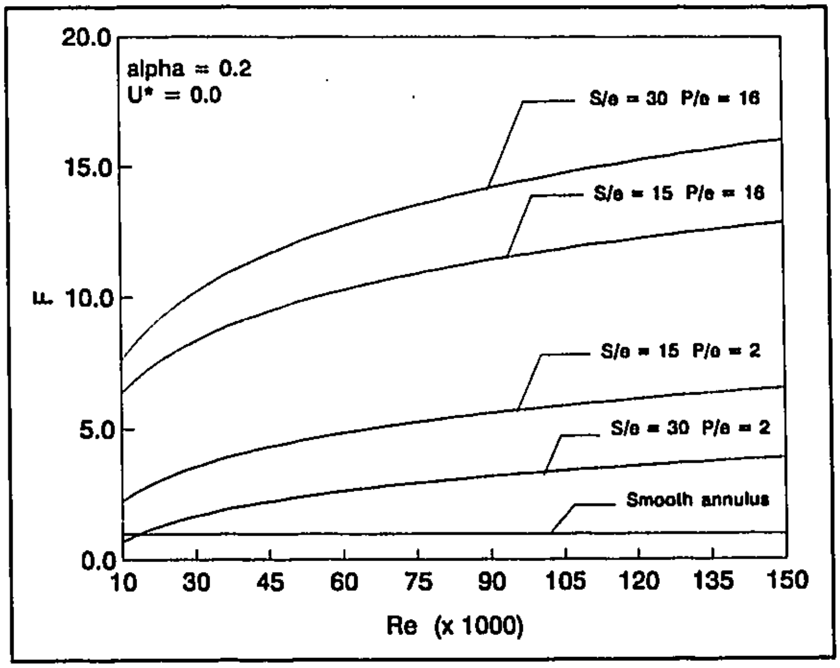

Figure 17: Effects of roughness on F (vs Re) - static core

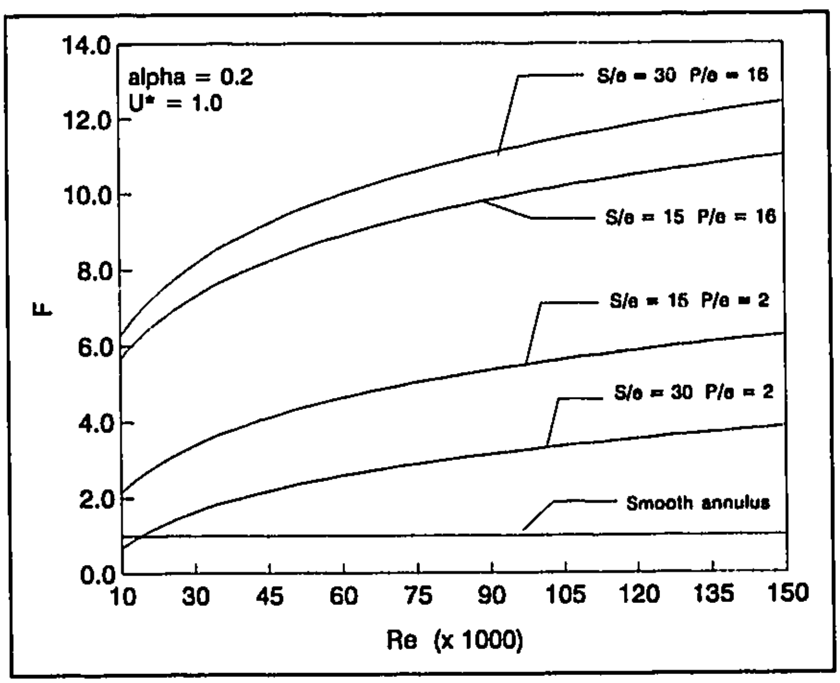

Figure 18: Effects of roughness on F (vs Re) - moving core

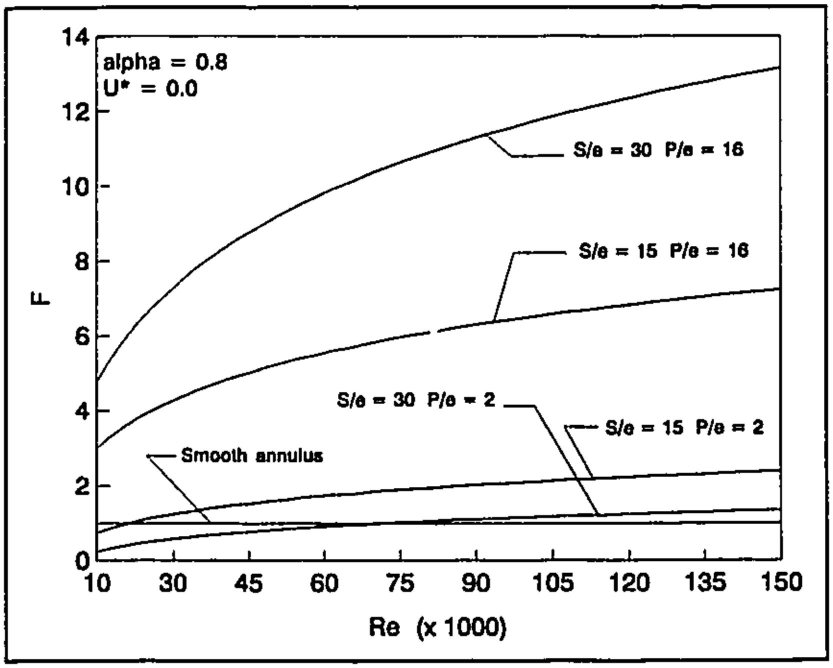

Figure 19: Effects of roughness on F (vs Re) - static core

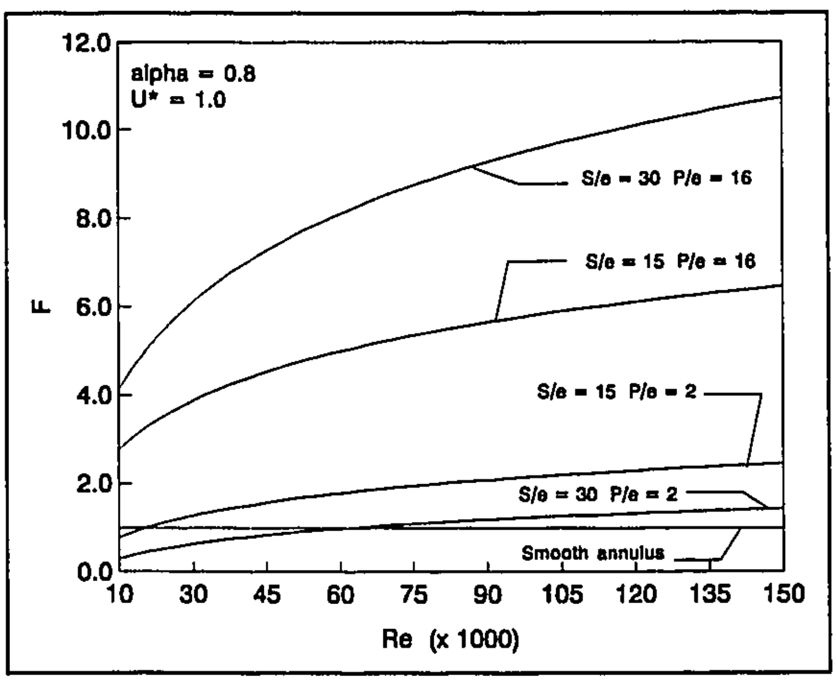

Figure 20: Effects of roughness on F (vs Re) - moving core

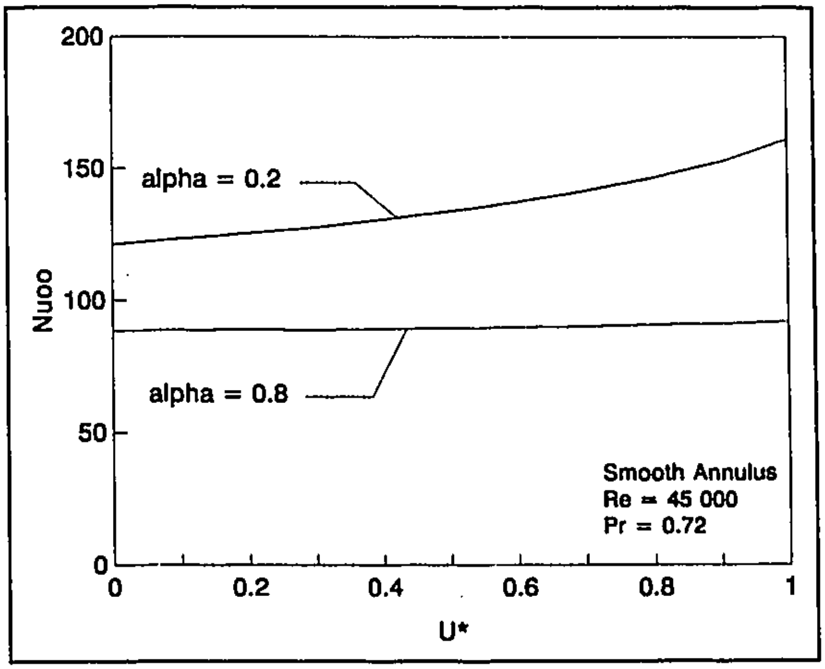

Figure 21: Outer Surface Nusselt number vs U* - smooth annulus

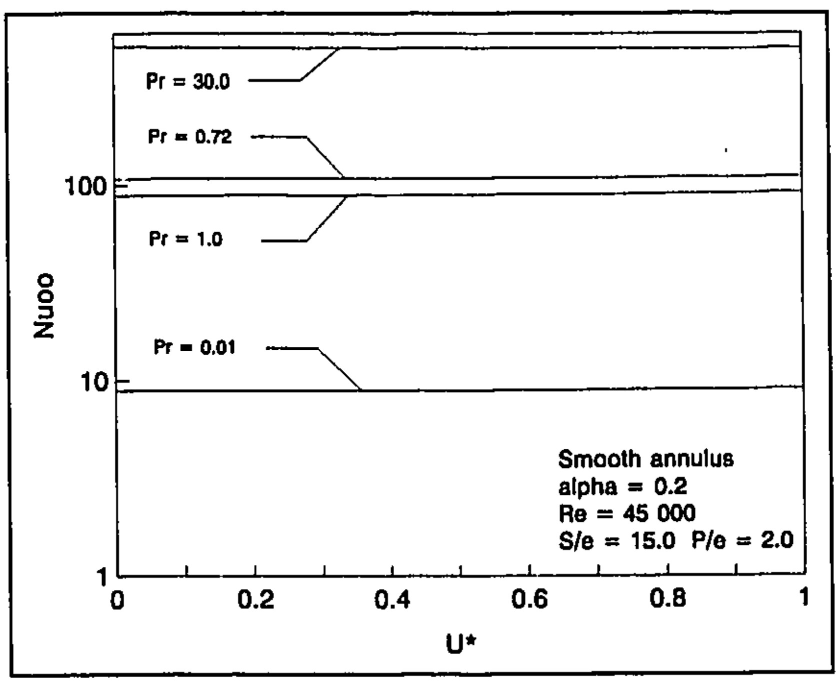

Figure 22: Effects of Pr and U* on Nuoo - smooth annulus

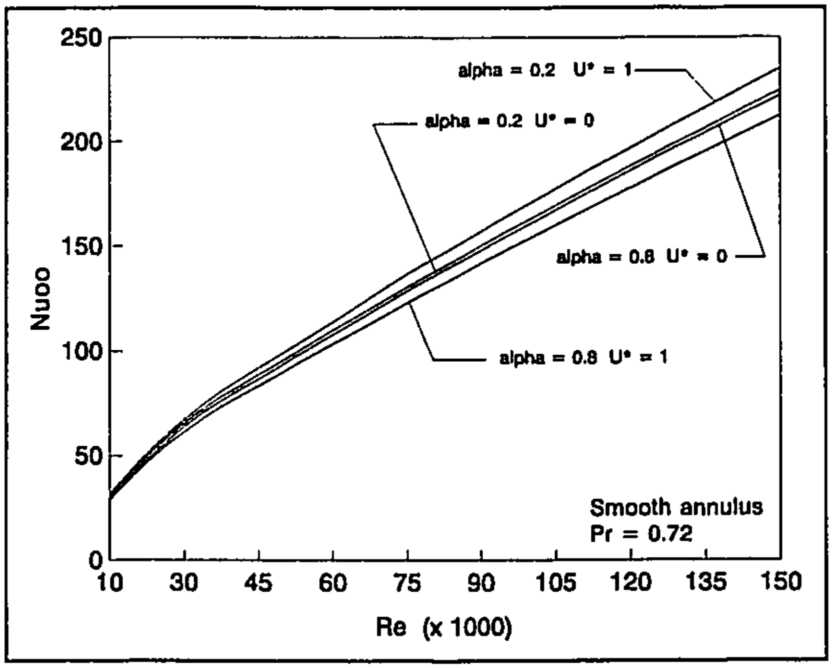

Figure 23: Effects of Re, α and U* on Nuoo - smooth annulus

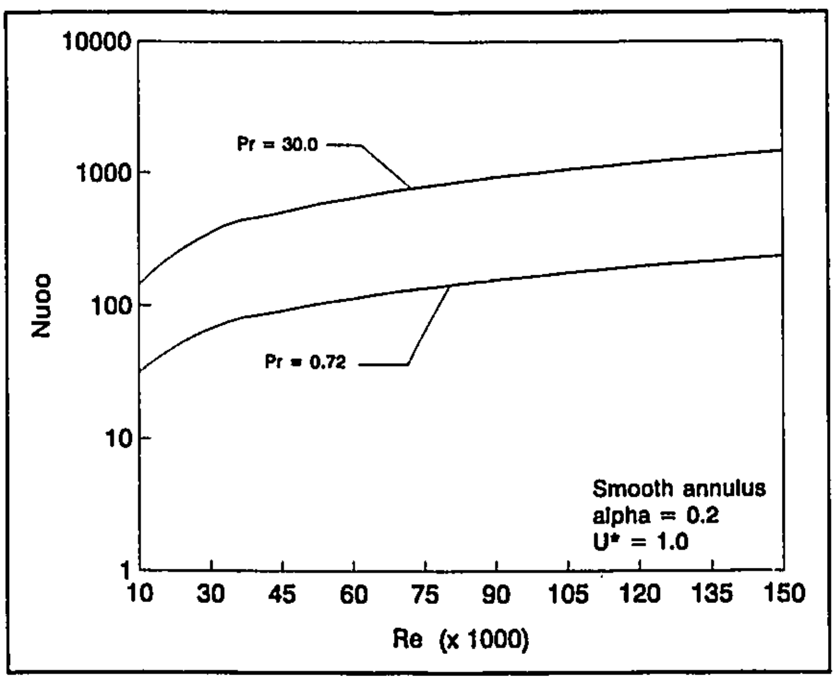

Figure 24: Effects of Pr on Nuoo - smooth annulus with moving core

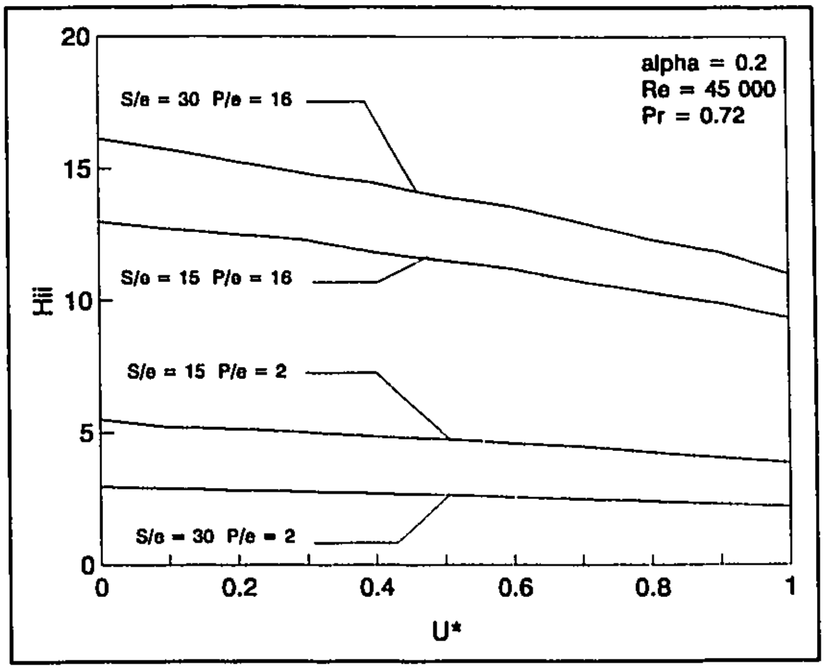

Figure 25: Effects of roughness on Hii (vs U*)

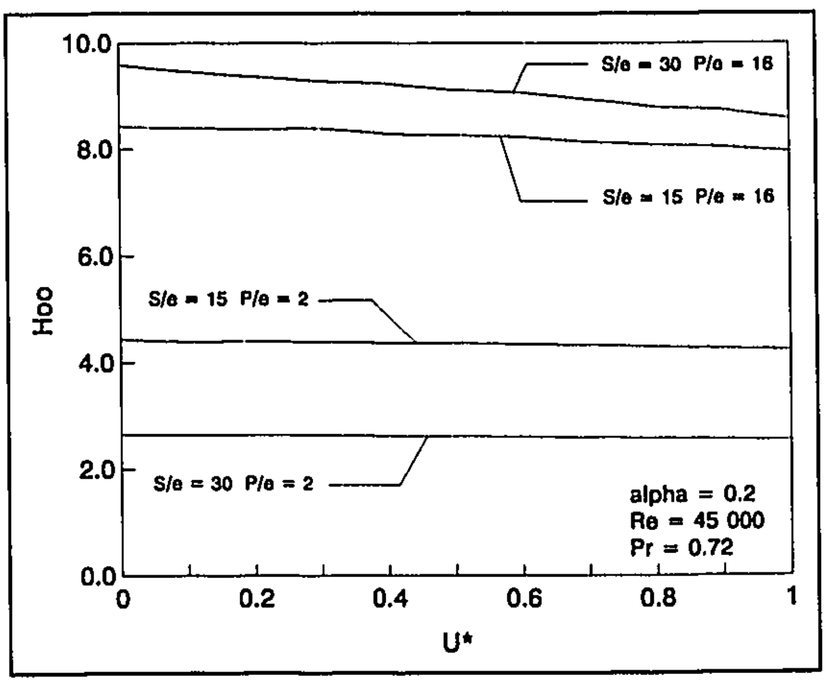

Figure 26: Effects of roughness on Hoo (vs U*)

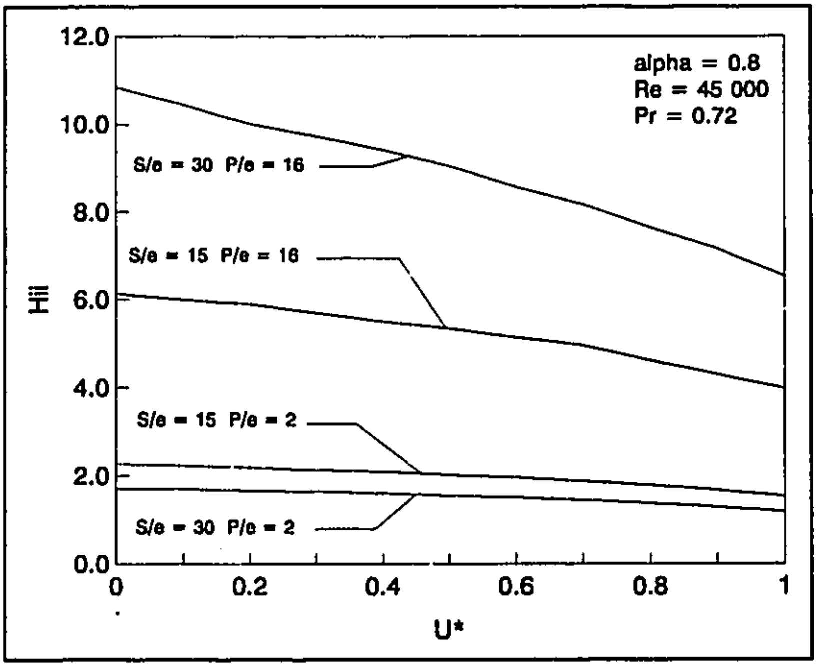

Figure 27: Effects of roughness on Hii (vs U*)

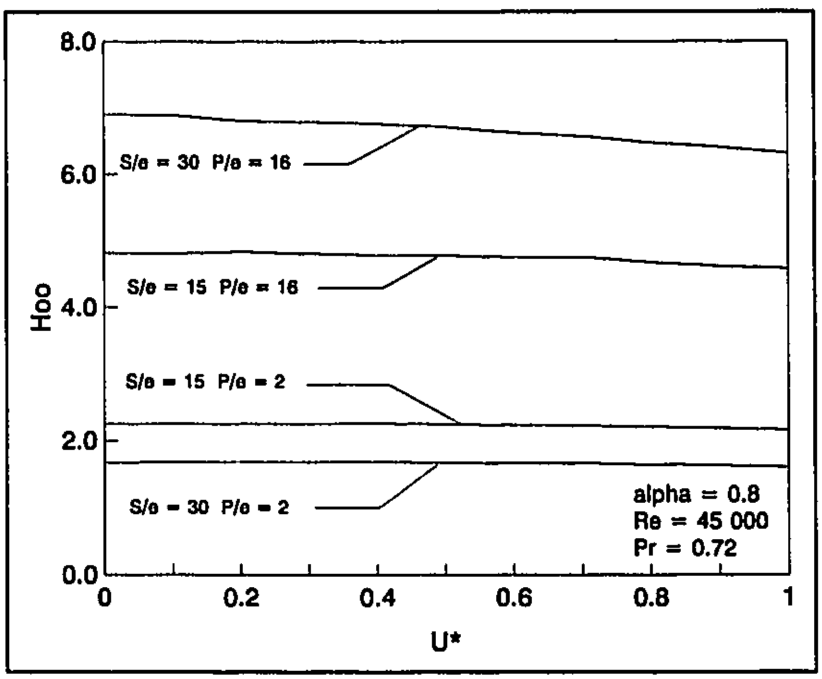

Figure 28: Effects of roughness on Hoo (vs U*)

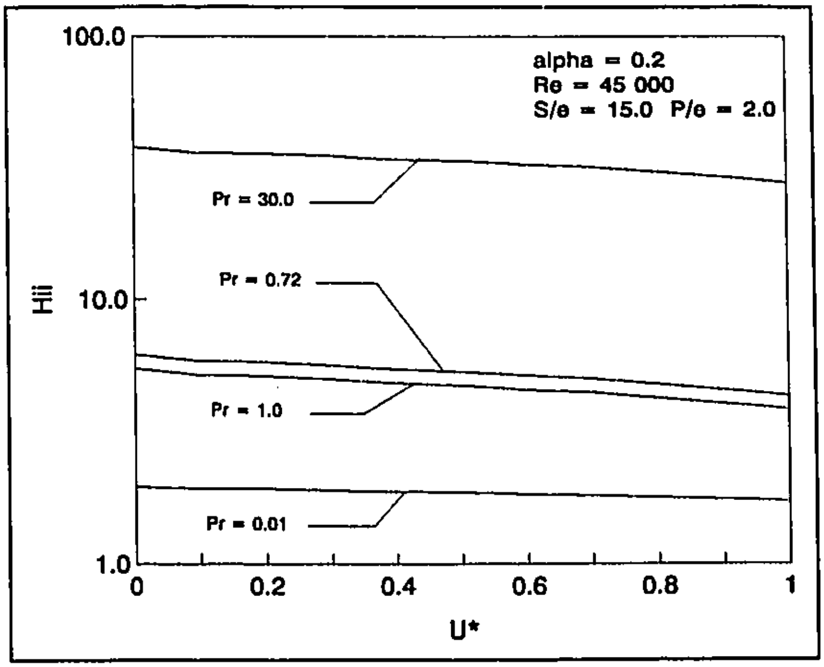

Figure 29: Effects of Pr on Hii (vs U*)

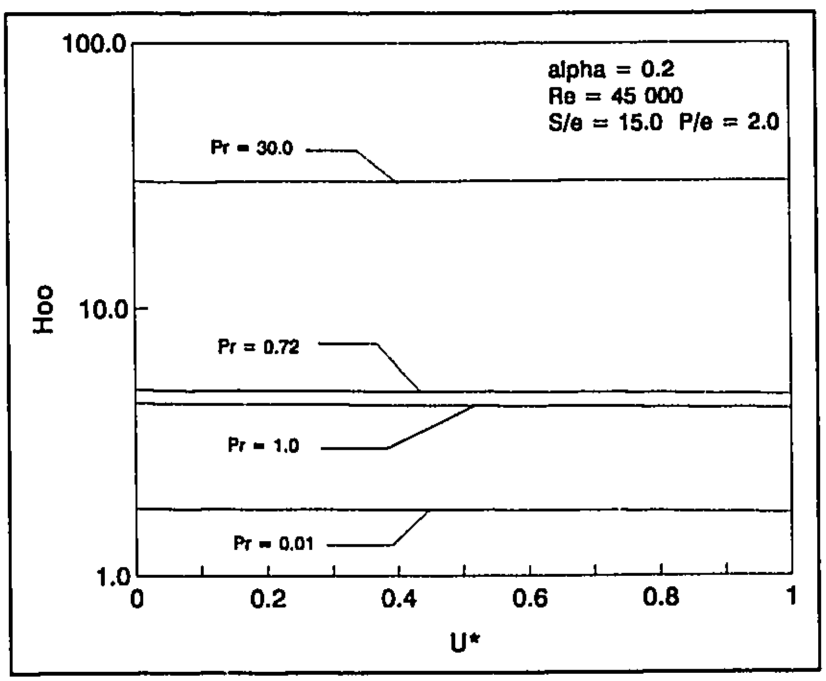

Figure 30: Effects of Pr on Hoo (vs U*)

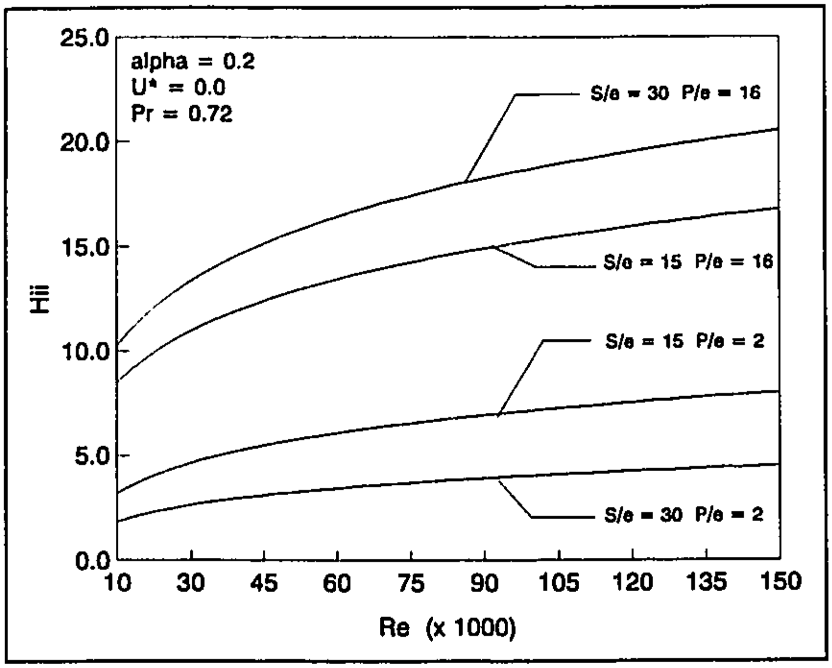

Figure 31: Effects of roughness on Hii vs Re - static core

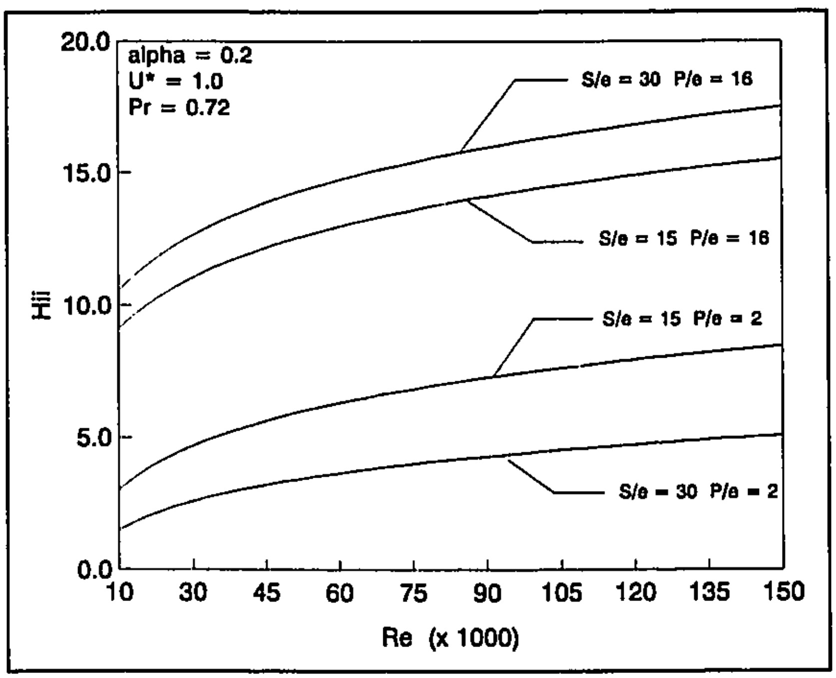

Figure 32: Effects of roughness on Hii vs Re - moving core

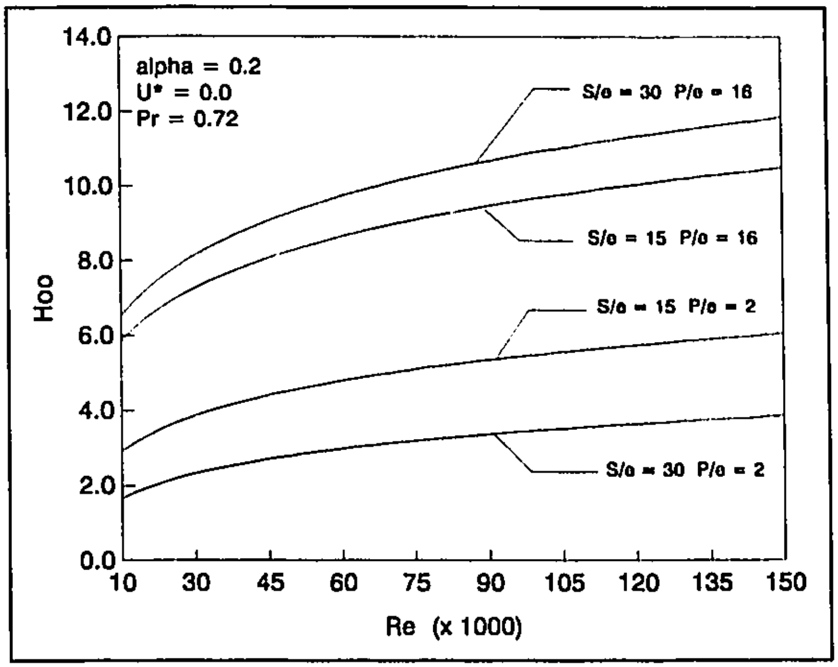

Figure 33: Effects of roughness on Hoo vs Re - static core

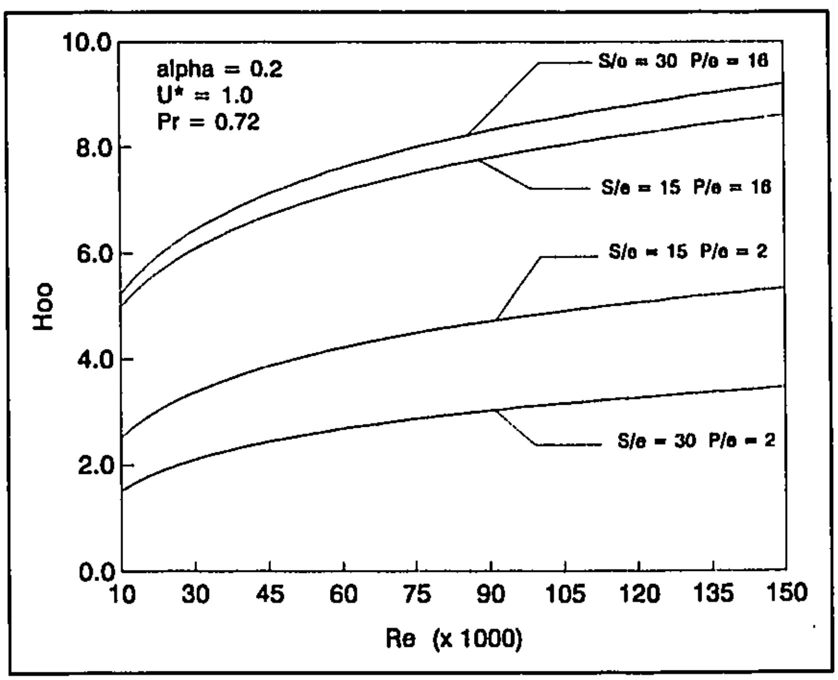

Figure 34: Effects of roughness on Hoo vs Re - moving core

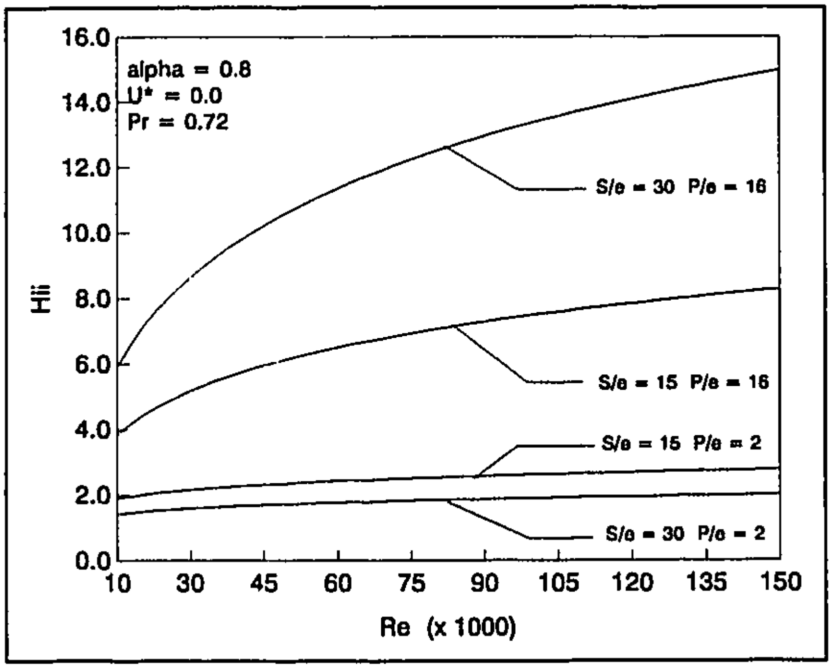

Figure 35: Effects of roughness on Hii vs Re - static core

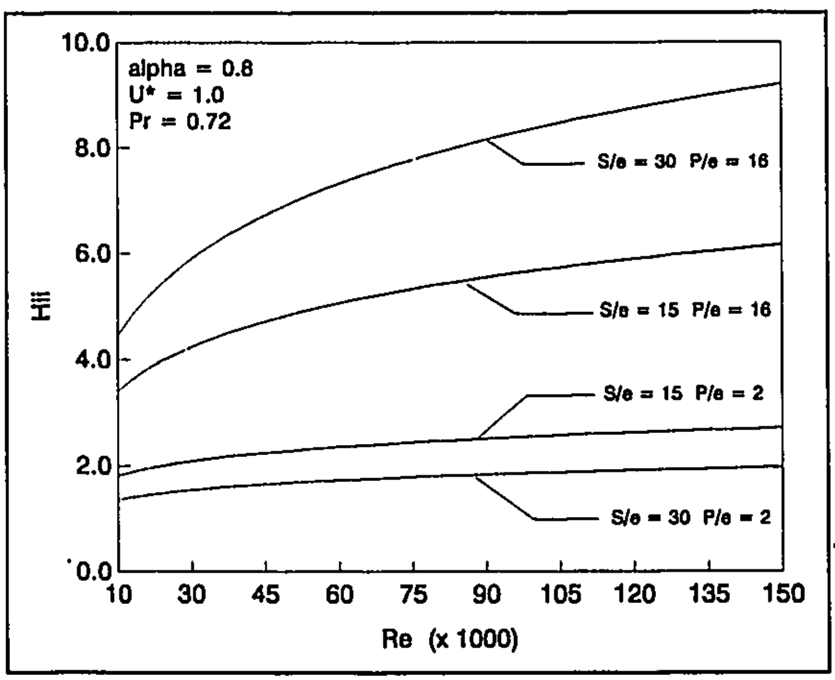

Figure 36: Effects of roughness on Hii vs Re - moving core

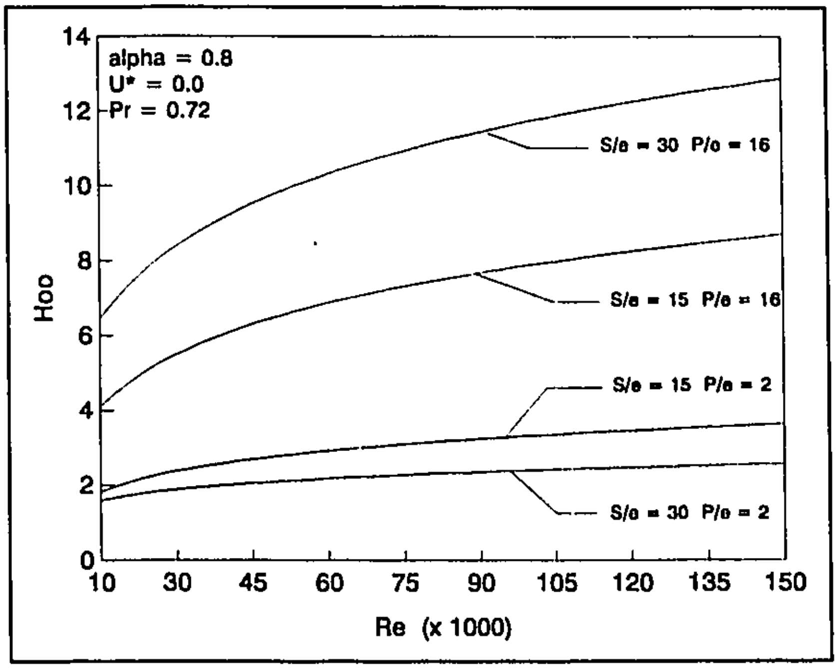

Figure 37: Effects of roughness on Hoo vs Re - static core

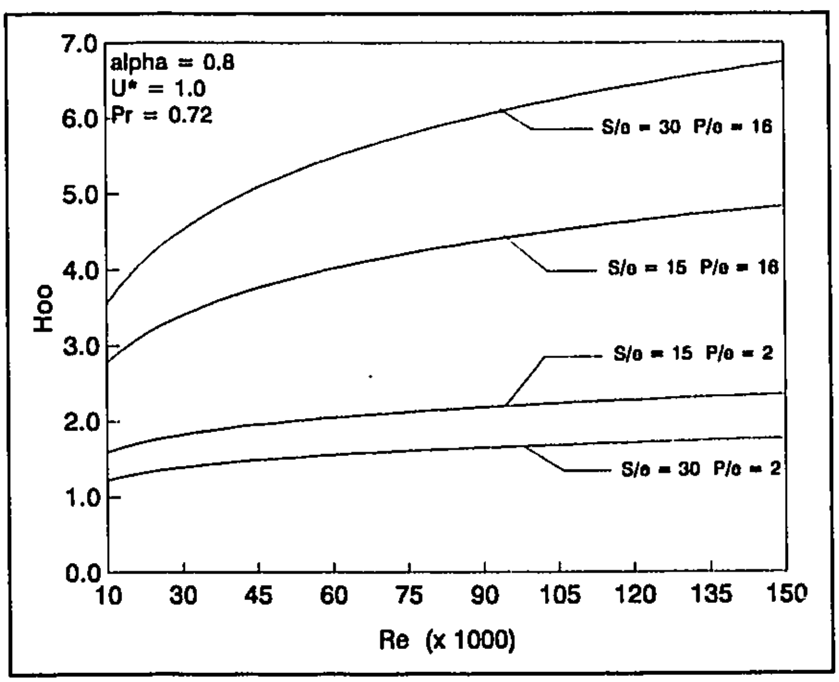

Figure 38: Effects of roughness on Hoo vs Re - moving core

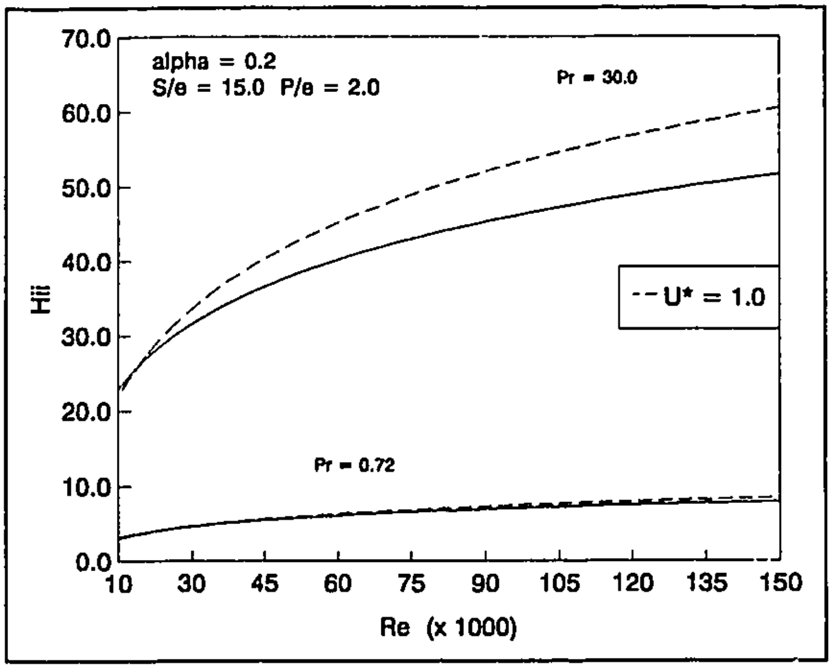

Figure 39: Effects of Pr and U* on Hii (vs Re)

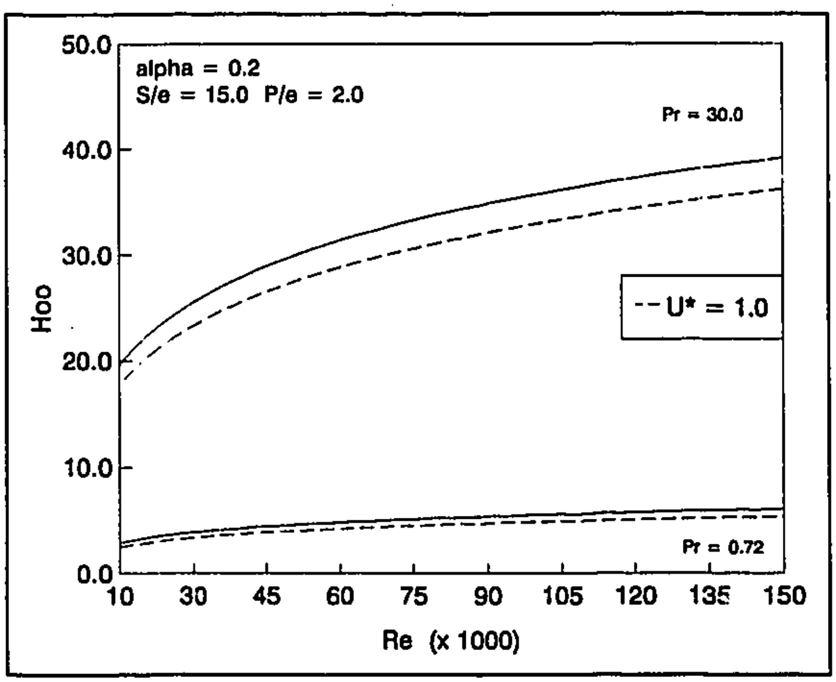

Figure 40: Effects of Pr and U* on Hoo (vs Re)

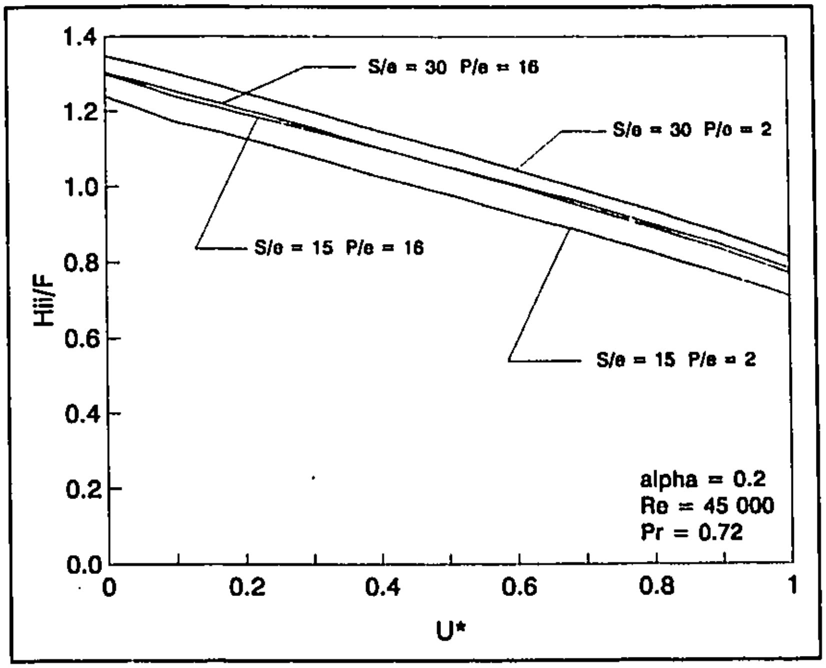

Figure 41: Effects of roughness on Hii/F (vs U*)

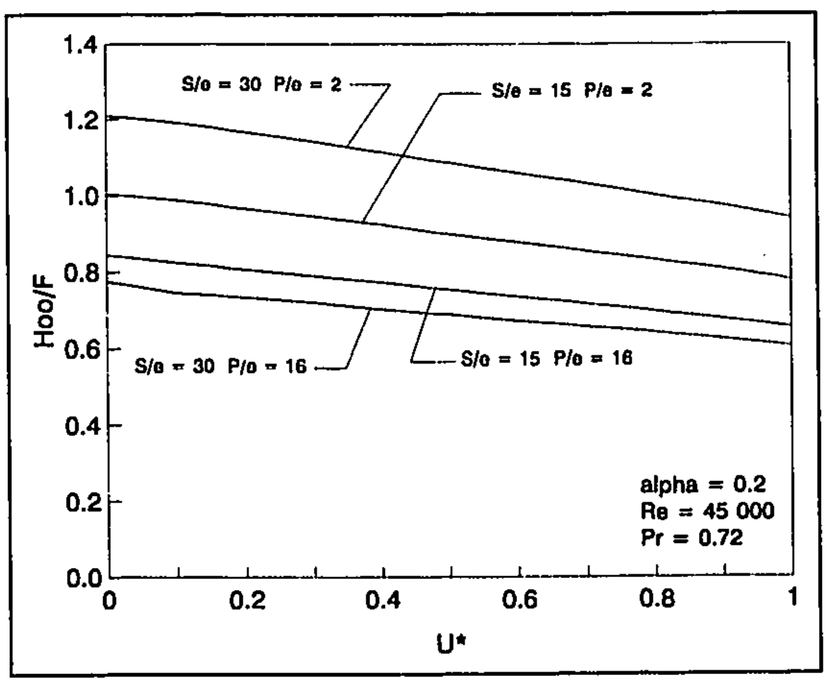

Figure 42: Effects of roughness on Hoo/F (vs U*)

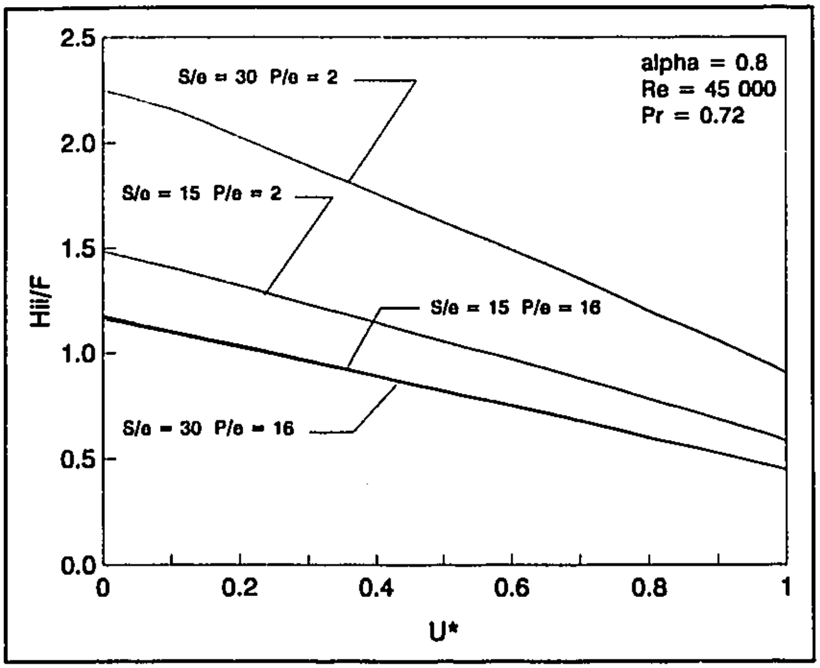

Figure 43: Effects of roughness on Hii/F (vs U*)

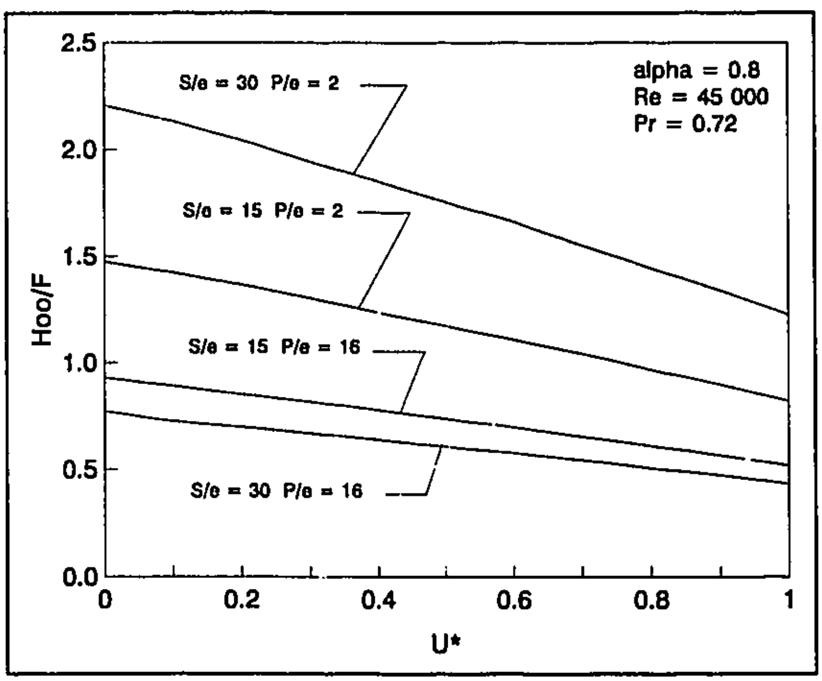

Figure 44: Effects of roughness on Hoo/F (vs U*)

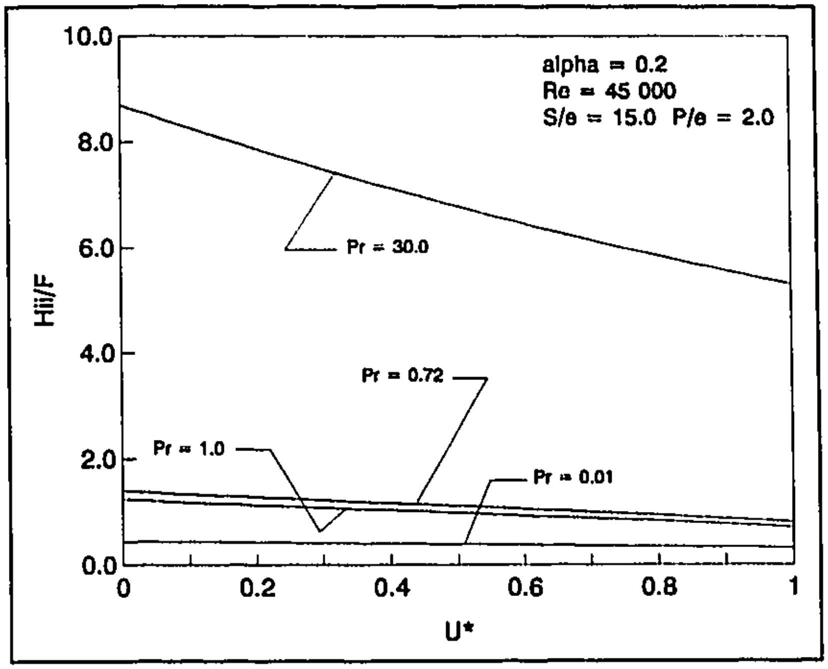

Figure 45: Effects of Pr on Hii/F vs U*

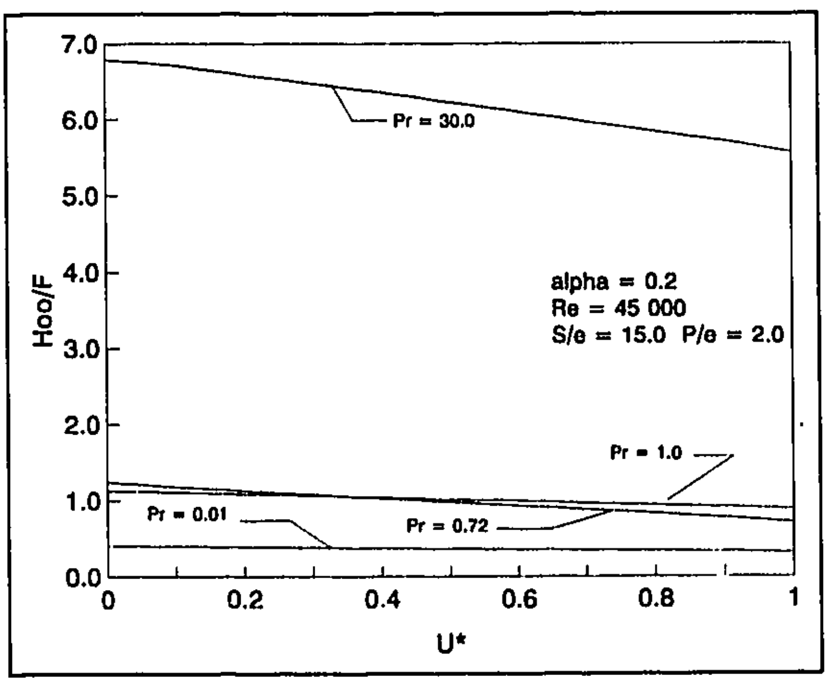

Figure 46: Effects of Pr on Hoo/F vs U*

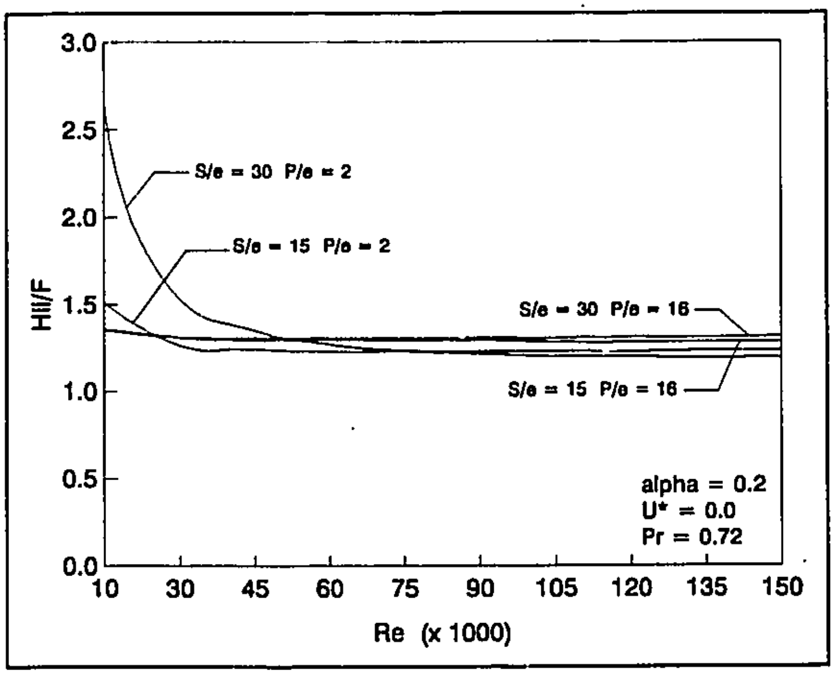

Figure 47: Effects of roughness on Hii/F (vs Re) - static core

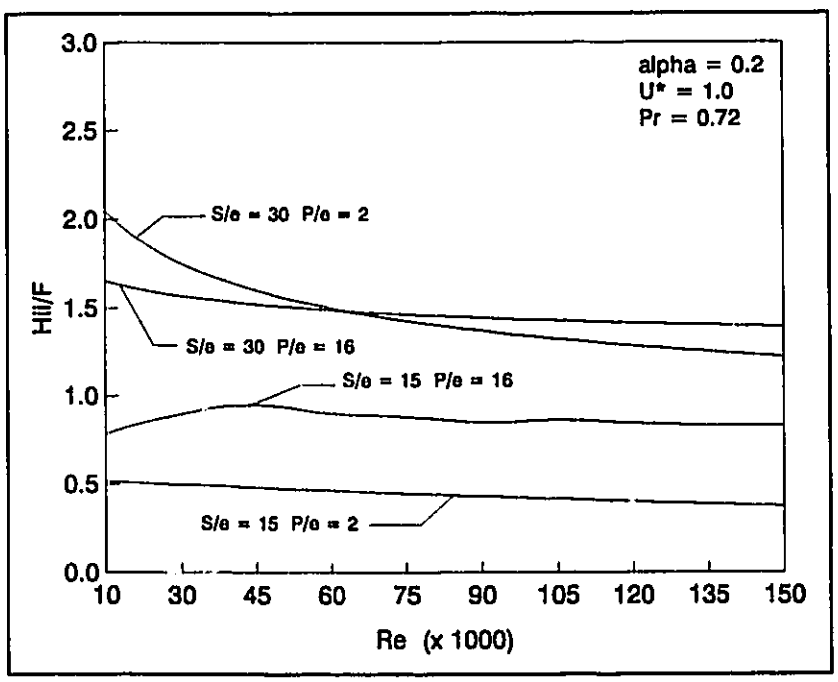

Figure 48: Effects of on Hii/F (vs Re) - moving core

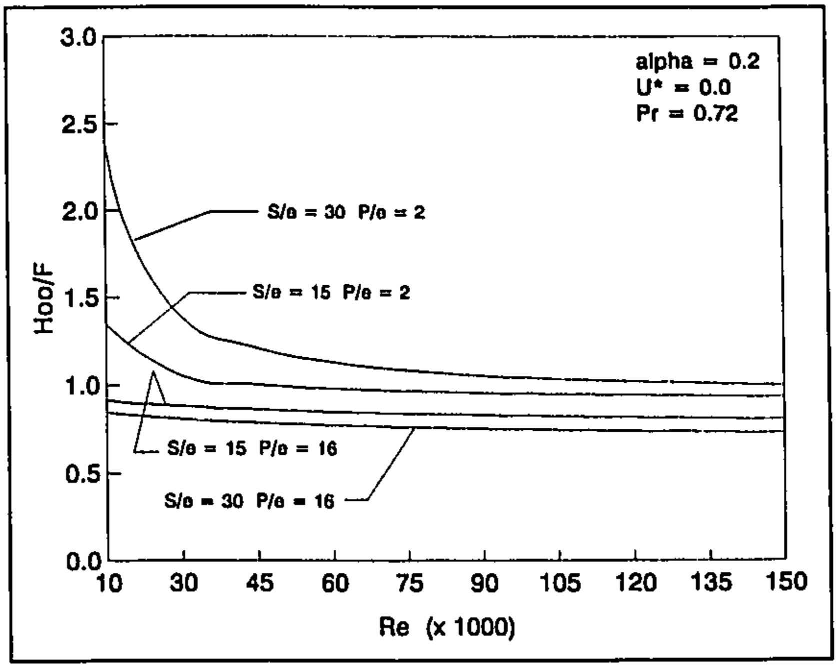

Figure 49: Effects of roughness on Hoo/F (vs U*) - static core

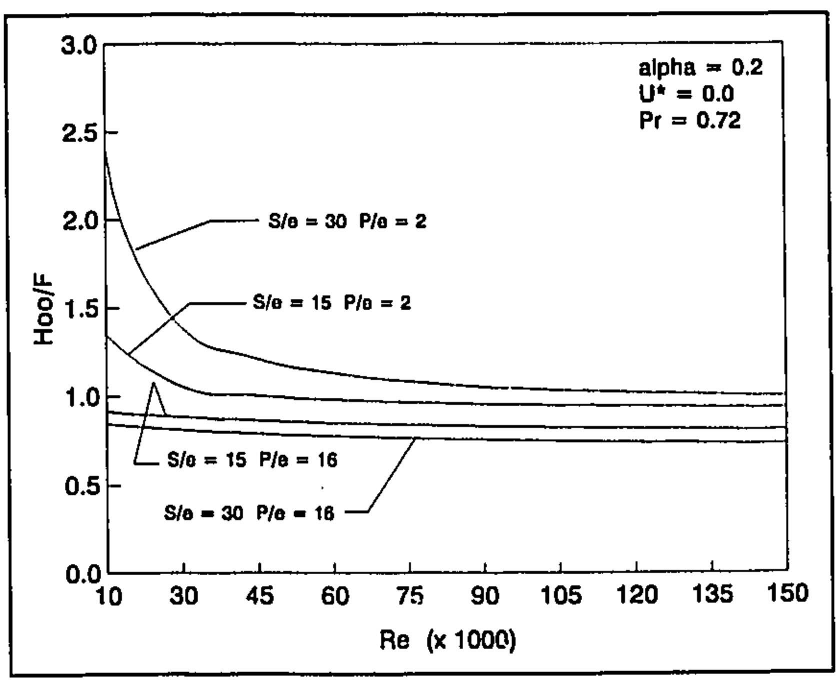

Figure 50: Effects of roughness on Hoo/F (vs U*) - moving core

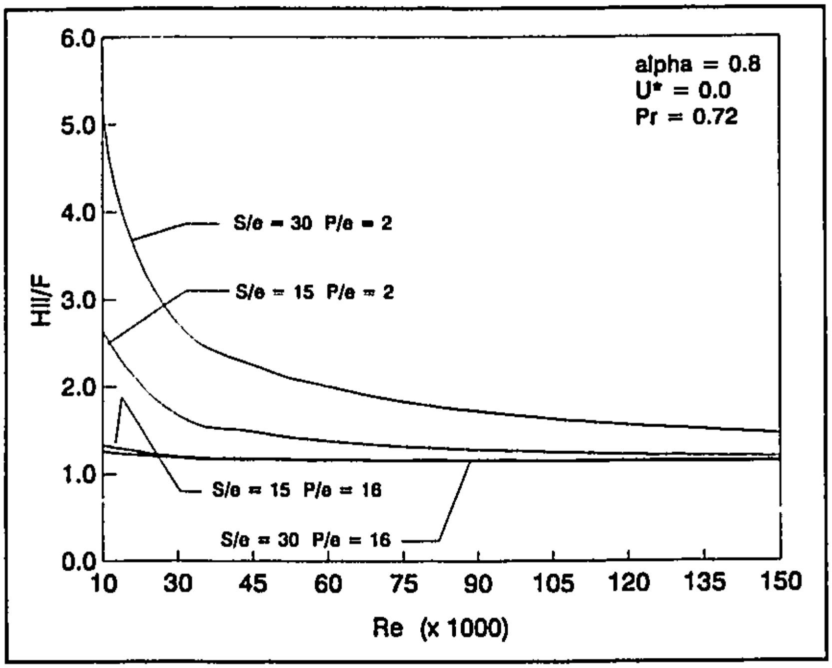

Figure 51: Effects of roughness on Hii/F (vs U*) - static core

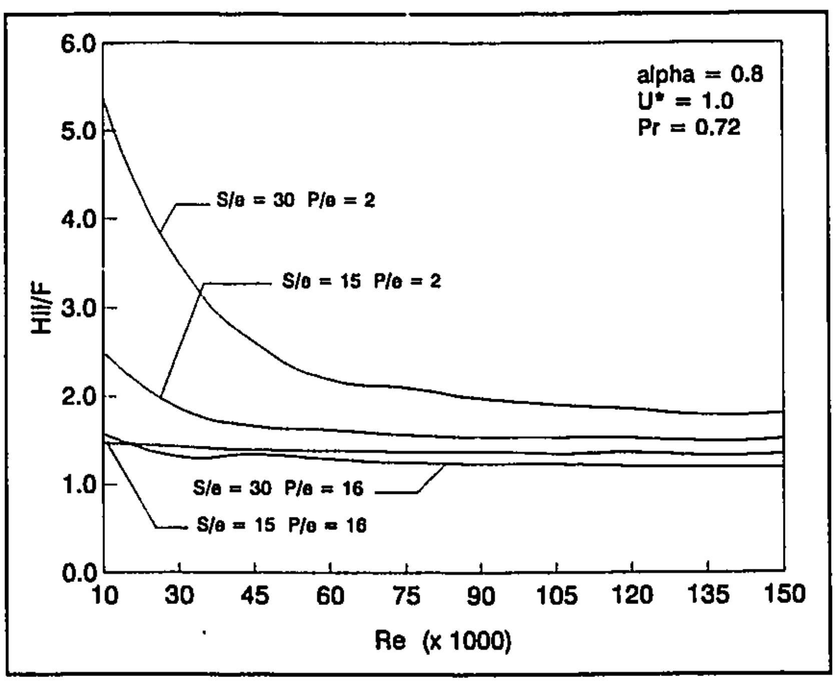

Figure 52: Effects of roughness on Hii/F (vs Re) - moving core

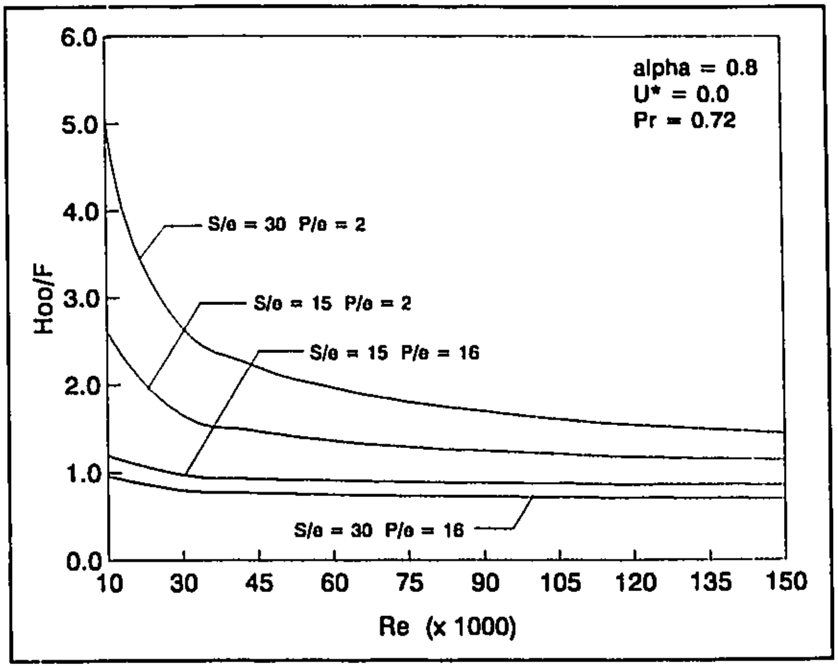

Figure 53: Effects of roughness on Hoo/F (vs Re) - static core

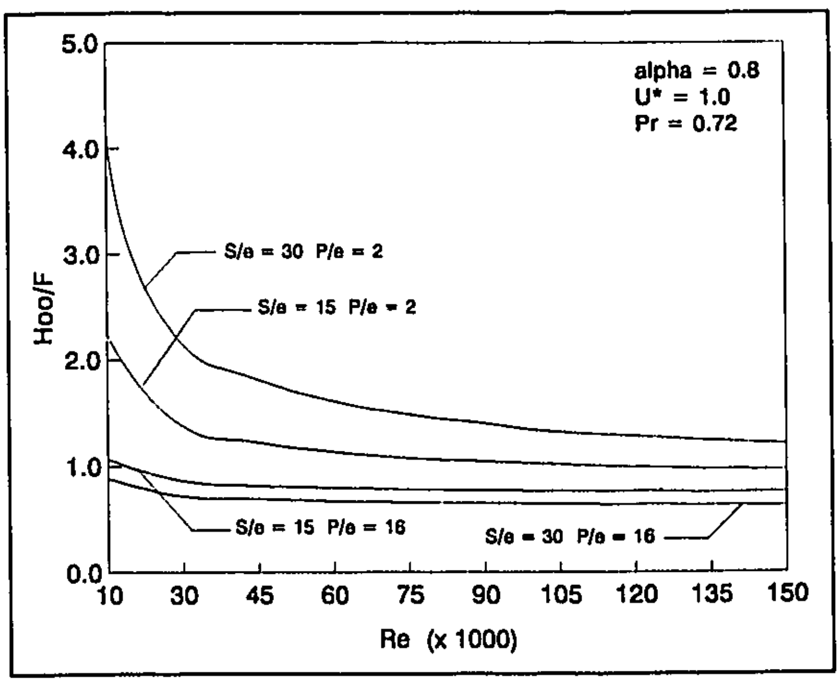

Figure 54: Effects of roughness on Hoo/F (vs Re) - moving core

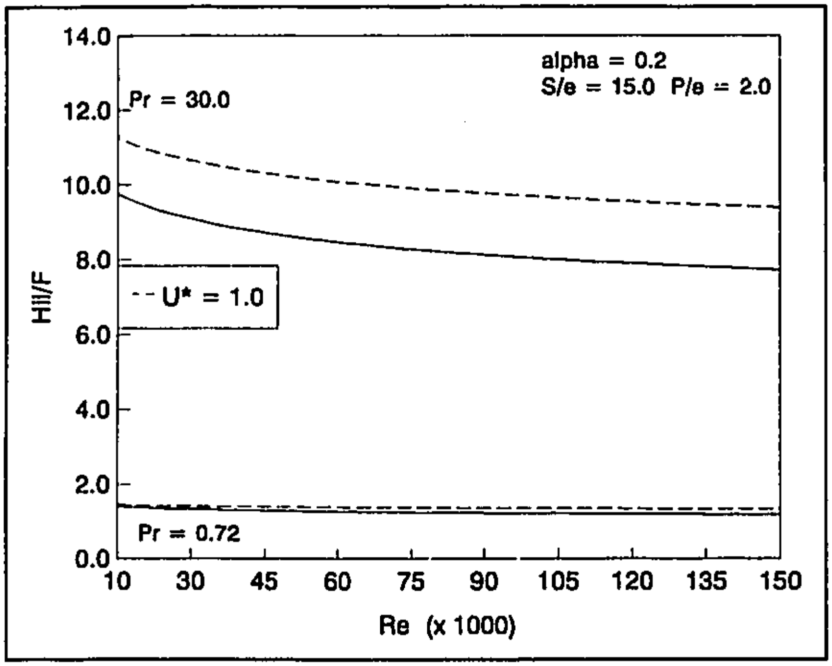

Figure 55: Effects of Pr and U* on Hii/F (vs Re)

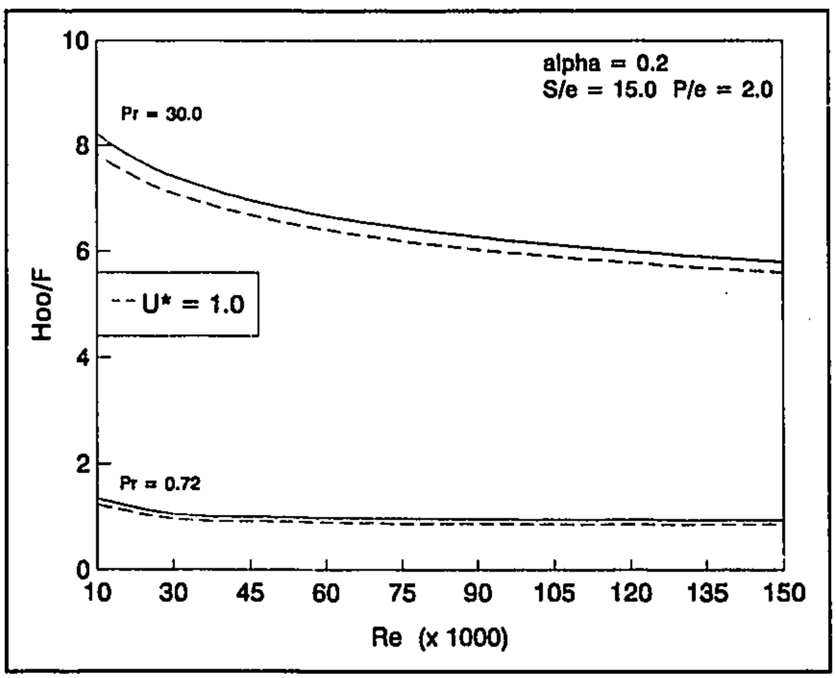

Figure 56: Effects of Pr and U* on Hoo/F (vs Re)